Recombinant pluripotency transcription factors for kinase studies and nanoparticle delivery

Dissertation

der Mathematisch-Naturwissenschaftlichen Fakultät

der Eberhard Karls Universität Tübingen

zur Erlangung des Grades eines

Doktors der Naturwissenschaften

(Dr. rer. nat.)

vorgelegt von

Peter Nader Zaki Malak

aus Asyut, Ägypten

Tübingen

2016

Gedruckt mit Genehmigung der Mathematisch-Naturwissenschaftlichen Fakultät der Eberhard Karls Universität Tübingen.

Tag der mündlichen Qualifikation:	24.06.2016
Dekan:	Prof. Dr. Wolfgang Rosenstiel
1. Berichterstatter:	Prof. Dr. Klaus Schulze-Osthoff
2. Berichterstatter:	Prof. Dr. Michael Schwarz

Table of Contents

Acknowledgements

In all your ways acknowledge Him, and He shall direct your paths.
(The Bible, Book of Proverbs 3:6)

Prof. Klaus Schulze-Osthoff
Thank you for providing me the chance to conduct my PhD study in your group.

Prof. Michael Schwarz
Thank you for being my co-supervisor and for your friendly support

Dr. Oliver Rothfuss
Thank you for your patience and guidance through the years of my PhD. I would not have gone so far without your encouragement.

Britta Merz, Benjamin Dannenmann and Perihan Mir
Thank you for the nice time we spent together in the lab and for the interesting conversations.

Salma Tammam, Benjamin Dannenmann, Alexander Hirth and Franziska Herster
Thank you for your efforts helping me with my projects. It has been an honor for me to work with you.

Frank Essmann, Stephan Hailfinger, Daniela Kramer and Simon Lehle
Thank you for your help during performing the experiments and writing the thesis.

My family
Thank you for your continuous support and for always reminding me that God will complete what he has started with me.

Stephan, Damaris Schnitzer, Dominik and Rosalie Schaebs
Thank you my friends for being always there for me whenever I needed help.

Reissner and Kuntzsch families
Thank you for your open hearts and houses through the last years.

Abbreviations

aa	Amino acid
AIR-1	Aurora kinase A homologue in *C. elegans*
Akt	v-akt murine thymoma viral oncogene homolog
APC/C CDH1	CDH1 activated Anaphase Promoting complex/Cyclosome
APS	Ammonium persulfate
AURKA	Aurora kinase A
AURKB	Aurora kinase B
AURKC	Aurora kinase C
BCA	Bicichoninic acid
bp	Base pairs
BR	Basic region
BSA	Bovine serum albumin
c-MYC	V-Myc Avian Myelocytomatosis Viral Oncogene Homolog
CDC25B	Cell division cycle 25B
CDH1	Cadherin 1
CDK1	Cyclin-dependent kinase 1
cDNA	Complementary DNA
CHX	Cycloheximide
Cp	Crossing point
Ctrl	Control
CV	Column volume
D-box	Destruction box
ddCp	Delta delta crossing point
ddH_2O	Double distilled water
DF1	Dharmafect 1
DFG	Aspartic acid, phenylalanine, glycine
DMEM	Dulbecco’s modified Eagle’s medium
DMSO	Dimethyl sulfoxide
DNA	Deoxyribonucleic acid
DTT	Dithiothreitol
E-box	Enhancer box
ECL	Enhanced chemiluminescence
EDTA	Ethylenediaminetetraacetic acid
EE	Encapsulation efficiency

EMSA	Electrophoretic mobility shift assay
EPDA	End point dilution assay
ESC	Embryonic stem cells
FCS	Fetal calf serum
FITC	Fluorescein isothiocyanate
For.	Forward
FRET	Förster resonance energy transfer
G2 phase	Gap II phase
GADD45A	Growth Arrest and DNA-Damage-Inducible protein 45 alpha
Gapdh	Glyceraldehyde-3-phosphate dehydrogenase
GFP	Green fluorescent protein
Gln	Glutamine
Gsk3ß	Glycogen synthase kinase 3ß
GST	Glutathione S-transferase
H3	Histone H3
HCl	Hydrochloric acid
HD	Homeodomain
HEK293 FT	Modified human embryonic kidney cell line
hFFn	Human neonatal foreskin fibroblasts
hFib	Human dermal fibroblasts
HLH-LZ	Helix-loop-helix-leucine zipper
HMG	High mobility group
hPSC	Human pluripotent stem cells
HRP	Horseradish peroxidase
HSV	Herpes simplex virus
ICM	Inner cell mass
IF	Immunofluorescence
Ig	Immunoglobulin
IP	Immunoprecipitation
iPSC	Induced pluripotent stem cell
kD	Kilo Dalton
KD	Kinase-dead mutant
KLF4	Krüppel-like Factor 4
KO	Knockout
L-NP	Large nanoparticle
L/I/H-NLS	Low/intermediate/high nuclear localization sequence

LIF	Leukemia inhibitory factor
M phase	Mitosis phase
MALDI	Matrix-assisted laser desorption/ionization
Max	Myc-associated factor X
Mdm2	Mouse double minute 2
mECC	Mouse embryonic carcinoma cells
MEF	Mouse embryonic fibroblasts
mESC	Mouse Embryonic stem cell
MOI	Multiplicity of infection
mRNA	Messenger RNA
MS	Mass spectrometry
mV	Millivolt
MWCO	Molecular weight cut-off
N-MYC	V-Myc Avian Myelocytomatosis Viral Oncogene Neuroblastoma Derived Homolog
Nanog	Nanog homeobox, transcription factor
NFκB	Nuclear Factor 'kappa-light-chain-enhancer' of activated B-cells
NLS	Nuclear localization sequence
NP	Nanoparticle
NT	Non-targeting
OCT4	Octamer-binding transcription factor
OSKM	OCT4, SOX2, KLF4 and c-MYC
p-AURKA	Phospho-Aurora kinase A
p-H3	Phospho-histone H3
P53	Tumor suppressor P53
PAK1	P21 Protein (Cdc42/Rac)-Activated Kinase 1
PBS	Phosphate buffered saline
PCR	Polymerase chain reaction
Pen/Strep	Penicillin/streptomycin
PFA	Paraformaldehyde
Pfu/ml	Plaque forming unit
PI3K	Phosphatidylinositol 3-kinase
PLK1	Polo-like kinase 1
POU5F1	POU class 5 homeobox 1 (OCT4 gene)
PP1	Protein phosphatase 1
PP2A	Protein phosphatase 2A

PR	Proline-rich region
PTD	Protein transduction domain
PTM	Post-translational modification
PVDF	Polyvinylidene fluoride
qRT-PCR	Quantitative real-time PCR
RALA	RAS-Like Protein A
Rev.	Reverse
RITC	Rhodamine B isothiocyanate
RNA	Ribonucleic acid
rpm	Revolutions per minute
RPMI	Roswell Park Memorial Institute
RT	Room temperature
S-NP	Small nanoparticle
S/T	Serine/Threonine
SD	Standard deviation
SDS	Sodium dodecyl sulfate
SDS-PAGE	Sodium dodecyl sulfate polyacrylamide gel electrophoresis
Sf9	Spodoptera frugiperda
shRNA	Short hairpin RNA
siNT	Non-targeting siRNA
siRNA	Small-interfering RNA
SOX2	Sex determining region Y-box 2
SPDP	N-succinimidyl 3-[2-pyridyldithio]-propionate
SR	Serum replacement
TAD	Transactivation domain
TBS-T	Tris-buffered saline + Tween-20
TEMED	Tetramethylethylenediamine
TF	Transcription factor
tk	Thymidine kinase
TPP	Tripolyphosphate
TPX2	Microtubule associated protein
UTF1	Undifferentiated embryonic cell transcription factor 1
w/v	Weight per volume
w/w	Weight per weight
WB	Western blot
WGA	Wheat germ agglutinin

wt	Wildtype
ZF	Zinc finger
ZP	Zeta potential
λem	Emission wavelength
λex	Excitation wavelength

1. Introduction

1.1. Pluripotent stem cells

Over the last two decades, pluripotent stem cells (PSCs) drew the attention of the scientific community because of their great promises in regenerative medicine. PSCs can give rise to all tissue and cell types of the human body. They are characterized by self-renewal, pluripotency and differentiation potential (Jaenisch and Young, 2008; Thomson et al., 1998). Self-renewal is defined not only as indefinite proliferation but also as the ability to simultaneously maintain pluripotency and inhibit differentiation.

Human (h) PSCs were first gained from the inner cell mass (ICM) of blastocysts (Thomson et al., 1998). However, this raised a great ethical debate because it involves the destruction of early embryos. Currently, hPSCs can be generated from terminally differentiated adult cells by different methods (Figure 1.1), i.e. by nuclear transfer to unfertilized oocytes in a process called somatic cell nuclear transfer (Tachibana et al., 2013) or by ectopic overexpression of a defined mixture of transcription factors in a process called reprogramming (Takahashi, 2007).

To maintain pluripotency, PSCs including embryonic stem cells (ESCs) and induced pluripotent stem cells (iPSCs) depend on intricate regulatory networks to simultaneously maintain self-renewal potential and to inhibit differentiation. These networks are governed by a relatively limited number of key transcription factors (TFs), primarily the Yamanaka factors OCT4, SOX2, KLF4 and MYC (Liu et al., 2008). The ectopic over-expression of solely OSKM is sufficient to reprogram terminally differentiated cells back to pluripotency in both human and mouse systems (Takahashi and Yamanaka, 2006; Takahashi et al., 2007).

OSKM are involved not only in pluripotency and differentiation regulation in stem cells but also in tumorigenesis (Wang et al., 2013; Herreros-Villanueva et al., 2013; Akaogi et al., 2009; Lin et al., 2012a). OSKM activity is fine-tuned in stem cells transcriptionally as well as by various post-translational modifications (PTMs) such as sumoylation (Tahmasebi et al., 2013; Wei et al., 2007), acetylation (Baltus et al., 2009) and phosphorylation (Van Hoof et al., 2009).

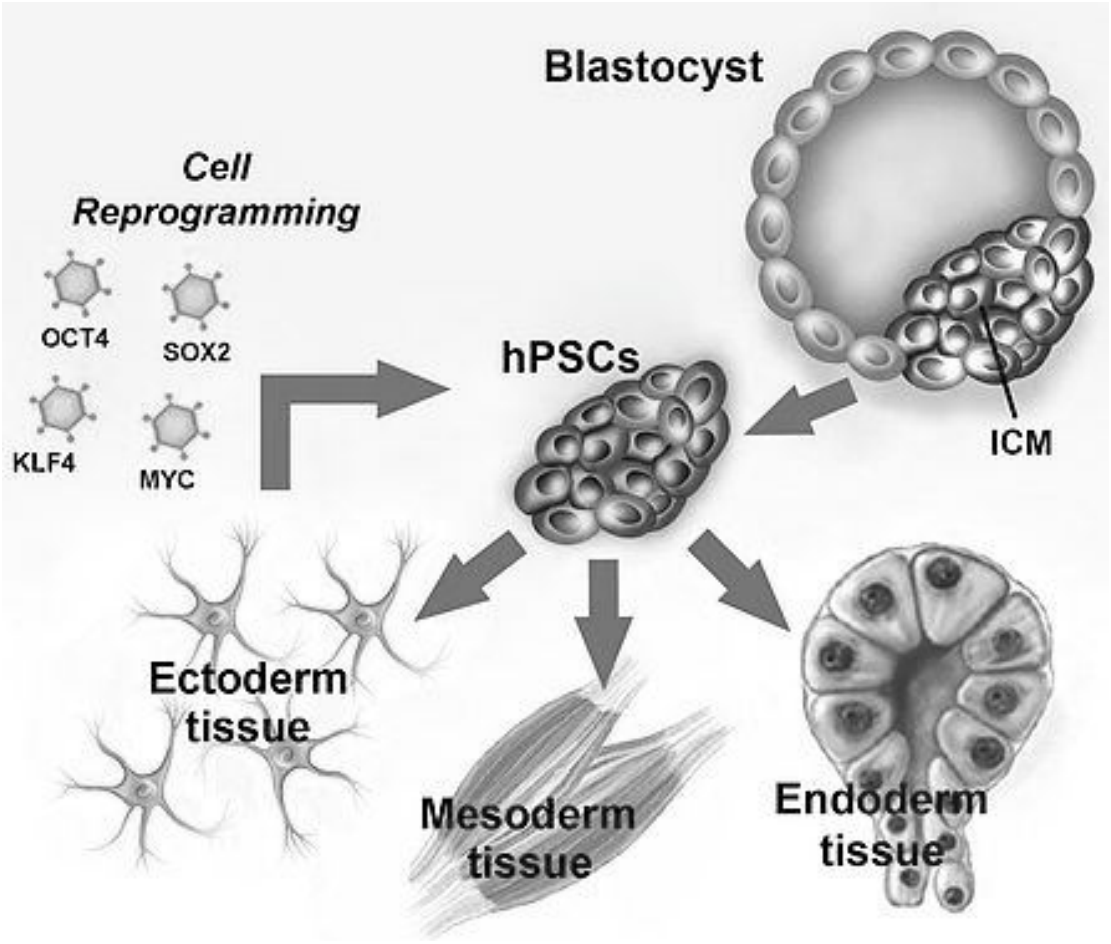

Figure 1.1: Derivation and differentiation of hPSCs

hPSCs can be derived from blastocysts of early embryos and cultured *in vitro*. Alternatively, terminally differentiated cells can be reprogrammed by ectopic overexpression of the transcription factors OCT4, SOX2, KLF4 and c-MYC (OSKM). In turn, hPSCs can be differentiated *in vitro* to give rise to cells from the three germ layers: Ectoderm, mesoderm and endoderm. Figure was adapted and modified from Wang et al., 2014

1.2. Role of Akt kinase in stem cells

Akt kinase is a serine/threonine (S/T) kinase which is highly active in pluripotent stem cells (Watanabe et al., 2006) and in numerous tumors (Altomare and Testa, 2005). It is well established that Akt kinase promotes pluripotency and self-renewal capacity in stem cells through the phosphatidylinositol 3-kinase (PI3K) pathway, suggesting that activation of Akt signaling is sufficient to maintain pluripotency in mouse and primate stem cells (Watanabe et al., 2006). Furthermore, there is accumulating evidence, that Akt directly phosphorylates the TFs Oct4, Sox2 and Klf4 modulating their nuclear localization, stability and transcriptional activity (Campbell and Rudnicki, 2013; Jeong et al., 2010; Schaefer and Lengerke, 2015).

In particular, Akt phosphorylates Oct4 at T235 enhancing its transcriptional activity and stability (Lin et al., 2012b) and this leads to enhanced apoptotic resistance and tumorigenic potential in mouse embryonic carcinoma cells (mECCs). Likewise, Akt phosphorylates Sox2 at T118 in mouse embryonic stem cells (mESCs) that results in decreased proteasomal degradation of Sox2 protein and enhanced the self-renewal capacity of the cells. However, Akt-mediated phosphorylation of Klf4 on T429 (T399 in mouse Klf4) accelerates its degradation and thereby impairs stemness (Chen et al., 2013).

The Akt-specific phosphorylation pattern on OSKM with the specific phosphorylation sites still needs to be more thoroughly defined. Yet, the available tools exhibit critical disadvantages and limitations. One of the widely applied methods to identify the specific phosphorylation sites is the co-expression of the kinase and target protein in mammalian cells. Different fragments of the protein must be expressed separately with the kinase to identify in which fragment the protein is phosphorylated, afterwards, the anticipated sites have to be mutated to a non-phosphorylatable residue, namely alanine, so the phosphorylation is diminished (Chen et al., 2013). This method is usually laborious, time-consuming and not compatible with high-throughput research.

The second common method is the *In vitro* phosphorylation analyses employing recombinant kinases and target proteins. This method provides a faster overview of kinase-specific phosphorylation patterns, but to date, all the proteins used for these studies are expressed in prokaryotic host cells (mainly *E. coli*). This system exhibits a crucial limitation, because the transcription factors are expressed in inclusion bodies and need to be denatured and refolded *in vitro* (Brumbaugh et al., 2012; Kim et al., 2009a; Lin et al., 2012b; Thier et al., 2012; Zhou et al., 2009). Recovering of overexpressed proteins from inclusion bodies is challenging and usually results in a poor yield of natively folded, bioactive proteins (Singh and Panda, 2005).

Therefore, we perceived a necessity to develop a reliable *in vitro* tool to identify the phosphorylation patterns of OSKM particularly by AKT kinase (Figure 1.2). To that end, we expressed and purified the transcription factors OCT4, SOX2, KLF4 and MYC in Sf9 Insect cells. This eukaryotic expression system is capable of performing mammalian-like PTMs (Klenk, 1996) such as phosphorylation which is crucial for the TF activity regulation (Cai et al., 2012).

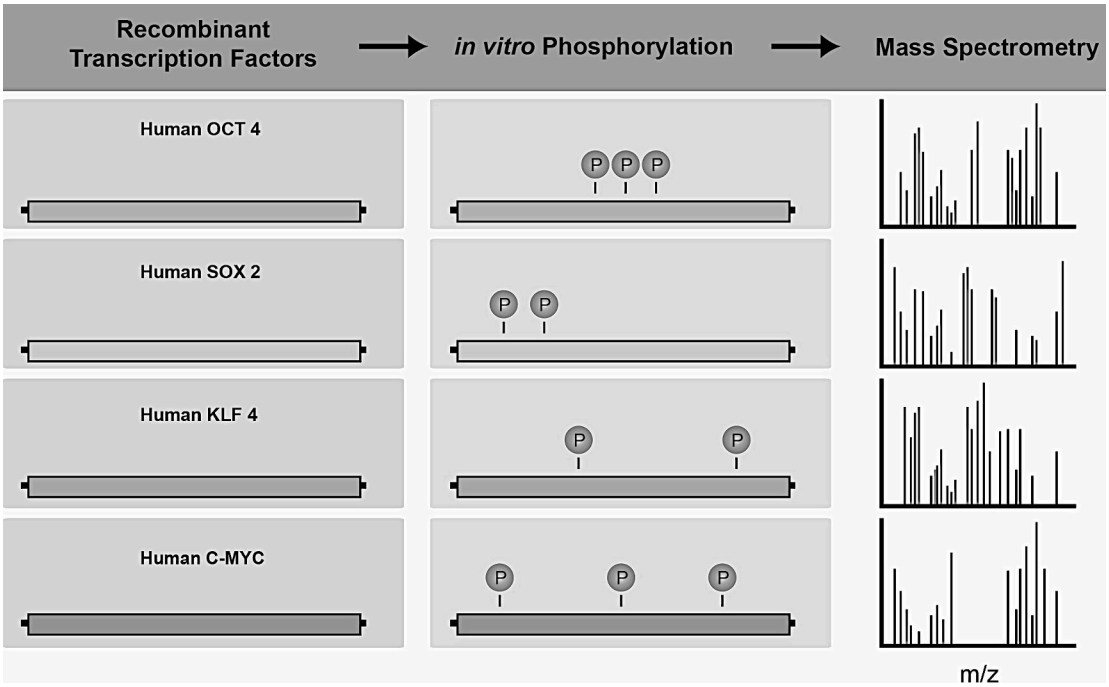

Figure 1.2: Simplified experimental overview of the developed *in vitro* tool

Human OSKM were expressed and purified from Sf9 insect cells. *In vitro* kinase assay were performed using human AKT expressed in Sf9 cells. Subsequently, the proteins were subjected to mass spectrometry and the AKT specific phosphorylation pattern was identified.

By the application of the Baculovirus Expression Vector System, we produced native, highly active recombinant TFs, capable of binding to DNA and similar to their mammalian counterparts in terms nuclear transport and intrinsic phosphorylation. Furthermore, using mass spectrometry-based phosphoproteomics analysis, we identified three novel AKT phosphorylation sites on OCT4, one site on SOX2 and four sites on KLF4. We were able to reproduce the phosphorylation sites described in previous studies as well.

1.3. Aurora kinase A in health and disease

Aurora kinases A/B/C are serine/threonine kinases first described in 1995 (Glover et al., 1995). They play a critical role in cell cycle and regulate different processes in mitosis (Barr and Gergely, 2007). Aurora kinase A (AURKA) gives the trigger for mitotic entry and is crucial for centrosome maturation and microtubule spindle assembly. However, Aurora kinase B (AURKB) is crucial for chromosome segregation and cytokinesis (Sasai et al., 2004). Aurora kinase C (AURKC) share many substrates and functions with AURKB and is thought to complement its function (Ruchaud et al., 2007).

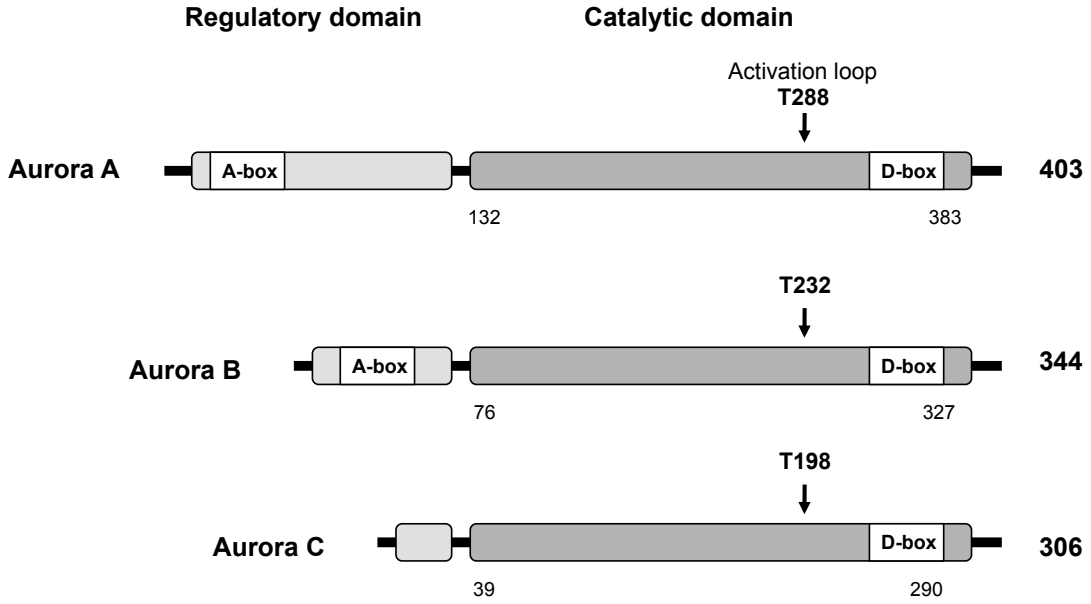

Figure 1.3: Structure of human Aurora kinases

Aurora kinases A/B/C harbor a regulatory and a catalytic domain. The start and the end of the catalytic domain are indicated as well as the length of the proteins.

Aurora kinases share a C-terminal catalytic domain, A and D boxes but a variable N-terminal domain (Figure 1.3). The A and D boxes are responsible for the proteasomal degradation of Aurora kinases A and B (Fu et al., 2007). The kinase activity of Aurora kinases A/B/C depends on autophosphorylation on a central threonine residue in their activation loop (T288, T232 and T198 in Aurora kinase A, B and C respectively). AURKA is expressed in all phases of cell cycle. However, its activity peaks in the late Gap II phase (G2) inducing the G2/M phase transition. Activation of AURKA is stimulated by interaction with several mitotic cofactors including Bora, Ajuba, PAK1

and TPX2 (Figure 1.4). TPX2, a microtubule-associated protein, is the main activator of AURKA. In the late G2 phase, it targets AURKA to the mitotic spindle and facilitates its autophosphorylation (Kufer et al., 2002). Moreover, it inhibits AURKA dephosphorylation by Protein phosphatase 1 (PP1) (Eyers et al., 2003).

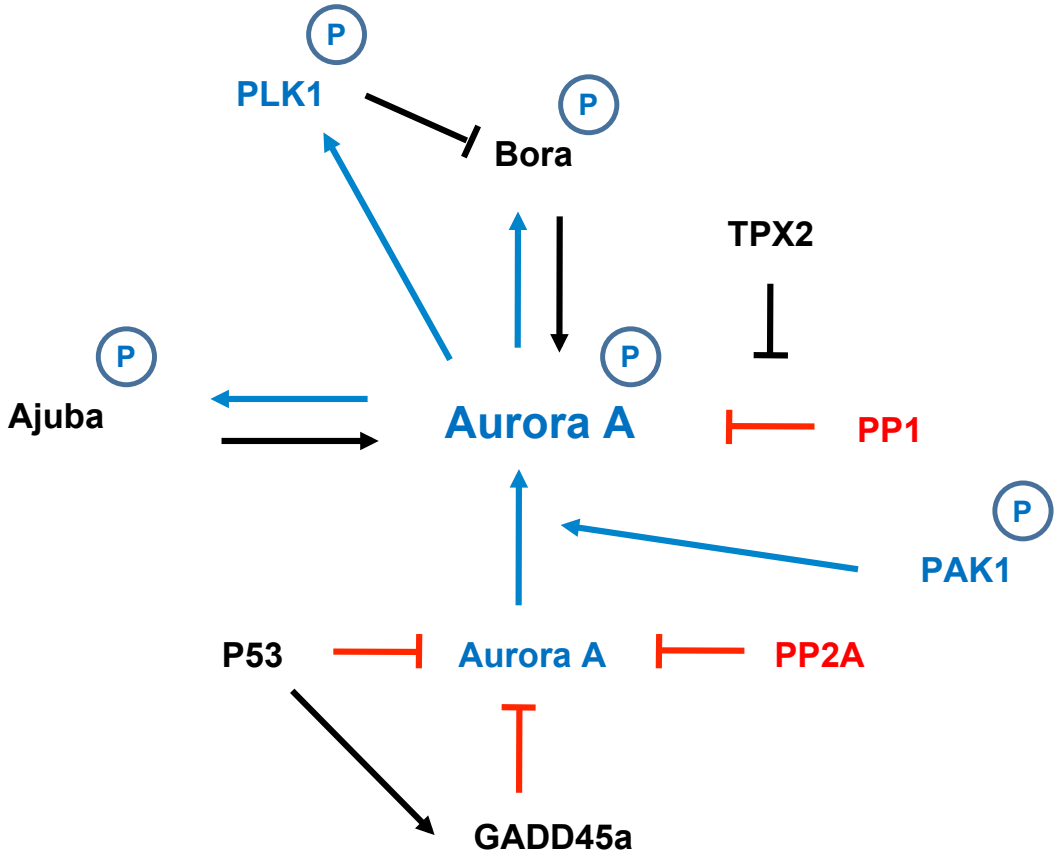

Figure 1.4: Regulators of human Aurora kinase A in cell cycle

AURKA activity in cell cycle is fine-tuned with many positive and negative regulators in a temporal manner. The kinases and phosphorylation events are indicated in blue. The inhibitory proteins and events are indicated in red.

AURKA initiates mitotic entry by phosphorylation of two important substrates CDC25B (Dutertre et al., 2004) and another mitotic kinase PLK1. The later promotes AURKA recruitment to the centrosome and provides a platform for interaction with other crucial mitotic substrates like Bora and for final activation of the cyclin B-CDK1 complex (Seki et al., 2008)

The activity of AURKA is tightly regulated in a temporal manner to ensure correct progression of cell cycle. During mitosis, PP1 dephosphorylates AURKA at T288 to decrease its kinase activity and PP2A dephosphorylates S51 to label AURKA for

proteasomal degradation (Eyers et al., 2003; Walter et al., 2000). Additionally, the tumor suppressor P53 inhibits AURKA kinase function through the expression of GADD45A, a DNA damage-inducible protein (Shao et al., 2006). At the end of mitosis, AURKA gets ubiquitinated by CDH1 activated Anaphase Promoting complex/Cyclosome (APC/C CDH1) and degraded by the proteasome (Crane et al., 2004)

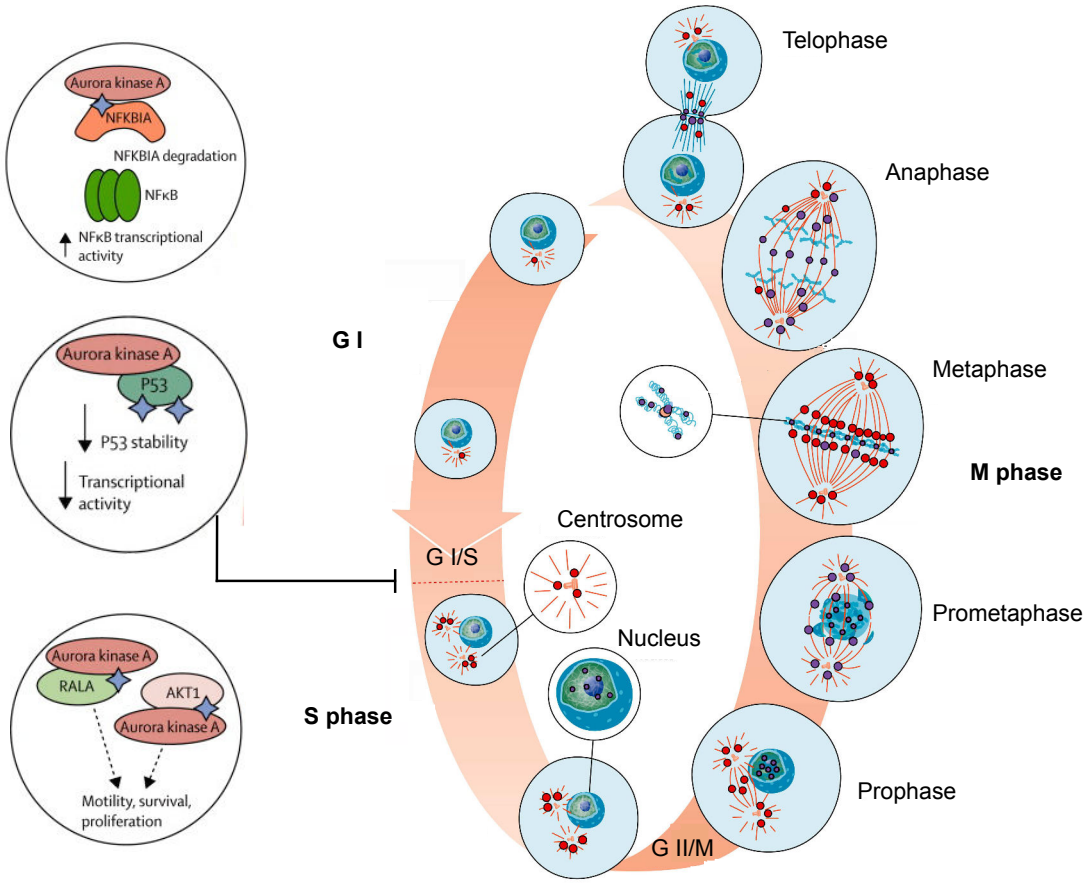

Figure 1.5: Aurora kinase A localization during mitosis and the main interaction partners in tumorigenesis

In the right panel, Aurora kinase A is indicated as red circles through the different phases of the cell cycle. Three of the most well known AURKA interaction partners are indicated in the left panel. The figure was adapted and modified from Mehra et al., 2013.

AURKA upregulation and/or exaggerated activity has been reported in different classes of solid tumors including breast, ovarian, prostate cancers and neuroblastoma (Bischoff et al., 1998; Zhou et al., 1998). The oncogenic potential is often attributed to spread of AURKA from its normal location near the centrosomes to the cytoplasm and even to the nucleus (Tatsuka et al., 2009). Furthermore, Increased AURKA expression leads to aneuploidy and genomic instability which is a

major stimulus for tumorigenesis (Marumoto et al., 2005). However, the aneuploidy caused by AURKA overexpression can trigger the mitotic checkpoints and even induce apoptosis (Meraldi et al., 2002). Despite the established evidence that AURKA is involved in tumorigenesis, AURKA heterozygosity (deletion of one allele) leads to enhanced tumor incidence in mice suggesting its role as a haploinsufficient tumor suppressor (Lu et al., 2008).

AURKA interacts with more than 60 tumorigenesis-associated partners including NFκB, AKT1, RALA, c-MYC, N-MYC and P53 (Figure 1.5) (Nikonova et al., 2013). For instance, AURKA phosphorylates P53 on two serine residues. Phosphorylation of S315 leading to its destabilization and subsequently degradation via MDM2 pathway (Katayama et al., 2004). Moreover, phosphorylation of S215 is reported to abrogate P53 transcriptional activity and P53-induced cell cycle arrest (Liu et al., 2004). Phosphorylation of NFKBIA by AURKA increases NFκB transcriptional activity on prosurvival genes (Briassouli et al., 2007). The interaction between c-MYC and AURKA was reported to augment the oncogenic potential of both in many solid tumors including colon cancer and hepatic cell carcinoma (Lu et al., 2014; Yang et al., 2010)

However, not all the interactions described in literature are dependent on AURKA's kinase function. There is growing evidence that AURKA has kinase-independent functions in mitosis as well as in cancer. Surprisingly, It has been reported that the kinase function of Aurora A is not required in the cell division of *C. elegans* embryos (Toya et al., 2011). Moreover, some described oncogenic functions of AURKA are kinase-independent. For instance, in neuroblastoma, AURKA stabilizes N-MYC in a kinase-independent manner (Otto et al., 2009).

In stem cells, Aurora kinase A role has been a matter of controversy. In a study performed by Lee et al., it has been identified as a fundamental kinase for self-renewal and pluripotency. Knockdown of Aurka in mESCs resulted in complete loss of self-renewal and led to differentiation to ectodermal and mesodermal lineages. Moreover, Aurka inhibition by the MLN8237 or knockdown reduced the reprogramming efficiency of MEFs to iPSCs (Lee et al., 2012a). However, Li and Rana in the same year identified Aurka as a barrier to reprogramming. They showed that Aurka inhibition by MLN8237 or knockdown greatly enhanced reprogramming efficiency (Li and Rana, 2012).

Preliminary experiments in our lab pointed to a direct interaction between AURKA and the transcription factors OCT4 and c-MYC. We further investigated the role of Aurka in mESCs and identified novel kinase-independent effects in regulating Oct4 and c-Myc. By performing luciferase assays, we found that AURKA enhanced the transcriptional activity of both transcription factors in a kinase-independent manner. In mESCs, Aurka overexpression stabilized c-Myc protein. However, knockdown of Aurka destabilized Oct4. Furthermore, we discovered that MLN8237 has diverse effects in mESCs. It destabilized Aurka, Oct4 and c-Myc proteins. Moreover, MLN8237 inhibited c-Myc mRNA expression in reprogrammed MEFs resulting in reduced reprogramming efficiency. Taken together, we conclude that Aurora kinase A is essential in stem cells. However, its kinase function is not the main regulator of pluripotency.

1.4. Chitosan nanoparticles for OCT4 nuclear delivery

The generation of human induced pluripotent stem cells from adult somatic cells represents a major advancement in stem cell biology, especially because of their many potential applications including patient-specific tissue replacement, drug screening and disease modeling (Okita and Yamanaka, 2011; Robinton and Daley, 2012). As mentioned before, human somatic cells can be reprogrammed to iPSCs by the ectopic expression of the four pluripotency-related transcriptional factors OCT4, SOX2, KLF4 and c-MYC, also known as the OSKM factors (Takahashi et al., 2007).

In most cases the OSKM factors are introduced into somatic cells via retroviral transduction, which however bears the risk of insertional mutagenesis of the genome-integrating viruses. Indeed, retroviral vector DNAs can insert at a large number of sites in the host genome and promote the expression of oncogenes or disrupt tumor suppressor genes, leading to the development of cancer. To address this concern, several protocols have been explored to circumvent the integration of foreign DNA into the genome. These include the transient expression of reprogramming factors using non-integrating adenoviruses, plasmids, RNA, episomal vectors or the excision of the transgenes after reprogramming by site-specific recombinases or transposases (Kaji et al., 2009; Okita et al., 2010; Sommer et al., 2010; Stadtfeld et al., 2008; VandenDriessche et al., 2009; Warren et al., 2010; Yu et al., 2009). While such approaches reduce the risk of insertional mutagenesis, the use of nucleic-acid-free approaches by the direct delivery of reprogramming proteins represents presumably the safest methods with respect to future clinical applications of iPSCs (Cho et al., 2010). In addition of reducing tumorigenicity, the use of proteins also avoids the sustained expression of transgenes after reprogramming. Since the transcription factor c-MYC is not only crucial for stemness but also is involved in tumor formation, its expression should be restricted to the reprogramming process.

A major hurdle for the intracellular delivery of proteins is their limited ability to cross the cell membrane. Small protein transduction domains (PTDs) from proteins (e.g., HIV-TAT or *Antennaria* peptide) can be fused to proteins of interest to facilitate the host delivery of reprogramming proteins (Kim et al., 2009a; Nemes et al., 2014; Zhou et al., 2009). Nevertheless, reprogramming by PTD-bearing proteins is very slow (≈8

weeks) and inefficient (≈0.001% reprogramming rate) compared to retrovirus-based protocols (≈0.01% of input cells). The low success of protein-induced stem cell generation is presumably caused by the low stability and solubility of recombinant reprogramming factors as well as their poor endosomal release. Therefore, further developments in protein delivery systems are required to enhance the efficiency of cellular reprogramming to iPSCs.

Polymeric nanoparticles (NPs), such as chitosan NPs, offer a more promising approach. Apart from their biocompatibility and biodegradability, their ability to encapsulate therapeutic proteins into their cores protects proteins from premature degradation (Agnihotri et al., 2004; Enríquez de Salamanca et al., 2006; Pan et al., 2002; Vila et al., 2004). Chitosan [poly(N-acetyl glucosamine)] is a biodegradable polysaccharide that can be used to formulate NPs by several methods e.g. by ionotropic gelation. The ionotropic gelation method is devoid of organic solvents, and the incorporation of a therapeutic protein into the NPs occurs via mild electrostatic interactions in aqueous, physiological conditions (Agnihotri et al., 2004). As cationic polymers chitosan NPs adhere to the negatively charged cell surface, facilitating their cellular uptake by endocytosis (Harush-Frenkel et al., 2007). The presence of primary amine groups on the NP surface facilitates endosomal escape via the proton-sponge effect (Richard et al., 2013). Moreover, tagging of nuclear localization sequences (NLS) to the chitosan NPs allows directing NPs to the cell nucleus (Tammam et al., 2015a).

Among the OSKM factors, the transcription factor OCT4 is of particular importance for reprogramming, stemness and the self-renewal of stem cells (Radzisheuskaya and Silva, 2014). OCT4 is highly expressed in pluripotent cells and becomes silenced upon differentiation. The precise expression level of OCT4 determines the fate of embryonic stem cells (Radzisheuskaya et al., 2013). DNA binding of OCT4 to promoter regions initiates transcription of various genes involved in pluripotency or self-renewal, such as *NANOG* and *SOX2* (Jerabek et al., 2014). OCT4 is therefore considered a master regulator for the maintenance of pluripotent cells and successful reprogramming with *OCT4* alone has been shown (Kim et al., 2009b). However, it was reported that recombinant OCT4 protein has a limited solubility and stability under cell culture conditions (Bosnali and Edenhofer, 2008; Thier et al., 2010). Furthermore, recombinant cell-permeant OCT4-TAT fusion proteins show a weak endosomal release after cellular uptake, which, in addition to their poor stability,

represents another bottleneck for achieving robust reprogramming by protein transduction (Bosnali and Edenhofer, 2008; Thier et al., 2010).

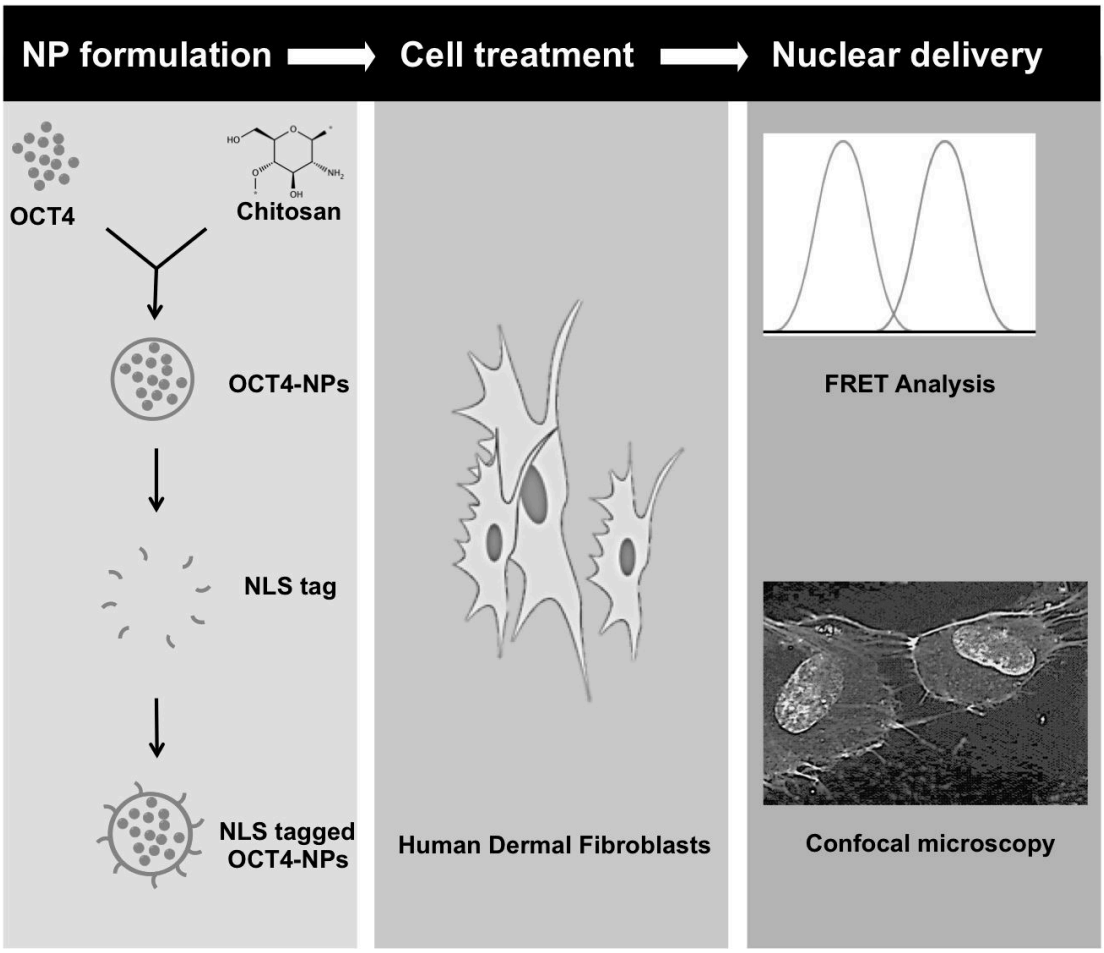

Figure 1.6: Simplified experimental overview of the developed integration-free reprogramming method

NPs were formulated from chitosan monomers and OCT4 recombinant protein, then tagged with NLS. Human dermal fibroblasts were treated with the NPs and analyzed for nuclear delivery using FRET analysis and confocal microscopy.

Various expression systems are available for recombinant protein production. Several groups reported the expression of OCT4 in *E. coli* or mammalian cells (Bosnali and Edenhofer, 2008; Nemes et al., 2014; Thier et al., 2010; Zhang et al., 2012; Zhou et al., 2009). As mentioned before, bacterially expressed OCT4 is usually found in inclusion bodies and needs to be denatured and refolded *in vitro*. The refolding process is cumbersome and results normally in very poor yields of properly folded active proteins. On the other hand, OCT4 expressed in mammalian cells can be purified in a native state, but production of large quantities of purified and active

protein remains challenging and expensive. This limitation might be overcome by the baculoviral expression system in Sf9 insect cells, which can provide high yields of functional proteins (Singh and Panda, 2005).

In order to develop an integration-free, protein-based reprogramming method, we formulated nuclear-targeted chitosan NPs for human OCT4. OCT4 was expressed in Sf9 insect cells, evaluated with respect to its activity and nuclear localization and encapsulated in chitosan NPs (Figure 1.6). Chitosan NPs were able to considerably stabilize the DNA-binding activity of recombinant OCT4 as well as to deliver the OCT4 cargo into nuclei of human fibroblasts. Our study therefore demonstrates a proof-of-concept for a DNA-free protein transduction system, making chitosan NPs as a promising and safe tool for cellular reprogramming and derivation of transgene-free iPSCs.

2. Aim of the study

Stem cells drew a vast attention in the last decades because they hold a great potential for regenerative medicine. Stem cells are capable of self-renewal and differentiation to almost any cell type in the human body. They possess a complex pluripotency network governed by a relatively small number of transcription factors, primarily, OCT4, SOX2, KLF4 and c-MYC (OSKM). In stem cells, these factors are tightly regulated on the post-translational level, mainly by phosphorylation. Therefore, the aim of the first project was to establish an *in vitro* tool to characterize the post-translational modifications (PTMs) in OSKM and to identify novel AKT phosphorylation sites using recombinant proteins expressed in insect cells.

The second project aimed to explore the role of the oncogene Aurora kinase A (Aurka) in stem cells. It has been reported that Aurka regulates the self-renewal and differentiation of stem cells through phosphorylation of the tumor suppressor p53 and Akt kinase. Moreover, There is a great contradiction in literature about the role of Aurka in stem cells and reprogramming. In 2012, Lee et al. defined Aurka as a fundamental kinase for self-renewal and pluripotency and showed that Aurka inhibition decreased reprogramming efficiency. However, in the same year, Li et al. identified Aurka as a barrier to reprogramming and upon Aurka inhibition, reprogramming efficiency was enhanced. Moreover, there is accumulating evidence about the kinase-independent functions of Aurka in mitosis and cancer. Preliminary results in our lab pointed to a direct interaction between Aurka and the pluripotency transcription factors c-Myc and Oct4. Therefore, the second project aimed to explore the effect of Aurka on the transcriptional activity and stability of c-Myc and Oct4. Furthermore, we wanted to disentangle the role of Aurka in reprogramming of MEFs to iPSCs.

Reprogramming of somatic cells to pluripotent stem cells circumvents the two major problems in stem cells research. Firstly, the ethical burden to kill human embryos to extract embryonic stem cells, secondly, the fear of immuno-rejection by allogeneic transplantations. Reprogramming is routinely performed by ectopic overexpression of OSKM using viral vectors increasing the risk of genetic manipulations by viral integrations in the host genome. Therefore, the aim of the third project was to establish an integration-free, protein-based reprogramming method using biodegradable chitosan nanoparticles (NPs).

3. Materials and Methods

3.1. Materials

3.1.1. Cell lines

Cell line	Description	Provider
hFib	Human dermal fibroblasts	Tuebingen University Hospital
hFFn	Human neonatal foreskin fibroblasts	Tuebingen University Hospital
HEK293FT	Human embryonic kidney cells	Invitrogen
MEF feeder cells	Mouse embryonic fibroblasts, feeders for mESCs	Own production
mESCs V64	Mouse embryonic stem cells	Stemgent
Sf9 cells	Spodoptera frugiperda clonal isolation of Sf21	Invitrogen

3.1.2. Cell culture media

Culture Media	Components
Feeder MEF medium	DMEM High Glucose + Glutamine 10% FCS 1% Penicillin/Streptomycin
hFib medium	RPMI-1640 10% FCS 1% Penicillin/Streptomycin
Infection medium	DMEM Knockout (KO)

	10% Serum replacement, 1% NEAA 0.5 mM β-mercaptoethanol 8 µg/ml protamine sulfate
MEF / HEK293FT medium	DMEM High Glucose + Glutamine 10% FCS 1% Penicillin/Streptomycin
MEF/ HEK293FT freezing medium	50% MEF/HEK293FT medium 40% FCS 10% DMSO
mES Freezing medium	50% mES medium 40% KO Serum Replacement 10% DMSO
mES medium	DMEM KO 20% KO Serum Replacement 1% MEM non-essential amino acids 1% Penicillin/Streptomycin 1% L-Glutamine 0.08 mM ß-Mercaptoethanol 1000 U/mL LIF (freshly added)
Sf9 medium	Ex-Cell 420 10% FCS 1% Penicillin/Streptomycin
siRNA Transfection medium for mESCs	DMEM KO
Transfection medium	DMEM + Glutamine + 10% FCS

3.1.3. Chemicals and reagents

3.1.3.1. Chemicals

Reagent	Provider
2-Propanol	VWR
4-Aminoantipyrine-phenol	Acros Organics
Acrylamide Rothiporese Gel 40	Carl Roth
Adenosine triphosphate	CST
Ammonium persulfate (APS)	Carl Roth
Ampicillin	Carl Roth
Bovine Serum Albumin (BSA) fraction V	Carl Roth
Bradford reagent	Fermentas
Bromophenol blue	Sigma-Aldrich
BSA-FITC	Own production
BSA-RITC	Own production
Calcium chloride dihydrate	Merck
Chitosan low molecular weight	Sigma
Complete Mini Protease Inhibitor	Roche
Deoxycholic acid sodium salt	Sigma-Aldrich
Disodium phosphate dihydrate	Merck
Dithiothreitol (DTT)	Carl Roth
DMSO	NeoLab
DNA Gel Loading Dye (6x)	Thermo Scientific
dNTP Mix (100 mM each)	Fermentas
ECL Western Blotting Substrate	Promega
EDTA	Carl Roth
Ethanol	VWR
Fluorescein isothiocyanate (FITC)	Thermo Scientific
Fluorescence-mounting medium	Dako
Glacial acetic acid	Carl Roth
Glycerol	AppliChem
Glycine	AppliChem
HEPES	Carl Roth
Horseradish peroxidase	Sigma Aldrich
Hydrochloric acid (HCl)	Carl Roth
Hydrogen peroxide	Carl Roth

Isopropanol	Merck
Kanamycin	Sigma Aldrich
KAPA 2G Hot Start Polymerase	KAPA Systems
Magnesium chloride dihydrate	AppliChem
Methanol	Merck
Midori Green Advance	Biozym Scientific
Monosodium phosphate monohydrate	Merck
Non-fat dried milk	Applichem
Nonidet P-40	AppliChem
Nuclear localization signal (CPKKKRKV)	Bio Basic Canada Inc.
Nuclease-free water	Ambion
O'GeneRuler 1kb Plus DNA ladder	Fermentas
Paraformaldehyde	Carl Roth
PhosSTOP Phosphatase Inhibitor	Roche
PMSF	Merck
poly(dI-dC)	Sigma Aldrich
ResoLight Dye	Roche
Rhodamine B isothiocyanate (RITC)	Sigma Aldrich
Sodium azide	Carl Roth
Sodium bicarbonate	Carl Roth
Sodium chloride	VWR
Sodium chloride	Carl Roth
Sodium deoxycholate	Carl Roth
Sodium dodecyl sulfate	AppliChem
Sodium hydroxide	Carl Roth
SPDP	Pierce Protein Biology Products
Spectra multicolor board range protein ladder	Thermo Scientific
TEMED	Carl Roth
Tripolyphosphate	Mistral chemicals
Tris base	Applichem
Triton X-100	Carl Roth
Tween-20	Merck
WGA-Alexa Fluor 488	Life Technologies
WGA-FITC	Sigma Aldrich

3.1.3.2. Cell culture reagents

Reagent	Provider
Aurora A Inhibitor I	Selleckchem
Cycloheximide	Sigma Aldrich
DharmaFECT 1	Dharmacon
Dimethyl sulfoxide (DMSO)	Sigma Aldrich
DMEM F12	Invitrogen
DMEM High Glucose (+ L-Glutamine)	Sigma Aldrich
Dulbecco's Phosphate Buffered Saline	Sigma Aldrich
Ex-Cell 420	SAFC- Biotechnologies
Fetal Calf Serum	Sigma Aldrich
Glutamine (100x)	Life Technologies (Gibco)
jetPEI Transfection Reagent	Polyplus Transfection
Knockout DMEM	Life Technologies (Gibco)
Knockout Serum Replacement	Gibco
L-Glutamine (100x)	Gibco
Leukemia inhibitory factor (LIF)	Biomol
MEM Non-essential amino acids	Sigma Aldrich
Mitomycin C	Santa Cruz
PBS	PAA
Penicillin/Streptomycin (100x)	Sigma Aldrich
RPMI-1640	Sigma Aldrich
Sodium chloride 150 mM	Polyplus Transfection
Sodium pyruvate	Gibco
ß-Mercaptoethanol	Sigma Aldrich
Trypsin/EDTA	Sigma Aldrich

3.1.3.3. Cloning reagents

Reagent	Provider
Agarose	Carl Roth
Baculogold Bright Linearized DNA	BD Biosciences
BamH1	Thermo Scientific
EcoR1	Thermo Scientific
LB medium	Carl Roth
NEB 5-alpha competent *E. coli*	New England Biolabs
pAcG2T transfer vector	BD Biosciences
Pfx polymerase	Life Technologies

PvuII	Thermo Scientific
SOC medium	New England Biolabs
T4 DNA ligase	New England Biolabs

3.1.3.4. Laboratory consumables

Cell culture plates and microplates	Greiner bio-one
Cell scraper	Greiner bio-one
Centricons 10 kD	Merck-Millipore
Falcon tubes	Greiner bio-one
Floatlyzers spectra/por, MWCO 100KD	Spectrum labs
Gel blotting paper	Whatman
GSTrap FF 1-mL columns	GE Healthcare
Half Area 96-well microplate	Perkin Elmer
LightCycler® 480 384-well plate, white	Roche
LightCycler® sealing foil	Roche
PVDF membrane	GE Healthcare
Reaction tubes 1.5, 2.0 mL	Eppendorf
Roti-Spin centrifugal filters (MWCO 100KD)	Millipore
T-flasks	Greiner bio-one

3.1.4. Buffers and solutions

Buffer/solution	Components
WB Running buffer (10x)	250 mM Tris 1.92 M Glycine 1% SDS (w/v)
WB Transfer buffer	25 mM Tris 192 mM Glycine 20% Methanol (v/v)
TAE buffer	40 mM Tris 1 mM EDTA pH 8 0.12% Glacial acetic acid (v/v)
Laemmli buffer (5x)	1 M Tris/HCl pH 6.8

	3% DTT (w/v) 40% Glycerol (v/v) 20% SDS (w/v) 0.05% Bromophenol blue (w/v)
Lysis buffer (WB)	10 mM Tris/HCl pH 7.5 300 mM NaCl 1% Triton X-100 (v/v) 2 mM $MgCl_2$ 5 mM EDTA pH 8 2% Protease inhibitors cocktail, 10% PhosSTOP (v/v) added freshly
Blocking buffer (WB)	TBS-T 5% Non-Fat dried Milk (w/v)
Blocking buffer (IF)	TBS-T 4% BSA (w/v)
TBS-T (10x)	0.5 M Tris base/HCl pH 7.4 1.5 M NaCl 0.05% Tween-20 (v/v)
Kinase assay buffer	25 mM Tris-HCl pH 7.5 5 mM ß-Glycerophosphate 2 mM DTT 0.1 mM Sodium orthovanadate 10 mM $MgCl_2$
Buffer A (Sf9 nuclear extraction)	10 mM Na-HEPES pH 7.9 10 mM KCl 0.1 mM EDTA 0.1 mM EGTA 1 mM DTT 0.5 mM PMSF (added freshly)

Buffer B (Sf9 nuclear extraction)	20 mM Na-HEPES pH 7.9 400 mM KCl 1 mM EDTA 1 mM EGTA 10% Glycerol (v/v) 1 mM DTT Protease inhibitors (added freshly) 10 nM Aprotinin, 10 µM Leupeptin, 0.5 µg/mL Pepstatin, 0.5 mM PMSF
RIPA lysis buffer	25 mM Tris-HCl pH 7.6 150 mM NaCl 1% NP-40 (w/v) 1% Sodium deoxycholate (w/v) 0.1% SDS (w/v)
Glutathione elution buffer	10 mM GSH 50 mM Tris/HCl pH 8.0
Coomassie staining solution	0.1% Coomassie Brilliant Blue R-250 (w/v) 50% Methanol (v/v) 10% Acetic acid (v/v)
Coomassie destaining solution	10% Acetic acid (v/v) 10% Isopropanol (v/v) 10% Methanol (v/v)
Silver staining fixation solution	10% Acetic acid (v/v) 40% Ethanol (v/v)
Silver staining sensitization solution	500 mM Sodium acetate 8 mM Sodium thiosulfate x 5 H_2O 40% Ethanol (v/v)
Silver stain	30 mM Silver nitrate

Silver staining developing solution	235 mM Sodium carbonate 50 µL 37% Formaldehyde 25 µL 10% Sodium thiosulfate x 5 H_2O Water to 100 mL
EMSA binding buffer (10 x)	100 mM Tris pH 7.5 500 mM KCl 10 mM DTT
TBE buffer (10 x)	1M Tris base 1M Boric acid 0.02 EDTA

3.1.5. Nucleic acids

3.1.5.1. EMSA IRDye 700 oligonucleotides

EMSA oligonucleotides were labeled from 5' end with phthalocyanine dye IRDye 700DX (Peng et al., 2006) (λex: 689 nm; λem 700 nm). Oligonucleotides were purchased from Integrated DNA Technologies.

Denotation	**Sequence (5´to 3´)**
OCT4 forward primer (For.)	GCCGAA**TTTGCAT**ATTTGCATGGCTG
OCT4 reverse primer (Rev.)	CAGCCATGCAAATATGCAAATTCGGC
SOX2 For.	TAGAAAC**ACAATG**CCTTTCTCGGC
SOX2 Rev.	GCCGAGAAAGGCATTGTGTTTCTA
KLF4 For.	GTAGGGGGTGTGCCCGCCAGGAGGG**GT** **GGG**TCTAAGGTGATAGAGCCTTC
KLF4 Rev.	GAAGGCTCTATCACCTTAGACCCACCCCTCCTGG CGGGCACACCCCCTAC
c-MYC For.	GTGTTAATTGGGAG**CACGTG**TAGGT C
c-MYC Rev.	ACCTACACGTGCTCCCAATTAACAC
UTF1 For.	CTGAAAGATGAGAGCCCT**CATTGTT*ATGCTAGT***G AAGTGCCAAGCTGA
UTF1 Rev.	TCAGCTTGGCACTTCACTAGCATAACAATGAGGG CTCTCATCTTTCAG

The DNA-binding sites are written in bold. In the UTF1 enhancer element, the OCT4-binding site is written in bold italic and the SOX2-binding site in bold.

3.1.5.2. Primers for qRT-PCR

All primers were purchased from Sigma-Aldrich unless otherwise indicated.

Denotation	Sequence (5´to 3´)
Mm-Oct4 For.	GCATACTGTGGACCTCAGGTT
Mm-Oct4 Rev.	TCGAAGCGACAGATGGTGGT
Mm-Sox2 For.	TGCACAACTCGGAGATCAGCA
Mm-Sox2 Rev.	CTCCTGCATCATGCTGTAGCT
Mm-Klf4 For.	GTGCCCCGACTAACCGTTG
Mm-Klf4 Rev.	GTCGTTGAACTCCTCGGTCT
Mm-Aurka For.	CTGGATGCTGCAAACGGATAG
Mm-Aurka Rev.	CGCTGGGAGTTAGAAGGACAC
Mm-Gapdh For.	AGGTCGGTGTGAACGGATTTG
Mm-Gapdh Rev.	TGTAGACCATGTAGTTGAGGTCA
Mm-Actb For.	GGCTGTATTCCCCTCCATCG
Mm-Actb Rev.	CCAGTTGGTAACAATGCCATGT
Hs-AURKA For.	GAGGTCCAAAACGTGTTCTCG
Hs-AURKA Rev.	ACAGGATGAGGTACACTGGTTG
Mm-c-Myc (QuantiTect Primer)	Qiagen (Proprietary sequence)

3.1.5.3. Primers for cloning

Denotation	Sequence (5´to 3´)
pAcG2T For.	CGCGGATCCGATTACAAGGATGACGACGATAAG ATG
OCT4 Rev.	CG GAATTC TCAGTTTGAATGCATGGGAGAGC
SOX2 Rev.	CGGAATTCTCACATGTGTGAGAGGGGCAGT
KLF4 Rev.	CGGAATTCTTAAAAATGTCTCTTCATGTGTAAGG C
c-MYC Rev.	CGGAATTC TTACGCACAAGAGTTCCGTAGCTGT

3.1.5.4. Plasmids

Denotation	Description	Provider
Ig µE4 luciferase reporter (6w-tk Luc)	Luciferase reporter with HSV tk gene promoter	Schöler Lab MPI Münster
c-Myc luciferase reporter	Luciferase reporter with	Qiagen

	minimal CMV promoter and tandem repeats of E-box sequence	
Octamer luciferase reporter	Luciferase expression plasmid with minimal CMV promoter and tandem repeats of Oct4 transcriptional response element	Qiagen
pBABE-AURKA	Retroviral expression vector for human Aurora A kinase	Addgene
pBABE-AURKA KD	Retroviral expression vector for human Aurora A kinase-dead mutant D274A	Addgene
pMX-GFP	Retroviral expression vector for GFP	Cell Biolabs
pMXs-c-MYC	Retroviral expression vector for human cMyc	Addgene
pMXs-hOCT4	Retroviral expression vector for human Oct4	Addgene

3.1.5.5. Small interfering RNA (siRNA)

Denotation	Description	Provider
siNT	SMART pool siRNA without a specific target	Dharmacon
siAurka	SMART pool siRNA targeting mouse Aurora A kinase	Dharmacon

3.1.6. Commercial kits

Kit	Application	Provider
AKT kinase kit	*In vitro* kinase assay	CST
Cignal Oct4/Myc reporter assay Kit	Tranfection for luciferase assay	Qiagen

Coomassie plus	Protein quantification	Pierce Biotechnology
GeneJET Gel Extraction Kit	PCR purification	Fermentas
GeneJET PCR Purification Kit	PCR product purification	Fermentas
GeneJET Plasmid Miniprep Kit	Plasmid isolation	Fermentas
Luciferase assay Kit	Luciferase assay	Promega
Pierce BCA Protein Assay Kit	Protein quantification	Thermo Scientific
QuantiTect Reverse Transcription Kit	cDNA synthesis	Qiagen
RedTaq Mastermix for colony PCR	Colony PCR	Genaxxon
RNeasy Mini Kit + *QIAshredder*	RNA isolation	Qiagen

3.1.7. Antibodies

Specificity	**Species**	**Provider**
Anti-mouse IgG HRP conjugate	Goat	Promega (# W4021)
Anti-rabbit IgG HRP conjugate	Goat	Promega (# W4011)
c-Myc	Rabbit	GeneTex (# GTX61117)
GAPDH HRP conjugate	Rabbit	CST (# 3683)
GST clone 1E5	Mouse	Santa Cruz (#sc-53909)
Human Aurora kinase A	Mouse	Bethyl lab. (#A300-071A)
Mouse Aurora kinase A	Mouse	BD Bioscience (# 610938)
Oct4	Rabbit	CST (# 2840)
Phospho-AKT substrate (RxRxxS/T)	Rabbit	CST (#9614)
Phospho-Aurora A/B/C	Rabbit	CST (#2914)

Phospho-Histone H3	Rabbit	CST (#9701)
Vinculin	Rabbit	CST (#13901)

3.1.8. Instruments and systems

Denotation	Application	Provider
Biorupture™ UDC200	Sonification	Diagenode
Dounce homogenizer	Nuclear extraction	Thermo Scientific
EasyLC nano-HPLC	Chromatography	Proxeon Biosystems
Eclipse Ti	Confocal icroscopy	Nikon
Epgradient S Master	PCR Cycler	Eppendorf
Fusion Software	Western blot imaging	Peqlab
FX Vilber Lourmat	Western blot imaging	Peqlab
Infinite M200 Reader	Spectrophotometry	Tecan
Lambda 12	Spectrophotometry	PerkinElmer
LEO SUPRA 55	Scanning electron microscopy	Carl Zeiss
LightCycler 480 II	qRT-PCR	Roche
LTQ Orbitrap Elite	Mass spectrometry	Thermo Scientific
MaxQuant software	Proteomic analysis	Max Planck Institute of Biochemistry, Martinsried
Mini-Protean	Western Blot	BioRad
Mithras LB 940 / MikroWin 2000 software	Luciferase assay	Berthold technologies
NanoDrop 1000	Spectrophotometry	Peqlab
Odyssey imaging system	EMSA imaging	LI-COR Biosciences
Zetasizer Nano ZS90	Size/charge measurement	Malvern Instruments Ltd

3.2. Methods

3.2.1. Cell culture

3.2.1.1. Sf9 insect cells

Sf9 insect cells, a clonal isolate of Sf21, were used for recombinant protein expression. Sf9 cells were kept at 27°C without CO_2 in both adherent and suspension cultures. Frozen cells were thawed for 1 min at 37°C and washed once with 10 mL fresh insect cell medium. After 5 min centrifugation at 800 rpm at room temperature (RT), cells were seeded in T-flasks with a density of 10^6 cells/cm^2. After 2-3 passages cells were transferred to suspension culture. Sf9 cells were passaged every 2-3 days. Briefly, cells were scraped using a rubber cell scraper, pipetted up and down 3 times and centrifuged for 5 min at RT at 800 rpm. Cells were resuspended in fresh medium and split 1:3 for adherent cell culture with a density of 0.5 x 10^6 cells/mL for suspension culture. For protein expression, suspension cultures were used in a density of 2 x 10^6 cells/mL.

3.2.1.2. Mouse embryonic fibroblasts (MEFs) feeder cells

MEF feeder cells were isolated from BL6 mouse embryos, which were a kind gift from Benjamin Schmid (Hertie Institute for Clinical Brain Research, Tuebingen). Cells were kept in hypoxic culture conditions (5% O_2, 5% CO_2, 37°C) and split 1:3 every 3 days. Briefly, 90% confluent cells were detached using trypsin/EDTA, washed once with PBS, centrifuged for 5 min at 800 rpm at RT and finally resuspended in fresh MEF medium. To make feeder cells for mES cell cultures, MEFs were mitotically inactivated by mitomycin C. Briefly, cells were grown to confluence followed by treatment with mitomycin C (10 µg/mL) for 3 h, washed once with PBS. After washing, cells were detached using trypsin/EDTA solution and frozen in 80% FCS + 20% DMSO with a density of 6 x 10^6 cells/cryo-vial. Frozen cells were thawed for 1 min at 37°C and washed once with 10 mL fresh MEF medium. After 5 min centrifugation at 800 rpm at RT, cells were resuspended and seeded as feeders in a density of 1.5 x 10^4 cells/cm^2.

3.2.1.3. Human dermal fibroblasts (hFib) feeder cells

Human primary fibroblasts were isolated from punch biopsies (diameter: 6 mm) of the skin (volar forearm) of healthy donors. The biopsies were fragmented and transferred into a 6-well plate in hFib medium and incubated at 37°C, 5% CO_2 for 10-

14 days. The cellular outgrowth was detached by trypsin/EDTA and split to a suitable plate size. After reaching 80-90% confluence, cells were split 1:3 every 3 days. hFib feeder cells were mitotically inactivated by mitomycin C with the same procedure mentioned in the previous section.

3.2.1.4. Mouse embryonic stem cells (mESCs)

mESCs were cultured under normal conditions (37°C, 5% CO_2, 20% O_2) using mES medium. For optimal growth of mESCs, MEFs were used as feeder cell layer. However, for qRT-PCR and western blot experiments, mESCs were seeded on hFib feeder layer. mESCs were passaged 1:50 to 1:500 every 3 days on feeder-coated plates. Briefly, feeder cells were seeded as previously described. Then, mESCs were detached using Trypsin/EDTA solution and resuspended in mES medium. To separate mESCs from feeder cells, we exploited the fact that feeder cells are bigger in size than mESCs. Therefore, the cell suspension was incubated at RT for 30 min and the supernatant was used for passaging or seeding for experiments. Cells thawing and freezing was performed with a similar procedure as for MEF feeder cells with the use of serum replacement instead of FCS in the freezing medium.

3.2.1.5. OSKM and hAURKA/KD retrovirus production

Retrovirus was produced under biosafety (S2) regulations. HEK293 FT cells were transfected in 175 cm^2 T-flasks using JetPei transfection reagent according to the manufacturer's instructions. The amounts of plasmids used for virus production were: 13.5 µg of either pMXs-GFP/Oct4/Sox2/Klf4/c-Myc or pBABE-hAURKA/ D274A (KD) + 12 µg pUMVC + 1.3 µg pCMV-VSV-G. All plasmids were purchased from Addgene. The medium of HEK cells was exchanged and the JetPei/DNA mixture was added dropwise. Cells were incubated for 72–80 h. Viral supernatants were harvested and concentrated with Vivaspin concentrators (Sartorius) at 3000 rpm.

3.2.1.6. Reprogramming of MEFs to iPSCs

Retroviruses encoding for the four transcription factors OSKM (4F) were produced as described in the previous section. The supernatant of a 175cm^2 flask was used for 3 wells in 6-well plates. For MEF transduction, concentrated viral supernatants were mixed with 1.5 ml infection medium and added to MEFs. One day after infection, the medium was exchanged to mESC medium (with or without MLN8237). After 4 days, MEFs were split on feeder MEFs on 10 cm plates. Colonies were counted after on

day 14 after infection and the reprogramming was calculated by normalization on the 4F samples.

3.2.1.7. Transient gene knockdown

In order to transiently knockdown Aurka in mESCs, small-interfering RNA (siRNA) against Aurka was used. SiRNA without specific target (siNT) was used as a control. mESCs were seeded on MEFs in 6-well plates at a density of 10^5 cells/well. Transfection was usually performed one day after seeding with a final concentration of 50 nM according to Dharmafect1 (DF1) transfection protocol. Briefly, siRNA was mixed with DMEM knockout medium for 5 min. DF1 transfection reagent was mixed with DMEM knockout medium in a different tube. siRNA mixture was added to DF1 mixture and incubated for 20 min at RT. The medium was removed from the cultured cells and siRNA/DF1 mixture was added to the cells to a final volume of 2 mL with serum replacement containing DMEM knockout medium supplemented with LIF. 24 or 48 h after transfection, knockdown was confirmed by western blot or qRT-PCR.

3.2.1.8. Treatment with kinase inhibitors

mESCs or HEK293 cells were seeded as described above. 24 h after seeding, the medium was exchanged to fresh medium containing the indicated final concentrations of the Aurora A kinase inhibitor MLN8237. Cells were harvested 24 h after treatment for western blot and qRT-PCR analysis.

3.2.2. Protein expression in Sf9 cells using baculovirus

3.2.2.1. Cloning of OSKM into pAcG2T baculovirus transfer vector

The cDNAs of human OSKM were amplified individually using Pfx polymerase and flanked with a flag tag and BamH1 site from 5` end and EcoR1 site from 3` end. After digestion with FastDigest EcoR1 and BamH1 and ligation with T4 ligase, the DNA amplicons were cloned into insect cell transfer vector pAcG2T encoding N-terminal GST fusion proteins. Following transformation of competent NEB 5-alpha *E. coli*, the correct cloning of the inserts was verified by restriction analysis using PvuII.

3.2.2.2. Baculovirus production and amplification

Recombinant baculoviruses were generated through homologous recombination using calcium phosphate co-transfection of the recombinant pAcG2T transfer vector and Baculogold Bright Linearized DNA including GFP gene according to the

manufacturer instructions. Success of homologous recombination was monitored by GFP expression. Baculoviruses were amplified to high-titer stocks by infecting Sf9 suspension cells with multiplicity of infection of 0.5 pfu/cell. 5 days post-infection the supernatant was collected by centrifugation at 2000xg and filtered through 0.22 µm filter. Virus stocks were stored up to 1 year protected from light.

3.2.2.3. Baculovirus quantification and Sf9 cells infection

End point dilution assay (EPDA) was performed to quantify the virus. Briefly, Sf9 cells were seeded in 96-well plates at a density of 2.5 x 10^4 cell/well. Serial dilutions of the virus (10^{-2} - 10^{-9}) were prepared and 12 wells were infected with each virus dilution. 2 days post-infection the number of GFP positive wells was counted. The virus titer was calculated by the infectivity calculator developed by Brett D. Lindenbach according to Reed and Muench method (Reed and Muench, 1938). Virus titer after two rounds of amplification was ≈ 1.5-2 x 10^8 pfu/mL. For protein production, Sf9 cells were infected with MOI of 10 pfu/cell.

3.2.3. Protein purification

Sf9 cells were harvested 2 days post-infection for SOX2, KLF4 and c-MYC, and 3 days post-infection for OCT4 at 2500xg for 10 min. OCT4, SOX2 and KLF4 were isolated from purified Sf9 cell nuclei. To this end, the cell pellet was washed with PBS and resuspended in Buffer A. After incubation on ice for 15 min, cells were homogenized with 25 strokes in a Dounce homogenizer. After centrifugation at 7000xg for 10 min at 4°C, the nuclear pellet was resuspended in 5 pellet volumes of Buffer B and incubated for 30 min at 4°C with rotation. For c-MYC, whole cell extraction was performed by incubating the cells for 45 min in ice-cold RIPA lysis buffer. Both the nuclear and whole cell lysates were centrifuged at 50,000xg for 15 min at 4°C to remove cellular debris and filtered through a 0.45 µm filter. Protein purification was performed using GSTrap FF 1-mL columns coupled to a peristaltic pump. The column was equilibrated with 5 column volumes (CV) of PBS before the lysates were loaded with a flow-rate of 1 mL/min. After sample application, the column was washed with 10 CV PBS and proteins were eluted in 0.5 mL fractions with 5 CV glutathione elution buffer at a flow rate of 0.2 mL/min. All steps were performed at 4°C. The purified protein was stored in GSH elution buffer + 25% glycerol in -80°C.

3.2.4. Protein phosphorylation analysis

3.2.4.1. *In vitro* kinase assay

Kinase assays were carried out in kinase buffer in the presence or absence of 200 μM ATP. 3 µg of the recombinant proteins OSKM and 0.5 µg of active human AKT1 protein were incubated for 2 h at 30°C.

3.2.4.2. Mass spectrometry and phospho-proteomic analysis

After performing the kinase assays, proteins were processed for MS analyses as described before (Olsen and Macek, 2009) with the following changes: In-solution digestion was performed with endoproteinases Lys-C, trypsin or AspN. LC-MS/MS analyses were performed on an EasyLC nano-HPLC coupled to an LTQ Orbitrap Elite mass spectrometer as described (Franz-Wachtel et al., 2012). For the analyses, 15 most intense precursor ions were sequentially fragmented in each scan cycle (90 min, HCD, top15). The MS data of all experiments was processed using default parameters of the MaxQuant software version 1.2.2.9 (Cox et al., 2009). Peak lists were searched against a human target-decoy database (taxonomy id 9606), containing 84946 forward protein sequences and 248 common contaminants, and GST-tagged versions of OCT4, SOX2 and KLF4. The following criteria were applied for the database search: Endoproteinases Lys-C, trypsin or AspN were defined as proteases and two missed cleavages were allowed. Carbamidomethylation of cysteine was set as fixed modification; N-terminal acetylation, oxidation of methionine, and phosphorylation of serine, threonine and tyrosine were set as variable modifications. Initial precursor mass tolerance was set to 7 ppm and 20 ppm at the fragment ion level. Identified MS/MS spectra were further processed by MaxQuant for statistical validation and quantification of peptides and protein groups. A false discovery rate of 1% was set at the peptide, protein and phosphorylation site level.

3.2.5. Chitosan nanoparticles (NPs) characterization

3.2.5.1. NPs formulation, size and charge determination

Small (S-NPs) and large (L-NPs) chitosan NPs were formulated by the ionotropic gelation method using low-molecular weight chitosan (50–190 kD) and tripolyphosphate (TPP) as described (Tammam et al., 2015a). NP average hydrodynamic diameter and zeta potential were determined using a Zetasizer Nano

ZS90. After dilution of the NP suspension with deionized water samples were measured in triplicate at 25°C and calculated as means ± SD.

3.2.5.2. Encapsulation efficiency measurement

Horseradish peroxidase (HRP; ~150 U/mg) was used as a model protein to study protein encapsulation. HRP-loaded chitosan NPs were formulated by dissolving HRP in TPP solution. To exclude that the NP encapsulation of proteins by inotropic gelation did affect protein activity, encapsulation efficiency (EE) was determined based on enzyme activity and protein content. For determination of protein EE, L-NPs were centrifuged at 14000xg for 30 min before un-entrapped protein was quantified in the supernatant. S-NPs were first centrifuged in Roti-Spin centrifugal filters (molecular weight cut-off 100 kD) for 20 min at 4000xg before the non-entrapped protein was quantified in the flow-through. EE based on total protein content was determined by Coomassie Plus following removal of excess chitosan. HRP L-NPs and S-NPs were purified as described above. To 1 mL of L-NP supernatant and S-NP flow-through 20 µL of 20% NaOH were added to each tube. Tubes were vortexed allowing the remaining chitosan to precipitate. Tubes were then centrifuged at 14000xg for 5 min before chitosan-free supernatants were used to quantify un-entrapped protein using Coomassie dye. In order to exclude effects of NaOH on protein stability, protein calibration curves were prepared in either S-NP flow-through or L-NP supernatant and treated with 20 µL of 20% NaOH similar to the test solutions.

3.2.5.3. *In vitro* release analysis

To determine the ability of S-NPs and L-NPs to release proteins, HRP-loaded NPs were purified, reconstituted in 1 mL deionized water and placed in spectra/por float-A-lyzers (molecular weight cut-off 100 kD). NP-loaded float-A-lyzers were submerged in 6 mL PBS and maintained at 37°C in a shaking water bath. At predetermined time intervals, 200 µL of the samples were removed, replaced with fresh buffer and analyzed for active HRP. Free HRP was used as a control. All samples were analyzed in triplicate and results are given as means ± SD.

Activity-based quantification of HRP was performed as described (Trinder, 1969). Briefly, 1.5 mL of 1.7 mM of hydrogen peroxide in 0.2 M potassium phosphate buffer was mixed with 1.4 mL of 4-aminoantipyrine-phenol solution (2.5 M 4-aminoantipyrene, 0.17 M phenol). The increase in absorbance at 510 nm was

recorded using a UV–Vis spectrophotometer every 30 sec for 5 min upon addition of 100 µL enzyme-containing test solution (L-NP supernatant or S-NP flow-through). Rate of reaction was determined and used to calculate the enzyme concentration from an HRP standard calibration curve.

3.2.5.4. NPs tagging with nuclear localization signal (NLS)

As a classical NLS, the octapeptide CPKKKRKV was used. NLS tagging to NPs was performed via N-succinimidyl 3-[2-pyridyldithio]-propionate (SPDP) an SH-NH_2 cross-linker utilizing the N-terminal SH group in the NLS and cationic amines in chitosan. S-NPs with low (L-NLS; 0.25 NLS/nm^2), intermediate (I-NLS; 0.5 NLS/ nm^2) and high (H-NLS; 2 NLS/ nm^2) NLS density were synthesized. NLS tagging and characterization of the modified NPs was performed as detailed previously (Tammam et al., 2015b).

3.2.5.5. Cellular uptake quantification

For NP treatment, human primary fibroblasts were plated in 96-well plates ($2x10^4$ cells/well) and cultured in hFib medium. After 48 h cells were washed with PBS and incubated with purified NP-encapsulated BSA-RITC in serum-containing phenol-red free RPMI-1640 medium. The non-modified and NLS-modified S-NPs were added to the cells at a concentration of 100, 250 and 500 µg/mL. After 24 h, culture supernatants were removed and cells were washed twice with PBS. The amount of cell-associated NPs was calculated by fluorometry from standard curves as described (Tammam et al., 2015b).

Based on the preferential affinity of wheat germ agglutinin (WGA) to chitosan, FITC-coupled WGA was exploited to distinguish between cell surface-absorbed and internalized NPs. In non-permeabilized cells at 4°C, WGA-FITC is not internalized and only labels extracellular chitosan NPs, whereas in permeabilized cells at RT WGA-FITC can enter the cell and label both surface-bound and internalized chitosan NPs. Therefore, fibroblasts were grown in two 96-well plates and loaded with the non-modified or NLS-modified S-NPs as described above. After 24 h, cells were washed twice with PBS. In the first plate, cells were fixed with 4% paraformaldehyde (PFA) for 15 min, washed with PBS, and permeabilized with 0.1% Triton X-100 for 15 min. After washing cells were incubated with 100 µL of 10 µg/mL WGA-FITC for 15 min at RT followed by 3 times washing in PBS. In the second plate, cells were incubated on ice for 15 min and then directly treated with WGA-FITC for 15 min on

ice. After three times washing in PBS, the amount of bound WGA-FITC was determined by fluorometry (λex: 494 nm; λem 518 nm) in both plates as described (Tammam et al., 2015a). Results are expressed as mean ± SD from three experiments performed in triplicate.

3.2.5.6. Nuclear uptake quantification

Nuclear uptake was quantified using Förster resonance energy transfer (FRET) fluorometry. The nuclear DNA dye Hoechst 33258 and FITC from FITC-coupled BSA were used as FRET donor and acceptor, respectively. Formulation and encapsulation of BSA-FITC in unmodified and the different versions of NLS-modified S-NPs was performed as described above. Fibroblasts were seeded at a density of $2x10^4$ cells/well in 96-well plates, treated with 250 µg/mL of the NP versions after 48 h and incubated for another 24 h. After aspiration of the culture supernatants cells, cells were stained with Hoechst dye (1.5 µg/mL). Cells were washed 3 times with PBS then analyzed by FRET spectroscopy. Three readings were obtained in the FRET channel (λex 366 nm; -λem 518 nm) either for Hoechst-stained and NP-treated cells, for NP-treated cells or for Hoechst-stained cells. FRET was determined from the increase in FITC emission due to a nuclear co-localization of both dyes. FRET efficiency was calculated as described previously(Tammam et al., 2015b).

3.2.5.7. Scanning electron microscopy

For morphological analysis, a drop of the diluted NP suspension was spread on glass slides and subjected to field-emission scanning electron microscopy using a LEO SUPRA 55 microscope. Prior to analysis, NP samples were coated with a fine gold layer using a gold sputter module.

3.2.5.8. Confocal laser scanning microscopy

Human fibroblasts were seeded on coverslips in 24-well plates at a density of $5x10^5$ cell/well. After 24 h, cells were treated with either 50 µg/mL of OCT4 encapsulated in S-NPs or soluble OCT4 and incubated for another 24 h. Following several washes in PBS, cells were stained with Hoechst 33258 (1.5 µg/mL) for 5 min, fixed with 4% PFA and permeabilized with 0.1% Triton X-100 in PBS. WGA-Alexafluor 488 was added to the cells for 15 min at RT. Cells were then washed twice with PBS and incubated in blocking buffer (1% BSA in PBS) for 30 min. OCT4 primary antibody (1:100) was incubated overnight at 4°C. After three washes in blocking buffer, FITC-conjugated goat anti-rabbit IgG (1:500) was applied for 1 h at RT. Coverslips were

washed in PBS, mounted in fluorescence-mounting medium and examined by confocal microscopy.

3.2.6. Luciferase assay

HEK293 FT cells were seeded in 24-well plates at a density of $5x10^4$ cells/well. 24 h after seeding, cells were transfected with the firefly reporter, renilla control and the different DNA mixtures OCT4, c-MYC, AURKA or AURKA KD. 48 h after transfection, cells were detached by pipetting, transferred to reaction tubes, washed twice with PBS and lysed by passive lysis buffer (PLB). Lysis was completed by freezing at -80 for 20 min. For luciferase measurement, 2.5 µL of the lysates were pipetted in a white half-area 96-well plate, 25 µL of luciferase assay substrate (LARII) were injected and firefly luminescence was measured by Mithras luminometer. After 1 sec delay, 25 µL of Stop & Glow (S&G) were injected and renilla luminescence was measured. Firefly luminescence values of each sample were normalized to its renilla control. Ratio of firefly/renilla of the test samples was normalized to the ratio of the GFP control.

3.2.7. Gene expression analysis

Total RNA was isolated with the RNeasy Mini Kit according to the manufacturer's instruction and was stored at -80. Routinely, 1 µg of RNA was reverse-transcribed using QuantiTect Reverse Transcription Kit with Oligo-dT and a mix of random primers according to the manufacturer's instructions.

The LightCycler 480 II System was used for qRT-PCR, KAPA2G was used as a polymerase and Resolight as a DNA-staining dye. Briefly, for each 384-well reaction, the mixture contained the following: 5 µL KAPA2G mix, 0.03 µL Resolight, 1.48 µL water, 1 µL primer mix and 5-10 ng of the test cDNA. The PCR program consisted of 3 phases: 3 min at 95°C followed by 45 cycles of amplification (10 s at 95°C, 10 s at 60°C, 10 s at 72°C) and finally one cycle for melting curve analysis (5 s at 95°C, 1 min at 65°C, 97°C). Gapdh and Actb were used for normalization and relative gene expression was calculated as 2^(-ddCp) as described before (Livak and Schmittgen, 2001).

3.2.8. Protein quantification

BCA protein assay was used for protein quantification. Briefly, serial dilutions of BSA (2-0 mg/mL) were prepared in the used lysis buffer. BSA dilutions and the different

samples were loaded on a flat-bottom transparent 96-well plate in duplicates. BCA reagents A and B were mixed in proportion 50:1 respectively and added to the wells. The plate was incubated at 37° C for 30 min and absorbance was measured at 562 nm. Samples concentrations were calculated using the BSA standard calibration curve. For the purified proteins, Bradford assay was used instead of BCA assay because GSH interferes with BCA measurement. Briefly, serial dilutions of BSA (2-0 mg/mL) were prepared in GSH elution buffer. BSA dilutions and the different column elutions were loaded on a flat-bottom transparent 96-well plate in duplicates, Bradford reagent was added to the wells at RT and absorbance was measured at 595 nm. Elution concentrations were calculated using the BSA standard curve.

3.2.9. Western blot analysis

Cells were harvested either by trypsin/EDTA (mESCs, MEFs) or by pipetting (HEK293 FT). After washing with PBS, cells were centrifuged for 5 min at 4500 rpm at 4°C. PBS was aspirated and a lysis buffer supplemented with protease/phosphatase inhibitors cocktail was added. The lysates were incubated for 30 min on ice. The lysates were sonicated with Bioruptor for 5 min (5 cycles of 10 s on, 50 s off), if phospho-antibodies were intended to be used. Furthermore, the lysates were centrifuged for 30 min at 14000 rpm at 4°C to remove remaining cellular debris.

The protein samples were mixed with 5x Laemmli buffer and boiled for 5 min at 95°C. 10-20 µg protein were loaded on 10% SDS-PAGE gels, *Multicolor Broad Range Protein Ladder* was used as a protein marker. After running the gels in WB running buffer for 1.5 h at 120 V, the proteins were transferred to polyvinylidene fluoride (PVDF) membranes in transfer buffer for 1 h at 100V. After transfer, the membranes were blocked using 5% milk or 4% BSA in TBS-T. The membranes were subsequently incubated in the corresponding primary antibody solution overnight at 4°C on a roller shaker. After washing 3 times in TBS-T, the membranes were incubated in secondary antibody (HRP-conjugate) solutions for 1 h at RT and subsequently washed 3 times with TBS-T. For protein bands detection, the membranes were incubated in ECL solution for 2 min and then the chemiluminescence signal was visualized with the *Fusion-FX7 Spectra* detection system.

3.2.10. Coomassie and silver staining

The recombinant proteins were separated by 10% SDS-PAGE. For Coomassie staining, gels were stained for 1 h in staining solution and destained overnight in destaining solution. For silver staining, gels were fixed for 30 min, sensitized for 30 min, and washed three times for 5 min in H_2O. After staining for 30 min in the silver nitrate stain, gels were washed in H_2O and developed in 100 mL of the developing solution.

3.2.11. Electrophoretic mobility shift assay (EMSA)

EMSA was performed using Odyssey® Infrared EMSA Kit according to the manufacturer's instructions. Briefly, the recombinant proteins or the nanoparticles were incubated with 1 µL of IRDye® 700 infrared dye-labeled double-stranded oligonucleotides, 2 µL of 10x binding buffer, 2.5 mM DTT, 0.25% Tween-20 and 1 µg of poly(dI-dC) in a total volume of 20 µL for 30 min at RT in the dark. Samples were separated on 4% native polyacrylamide gels in 0.5x Tris-borate-EDTA buffer at 70 volts for 1 h. The gel was scanned by direct infrared fluorescence detection on the Odyssey imaging system.

3.2.12. Statistical analyses

Unless stated otherwise, data were expressed as mean ± standard deviation (SD) of at least three independent experiments. P-values were determined by unpaired, two-tailed Student's T-Test.

4. Results

4.1. OCT4, SOX2, KLF4 and c-MYC (OSKM) expression and purification

4.1.1. OSKM expression and protein integrity depended on time post-infection

To optimize protein expression, Sf9 cells were infected with different amounts of OCT4 baculovirus to different multiplicities of infection: 3, 5 and 10 plaque forming unit (pfu)/cell. No difference was observed between the different MOIs. However, the time post-infection affected the protein expression significantly. Full-length OCT4 protein expression increased 72-84 h post-infection, while the lowest expression level was observed 60 h post-infection. Three distinct degradation products were detected by OCT4 antibody (Figure 4.1). Matrix-assisted laser desorption/ionization (MALDI) analysis showed that these degradation products consist of part of the GST moiety and the POU-specific DNA binding domain which was still able to bind to DNA in EMSA analyses (data not shown).

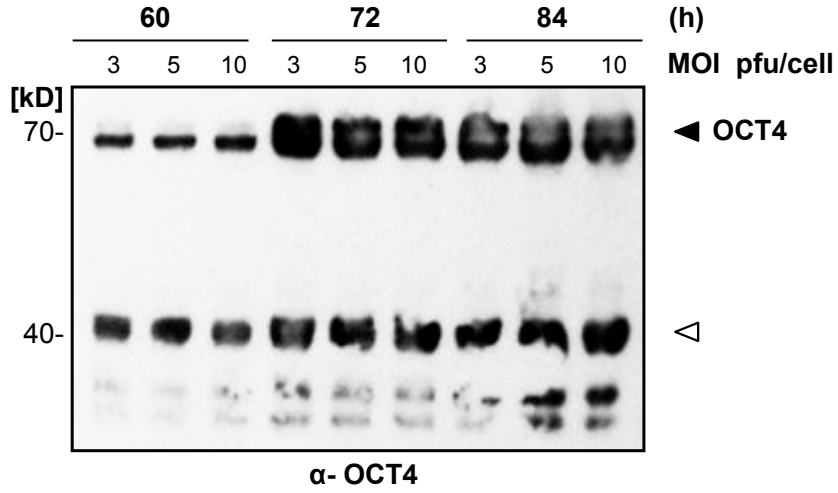

Figure 4.1: OCT4 expression in Sf9 cells increased with time post-infection

Western blot of Sf9 insect cells infected with baculovirus coding for human OCT4 preceded by GST-tag. Virus titer was quantified as number of plaque forming units/ml (pfu/ml). Cells were infected with the indicated MOI (pfu/cell) and harvested at the indicated time points. Cell pellets were lysed using RIPA buffer and subjected to immunoblotting using OCT4 antibody. Closed arrowheads refer to the full-length protein and open arrowheads to the degradation products.

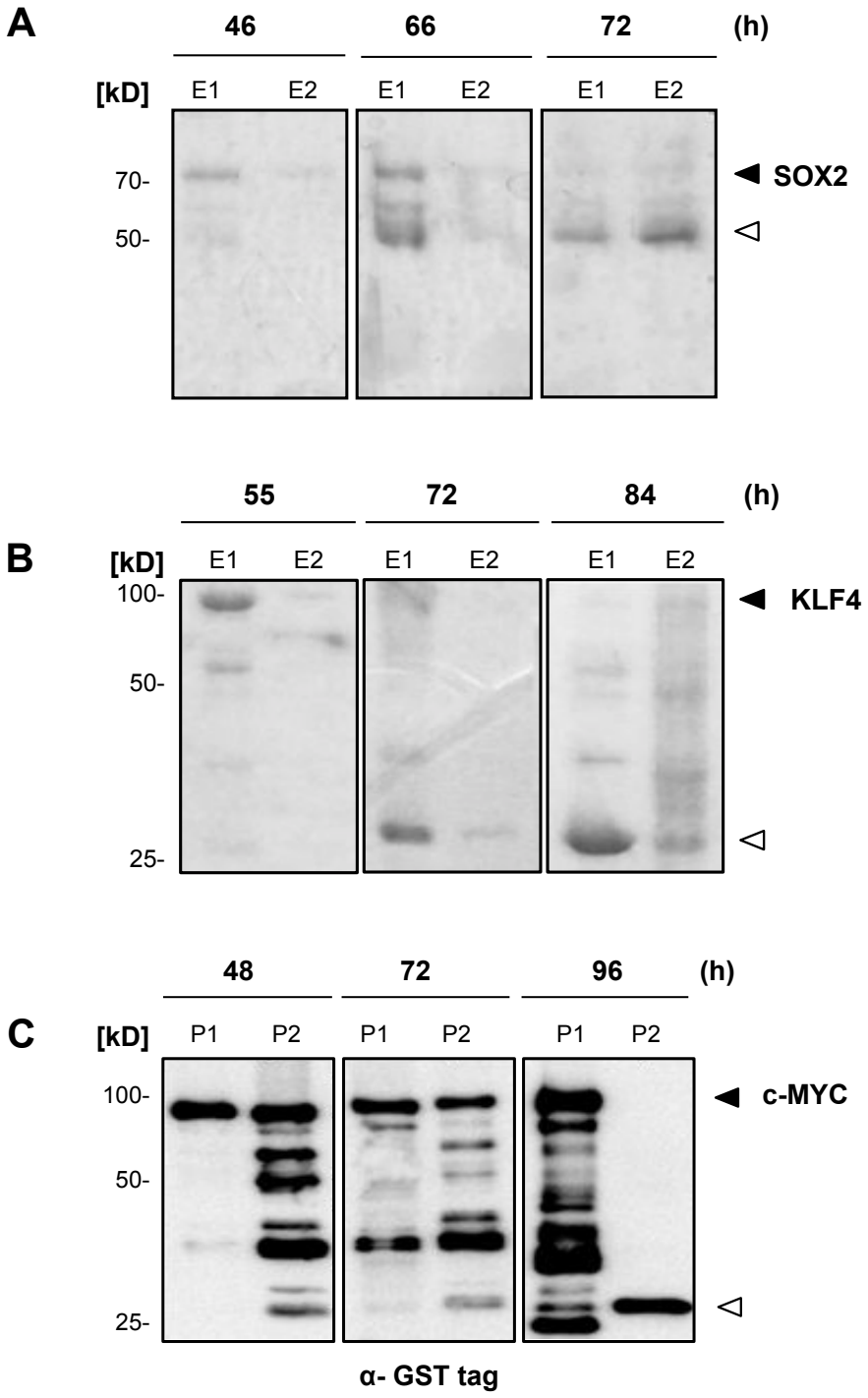

Figure 4.2: Time post-infection was crucial for SOX2, KLF4 and c-MYC protein integrity

Insect cells were infected with baculovirus encoding GST-tagged human SOX2 or KLF4 or c-MYC and harvested at the indicated time points. Cells were lysed by RIPA buffer and lysates were loaded on GST-affinity columns. Proteins were eluted and the elutions were analyzed by SDS-PAGE. (**A**) Coomassie staining of SOX2 elutions (E1: 0-1.5 ml, E2: 1.5-3 ml). (**B**) Coomassie staining of KLF4 elutions (E1: 0-1.5 ml, E2: 1.5-3 ml). (**C**) Western blot of c-MYC elutions by GST antibody. P1: first purification, E2: second purification. Closed arrowheads refer to the full-length protein and open arrow heads to the degradation products.

SOX2 and KLF4 protein integrity was checked by Coomassie staining. For SOX2, full-length protein was most pronounced 46 h post-infection with almost no degradation products. However, after 66 h infection degradation started and 3 bands were observed ≈ 50 kD. 72 h post-infection, only degradation products were observed. The degradation products were analyzed by MALDI and found to be the first 120 amino acid of SOX2 protein (Figure 4.2 A). For KLF4 a similar pattern was observed. 55 h post-infection, minor degradation products were observed at ≈ 55 and 40 kD. Degradation products increased after 72 h. 84 h post-infection, no full-length protein was observed; only degradation products mostly at ≈ 25 kD (Figure 4.2 B).
Similarly, GST antibody showed that c-MYC degrades in cell culture if incubated longer than 48 h. A ladder of indistinct degradation products was observed 72-96 h post-infection (Figure 4.2 C). Moreover, if the lysates were purified two times (purification of the column flow-through), a similar degradation pattern is observed.
To maintain the highest expression and protein integrity levels for all further protein expression and purification experiments, OCT4 expressing Sf9 cells were harvested 84-94 h post-infection. For SOX2, KLF4 and c-MYC, the cells were harvested 48 h post-infection.

4.1.2. Recombinant OSKM localized to the nucleus of Sf9 insect cells

A major advantage of the Sf9 baculovirus system is that, unlike bacterial expression systems, proteins can be produced in a native form retaining the correct subcellular compartmentalization and post-translational modifications. To produce human OSKM proteins their cDNAs were cloned into the N-terminal glutathione S-transferase (GST) fusion plasmid pAcG2T. After cotransfection of the vector with linearized wildtype baculovirus DNA high-titer virus stocks were produced. In first fractionation experiments we noticed that OCT4, SOX2 and KLF4 were predominantly localized in the nucleus of Sf9 cells, whereas c-MYC was distributed both in cytoplasmic and nuclear fractions, as revealed by Coomassie staining and Western blotting (Figure 4.3 A). For the purification of OCT4, SOX2 and KLF4 we therefore developed a single-step nuclear extraction protocol, allowing an easy enrichment of the transcription factors by nuclear fractionation, whereas c-MYC was purified from whole cell lysates.

To prepare nuclear fractions Sf9 cells were swollen in hypotonic buffer and broken up with a Dounce homogenizer. Representative microscopic pictures show the successful nuclear extraction after disruption of the cell membrane (Figure 4.3 B).

Following lysis of the nuclei for OCT4, SOX2 and KLF4 or of whole cells for c-MYC, GST-affinity chromatography was performed. As revealed by silver staining, all transcription factors could be purified to near homogeneity (Figure 4.3 C).

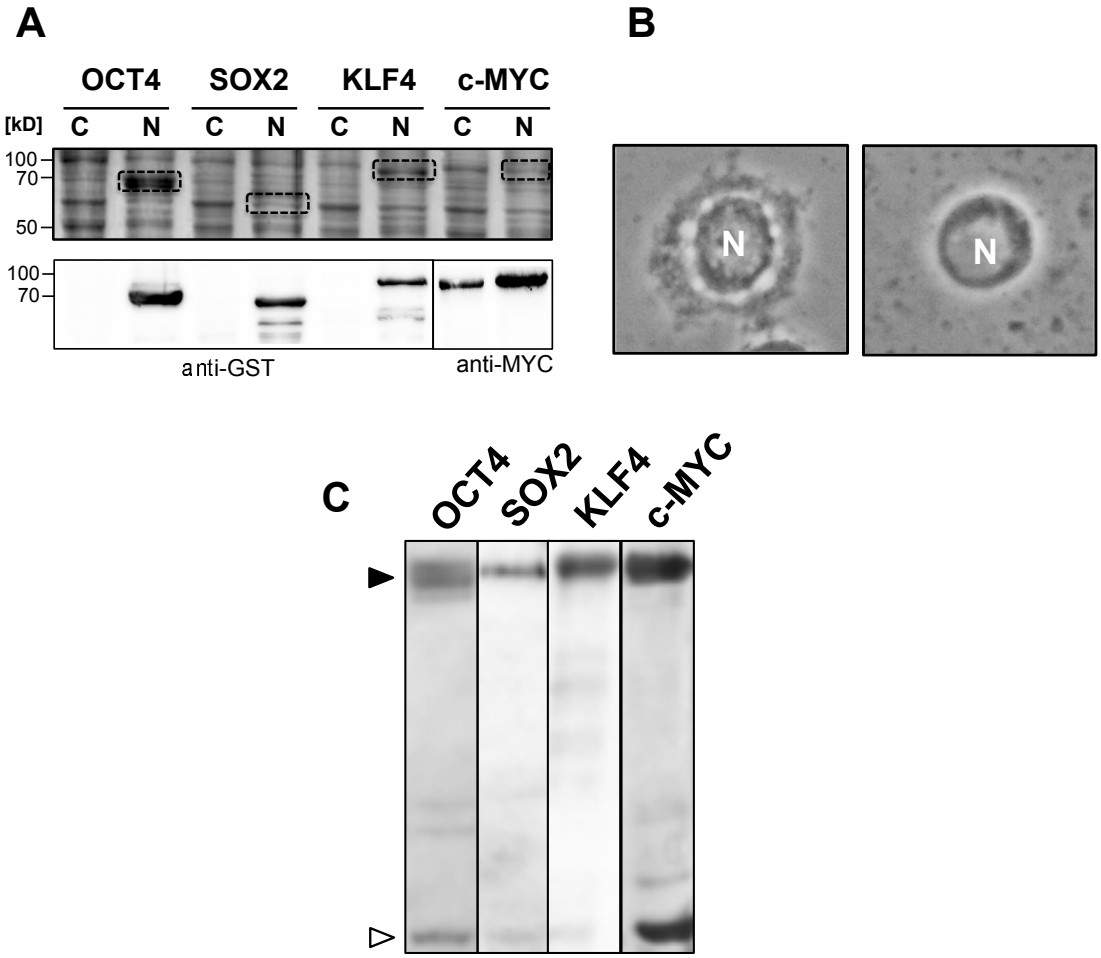

Figure 4.3: Nuclear extraction and purification of OSKM

(**A**) Upper panel shows Coomassie staining and lower panel shows western blot of cytoplasmic (C) and nuclear (N) fractions of Sf9 cells infected with baculoviruses encoding O/S/K/M. Sf9 cells were harvested 2 days post-infection for SKM and 3 days post-infection for O. (**B**) Microscopic pictures of Sf9 cells before (left) and after (right) cell membrane disruption by dounce homogenization (200x). N: nucleus. (**C**) Purified OSKM proteins by GST affinity chromatography after nuclear extraction (for OSK) and total cell lysis (for M). The full-length proteins are marked with a close arrowhead, and the 27 kD GST fragment of the fusion proteins with an open arrowhead.

Purified KLF4 showed minor protein bands at 50 and 70 kD, which were recognized by the KLF4 antibody and, as revealed by MALDI analysis, represented fragments of the transcription factor (data not shown). In addition, a minor GST band was found at 27 kD, which was most pronounced for c-MYC, presumably due to its purification

from cell lysates (Figure 4.3 C). Importantly, from Sf9 suspension cultures considerable protein yields of the transcription factors could be obtained: i.e. OCT4: 6.1 mg/l; SOX2: 1.5 mg/l; c-MYC: 2.8 mg/l and KLF4: 3.8 mg/l.

4.1.3. Recombinant OSKM bound to their consensus DNA binding sites

We next tested the DNA-binding activity of the purified factors using electrophoretic mobility shift assays (EMSAs) with different DNA consensus motifs (Figure 4.4).

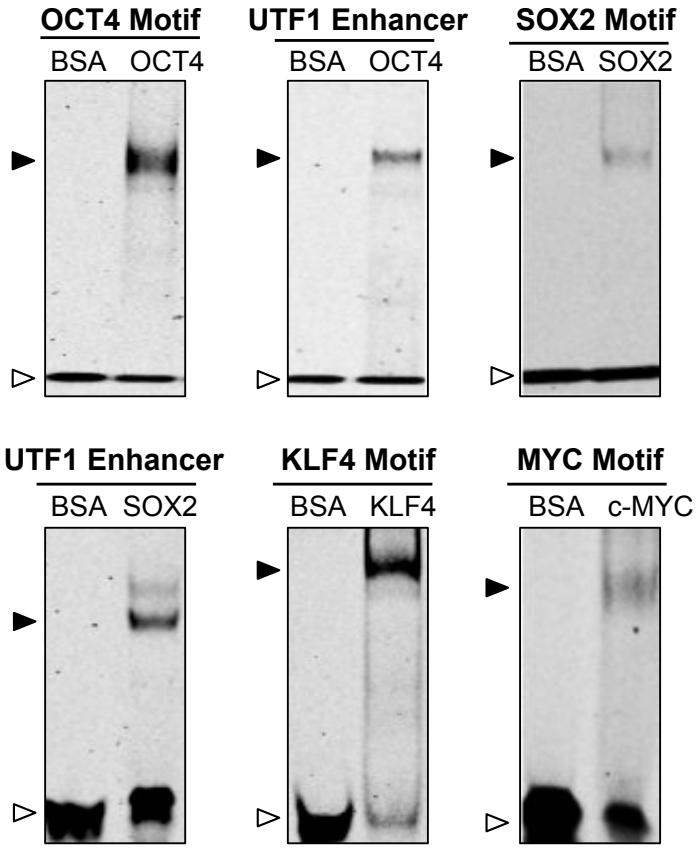

Figure 4.4: *In vitro* DNA binding analysis of OSKM by electrophoretic mobility shift assay (EMSA)

The DNA-binding activity of OCT4 was analyzed using oligonucleotides containing the OCT4 1W consensus motif or UTF1 enhancer sequence. SOX2 DNA binding was analyzed using oligonucleotides containing the SOX2 consensus motif or the UTF1 enhancer sequence. Similarly, the DNA-binding activity of KLF4 and c-MYC was tested with oligonucleotides containing the DNA consensus sequences of the transcription factors. Bovine serum albumin (BSA) was used as a negative control. The closed arrowheads indicate the specific protein-DNA complexes and the open arrowheads the unbound oligonucleotides.

Even a small amount (75 ng) of recombinant OCT4 was sufficient to reveal strong DNA binding to an octamer-binding site from the Ig heavy chain enhancer (1W motif). A slightly weaker DNA binding of OCT4 was detected to the OCT4-binding site from the enhancer of undifferentiated embryonic cell transcription factor 1 (UTF1), which contains an additional adjacent SOX2-binding site (Figure 4.4). In addition, DNA binding of recombinant SOX2 could be demonstrated to the classical DNA consensus site present in the miR-302 promoter as well as to the UTF1 site (Boyer et al., 2005). Moreover, KLF4 bound efficiently to the typical DNA consensus sequence of the Nanog promoter. DNA binding of recombinant c-MYC to the classical E-box element was somewhat weaker but clearly detectable. For all transcription factors DNA-binding was abolished by competition with unlabeled oligonucleotides (data not shown). These results therefore suggest that recombinant OSKM factors retain not only their typical nuclear localization, but also their DNA-binding activity.

4.2. Identification of novel AKT phosphorylation sites in OSK

In order to investigate AKT phosphorylation sites of the different transcription factors, we incubated all four OSKM factors with active baculovirus-derived recombinant AKT1 in an *in vitro* kinase assay. Subsequent immunoblotting of the reactions mixtures with an anti–phospho-(Ser/Thr) AKT substrate antibody, which recognizes AKT phosphorylation motif sequences, revealed that OCT4, SOX2 and KLF4 were efficiently phosphorylated by AKT (Figure 4.5 A). OCT4 showed several degradation products, which were strongly phosphorylated by AKT, whereas no phosphorylation of c-MYC could be detected.

To identify the AKT phosphorylation sites of the different transcription factors we subjected *in vitro* phosphorylated as well as the control OSKM factors to mass spectrometry (MS)-based phosphoproteomic analysis. As expected, we identified several intrinsic phosphorylation sites on OCT4 and KLF4 that were phosphorylated in the absence of ATP, indicating that the proteins were modified by the intrinsic phosphorylation machinery of Sf9 cells. Most phosphorylation sites however were dependent on AKT. A representative spectrum of phosphorylation at of OCT4 at T225 is shown in Figure 4.5 B.

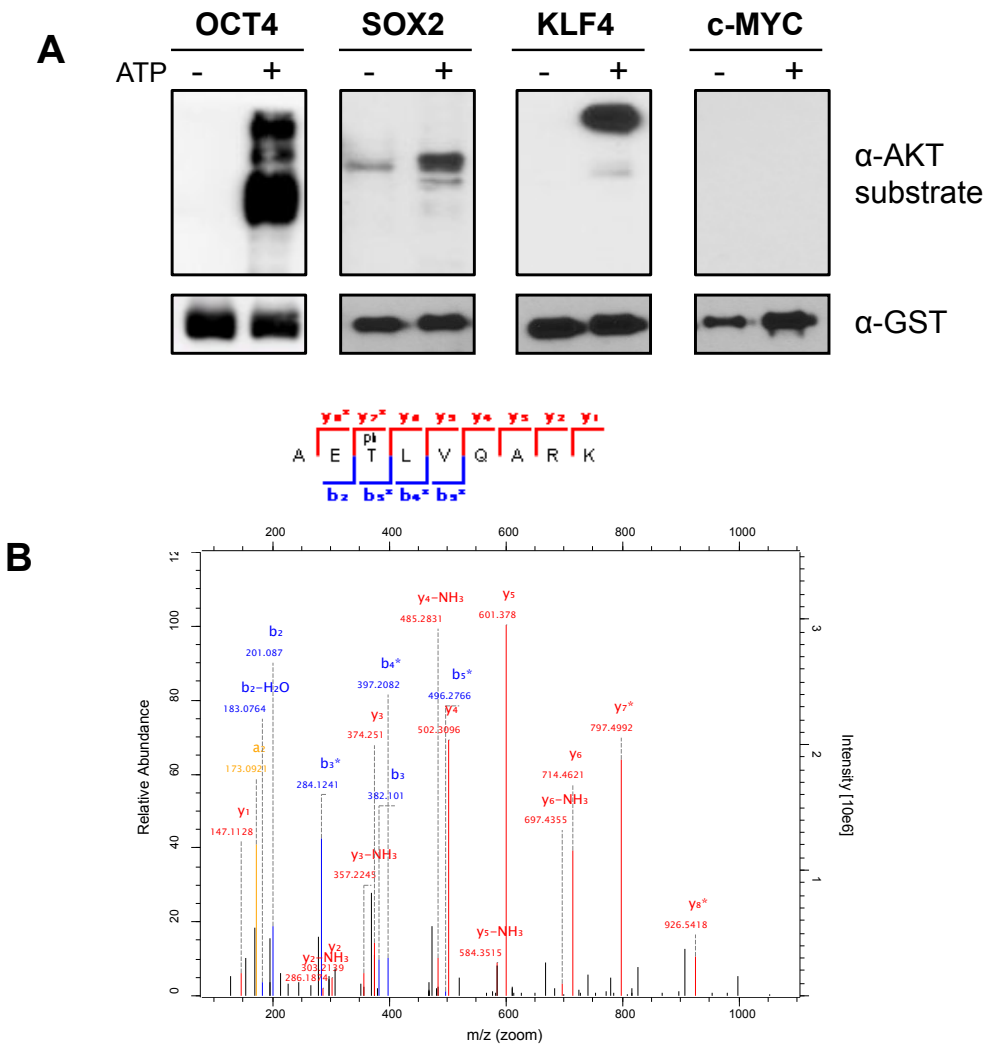

Figure 4.5: OCT4, SOX2 and KLF4, but not c-MYC were phosphorylated by AKT *in vitro*

(**A**) *In vitro* kinase assay: The purified OSKM factors were incubated with active AKT1 protein in the absence or presence of ATP, and immunoblotted with the indicated antibodies. (**B**) Representative mass spectrum demonstrating AKT-mediated phosphorylation of OCT4 at T225 following digestion with LysC.

As published previously (Lin et al., 2012b) OCT4 was found to be further phosphorylated by AKT at T235. Importantly, our phosphoproteomic analysis identified four further unreported sites in OCT4 that were phosphorylated by AKT, namely, S136, T159, T225 and S236 (Figure 4.6). In addition to OCT4, we found that AKT phosphorylated SOX2 at S83, which has been also yet not described. KLF4 was phosphorylated by AKT at five different sites: the already known residue T429, which is homologous to T399 in mouse (Chen et al., 2013), and four further novel sites, namely, S19, T33, S234 and S326 (Figure 4.6).

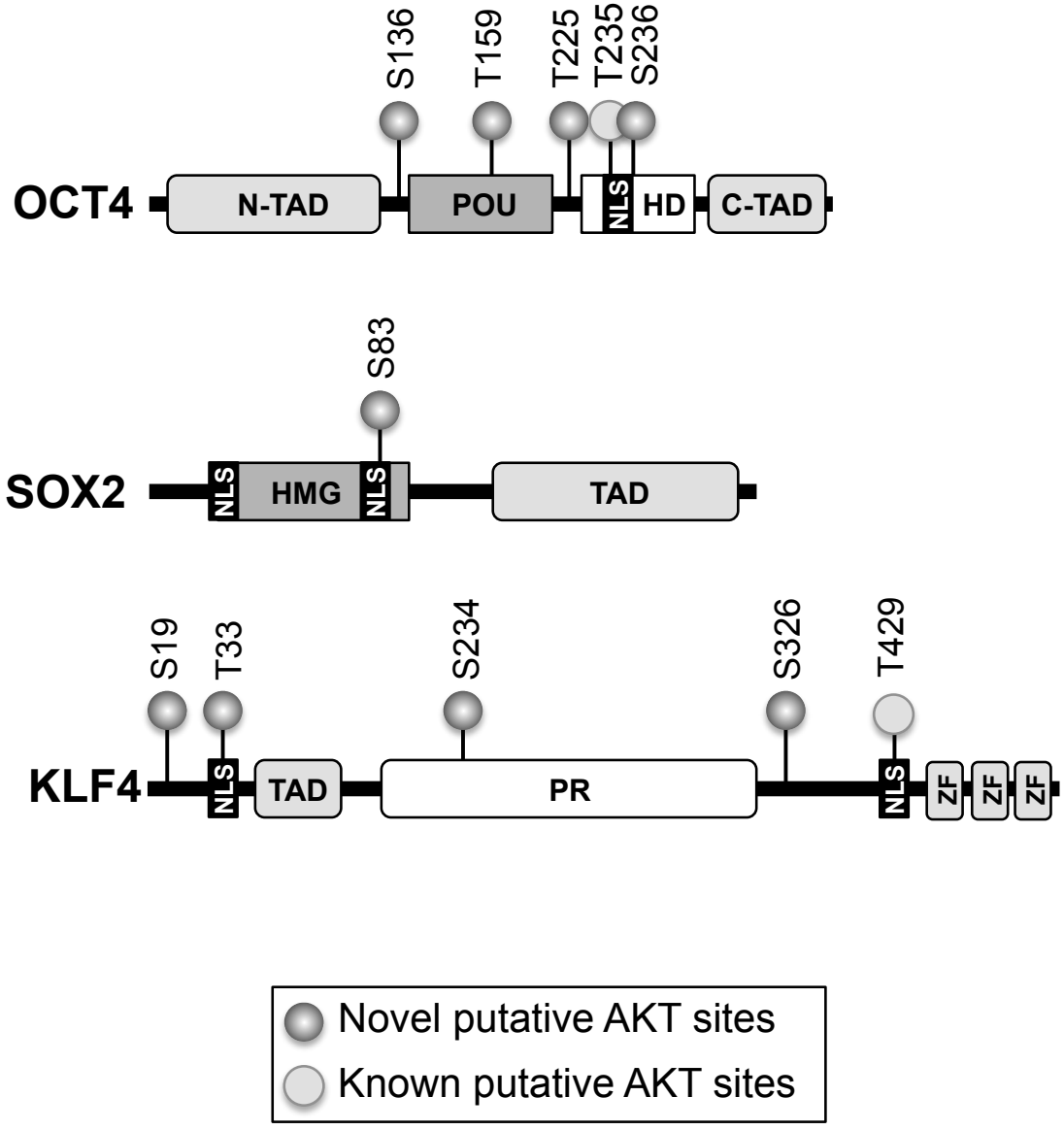

Figure 4.6: Novel AKT phosphorylation sites identified in OCT4, SOX2 and KLF4

The scheme shows the novel and previously reported AKT phosphorylation sites with the functional domains of OCT4, SOX2 and KLF4. OCT4 contains POU-specific and homeodomain (HD) DNA-binding domains as well as transactivation domains located at the N-terminus (N-TAD) and C-terminus (C-TAD). SOX2 has a high mobility group (HMG) DNA-binding domain and a transactivation domain (TAD). KLF4 contains a single N-terminal TAD, a central proline-rich region (PR) and three zinc-finger (ZF) DNA-binding domains. NLS marks the nuclear localization sequences of the transcription factors.

4.3. Aurora kinase A regulated c-Myc and Oct4 in a kinase-independent manner in stem cells

4.3.1. c-MYC and OCT4 were identified as AURKA substrates

Aurora kinase A (Aurka) plays an important role in maintenance of pluripotency and self-renewal in stem cells. It has been reported that Aurka protein expression correlated with the expression of the core transcription factors Oct4, Sox2 and Nanog in mouse embryonic stem cells (Lee et al., 2012a). Moreover, upon knockdown of Aurka, Oct4 is downregulated and mES cells started to differentiate into mesodermal and ectodermal germ layers. However, the exact regulation mechanism was poorly described. Therefore, we investigated whether there is a direct interaction between Aurka and the pluripotency transcription factors, especially, Oct4 and c-Myc.

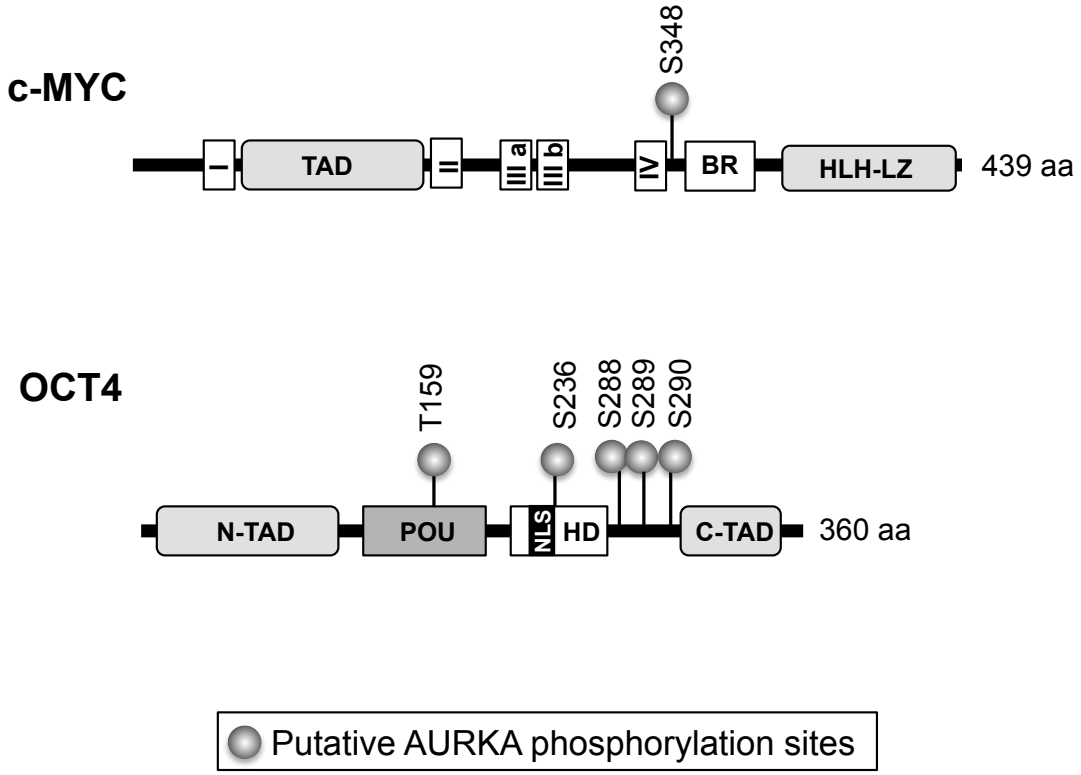

Figure 4.7: Putative AURKA phosphorylation sites on c-MYC and OCT4

The scheme shows predicted putative AURKA phosphorylation sites with the functional domains of c-MYC and OCT4. c-MYC contains a transactivation domain (TAD), basic region (BR), Helix-loop-helix-leucine zipper (HLH-LZ) and the MYC boxes (I, II, IIIa, IIIb, IV). OCT4 contains POU-specific and homeodomain (HD) DNA-binding domains as well as transactivation domains located at the N-terminus (N-TAD) and C-terminus (C-TAD). The full-length of the proteins is indicated as number of amino acids (aa). Serine and threonine are referred to as S and T respectively. Prediction was performed using GPS 3.0 phosphorylation prediction software.

To that end, we performed an *in silico* analysis of AURKA putative phosphorylation sites on human c-MYC and OCT4 using GPS phosphorylation prediction software. With the highest threshold set, putative phosphorylation sites were identified on c-MYC and OCT4. AURKA was predicted to phosphorylate c-MYC on one single site, namely, S348, which is located between the fourth MYC box and the basic region of c-MYC (Figure 4.7 upper panel). OCT4 had five putative phosphorylation sites, namely, T159, S236, S288, S289 and S290 (Figure 4.7 lower panel). These phosphorylation sites are located on three domains on the OCT4 protein. T159 is located in the POU-specific DNA binding domain, S236 is located in the homeodomain (HD) directly next to the nuclear localization sequence (NLS). Moreover, S288, S289 and S290 are located in the spacer between the HD domain and the C-terminal transactivation domain (C-TAD). These results pointed that there might be a kinase-dependent interaction between AURKA and the transcription factors c-MYC and OCT4.

4.3.2. AURKA increased the transcriptional activity of c-MYC and OCT4 in a kinase-independent manner

In order to investigate the *in vivo* interaction between AURKA on one side and c-MYC and OCT4 on the other side and whether the interaction is kinase-dependent or not, transcriptional analyses of these transcription factors were performed using luciferase assays. Human AURKA gene or the kinase-dead mutant (KD) was overexpressed in HEK293 FT cells in single transfection or in co-transfection with c-MYC or OCT4 or both. The KD mutant of AURKA was prepared by mutating the aspartic acid residue at the position 274 to alanine (D274A) in the DFG domain of the kinase rendering the kinase catalytically inactive (Crane et al., 2004).

The used luciferase reporter, Ig μE4, was first described in 1990 (Schöler et al., 1990). It encodes for firefly luciferase gene under control of thymidine kinase (tk) promoter and tandem repeats of μE4 region of the immunoglobulin heavy chain gene enhancer (Ig μE4). It harbors a non-canonical E-box sequence CACCTG and an Octamer binding site ATTTGCAT (Figure 4.8 A). Luciferase assays were conducted in HEK293 FT after transfection of the previously described firefly luciferase reporter and the indicated DNA (Figure 4.8. B). A constitutively expressing renilla luciferase construct with tk promoter was used as internal control for normalizing transfection efficiencies and monitoring cell viability.

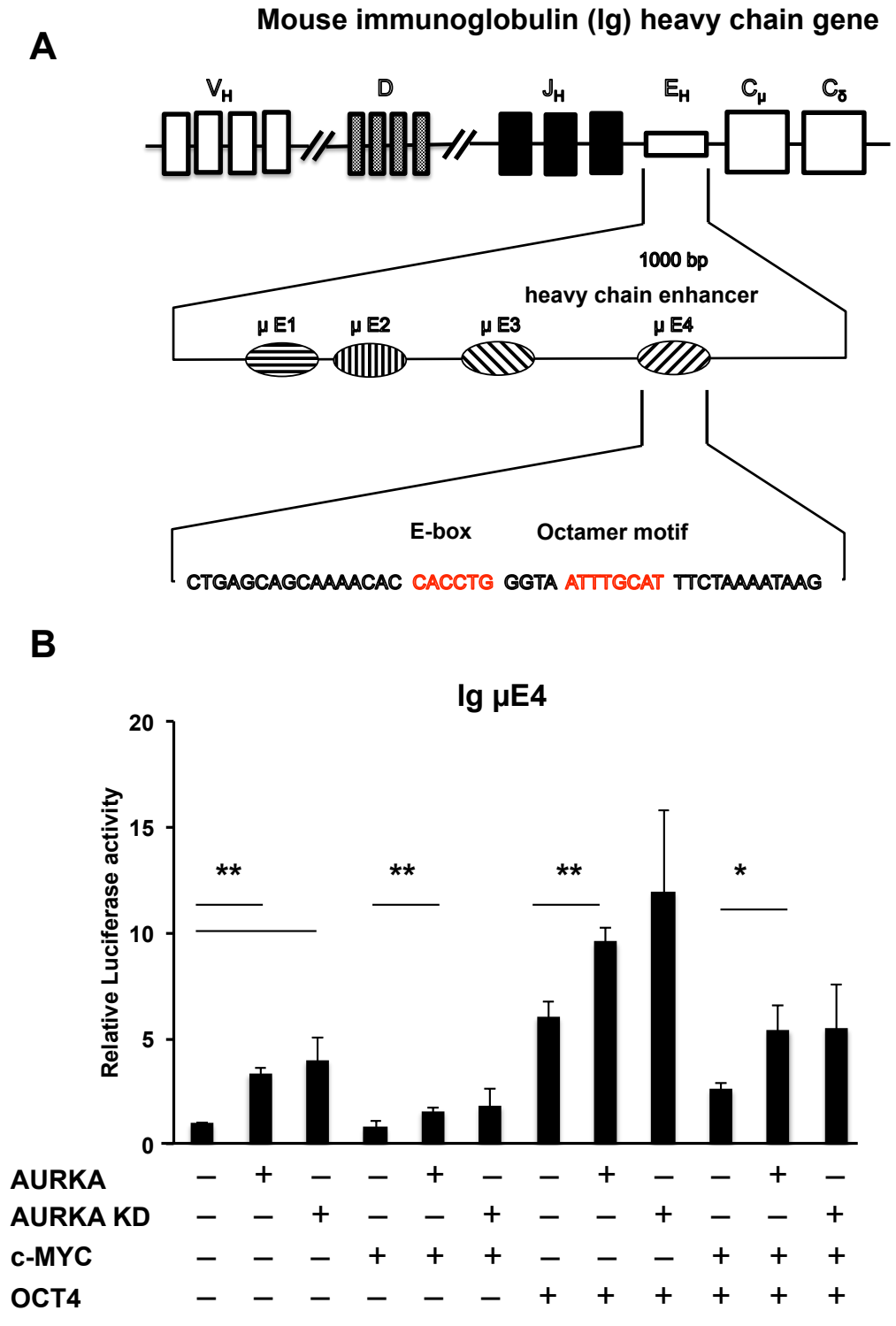

Figure 4.8: AURKA increased c-MYC/OCT4 transcriptional activity on Immunoglobulin heavy chain enhancer (Ig μE4)

(**A**) Mouse immunoglobulin (Ig) heavy chain gene: Variable (V), Diversity (D) and Joining (J) segments are followed by the enhancer gene (E) which contains in its μ E4 region a non-canonical E-box and an octamer motif (written in red). (**B**) Luciferase assay in HEK293 FT cells upon overexpression of c-MYC, OCT4, AURKA or AURKA kinase dead mutant (KD) using a firefly reporter coding for μE4 of the Ig heavy chain enhancer. Cells were transfected

with the indicated DNA, µE4 firefly reporter and a constitutively expressing renilla construct as a transfection control. Cells were harvested 48 h after transfection. Luminescence values were normalized on renilla and GFP controls (relative luciferase activity). n=3, results are expressed as mean + SD. * p< 0.05, ** p< 0.01.

AURKA overexpression activated the reporter in the absence of ectopically expressed c-MYC and OCT4. Surprisingly, overexpression of the inactive kinase AURKA KD showed the same effect. c-MYC reduced the relative luciferase signal which was restored by overexpression of AURKA or AURKA KD. OCT4 overexpression increased the relative luciferase activity and co-expression of AURKA or AURKA KD increased the signal even more. Adding c-MYC repressed the reporter signal in all combinations (Figure 4.8 B). The KD mutant was confirmed to be catalytically inactive by western blot. Successful overexpression of the genes was confirmed by western blot (Figure 4.9 A). Upon overexpression of the KD mutant, less autophosphorylation was observed by using phospho(p)-AURKA antibody (Figure 4.9 B).

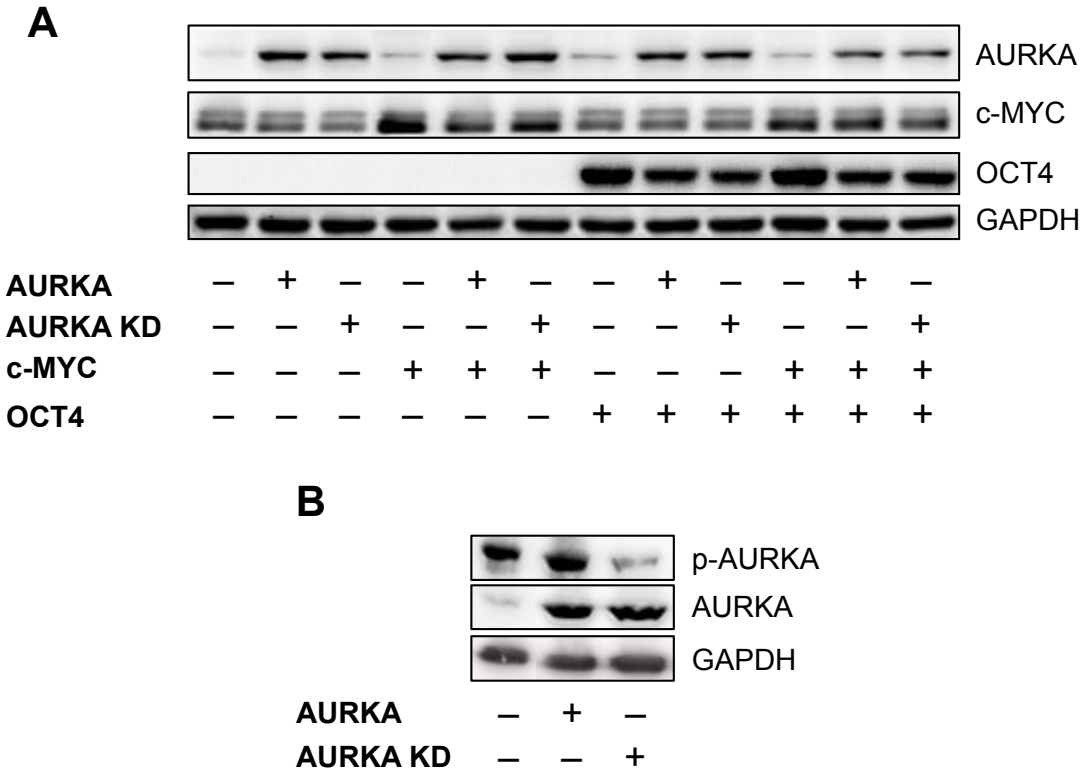

Figure 4.9: Confirmation of successful overexpression of AURKA/KD, c-MYC and OCT4

(**A-B**) Western blot of HEK293 FT cells transfected with the indicated DNA. Cells were harvested 48h after transfection, lysed and subjected to immunoblotting using the indicated antibodies.

4.3.3. Aurora kinase A regulated c-Myc and Oct4 protein stability and mRNA expression in mESCs

To disentangle the regulatory networks of Aurka in mESCs, we used different approaches. Initially, we infected the cells with retroviruses encoding human AURKA or AURKA KD. Amino acid sequence alignment showed 84% identity match between mouse and human AURKA.

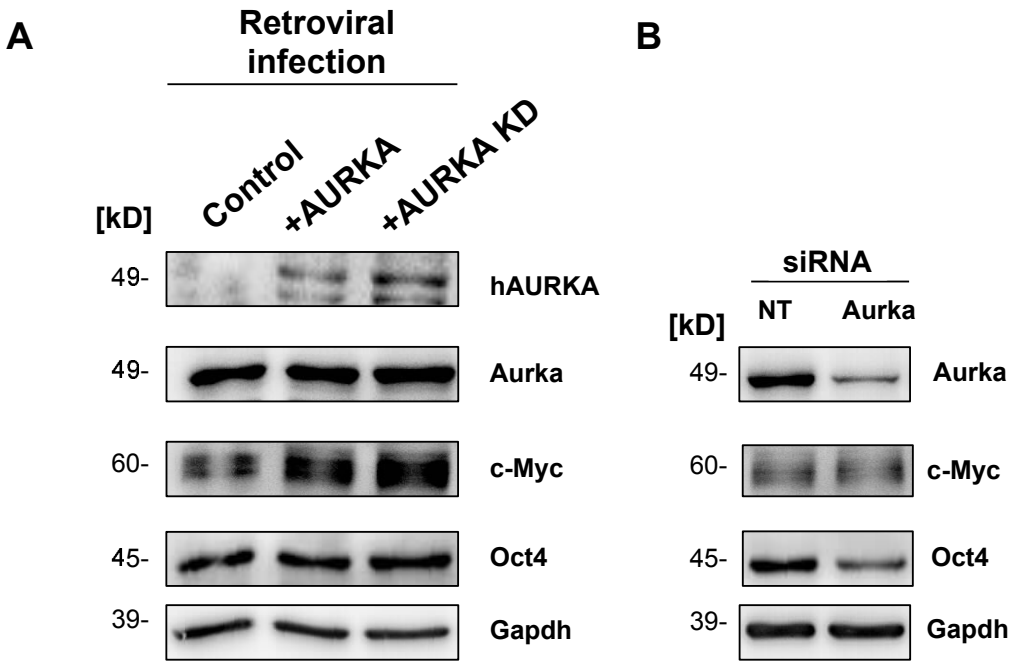

Figure 4.10: AURKA increased the protein levels of c-Myc in mESCs

(**A**) Western blot of mESCs infected with retroviruses encoding AURKA or AURKA KD. (**B**) Western blot of Aurka knockdown in mESCs. Cells were transfected with small interfering RNA (siRNA) against no target (siNT) or against Aurka. Cells were harvested 48 h after transfection, lysed and immunoblotted against the indicated antibodies.

Remarkably, overexpression of AURKA led to higher levels of c-Myc protein. The same effect was noticed upon overexpression of the KD mutant. The levels of mouse endogenous Aurka did not change upon overexpression of the human genes AURKA or AURKA KD, neither did Oct4 levels (Figure 4.10 A). Subsequently, we transiently knocked down Aurka using small interfering RNA (siRNA). Knockdown was efficient and western blot showed ≈80% reduction on Aurka protein level compared to the control (Fusion software, Peqlab). On protein level, Aurka knockdown destabilized Oct4 protein. However, no change was noticed in c-Myc levels (Figure 4.10 B).

4.3.4. Aurora kinase A inhibitor, MLN8237, modulated the protein and mRNA levels of c-Myc and Oct4 in mESCs

MLN8237 is a selective Aurora kinase A inhibitor, which has been described to have diverse effects on Aurora kinase A and its interaction partners in stem cells (Li and Rana, 2012).

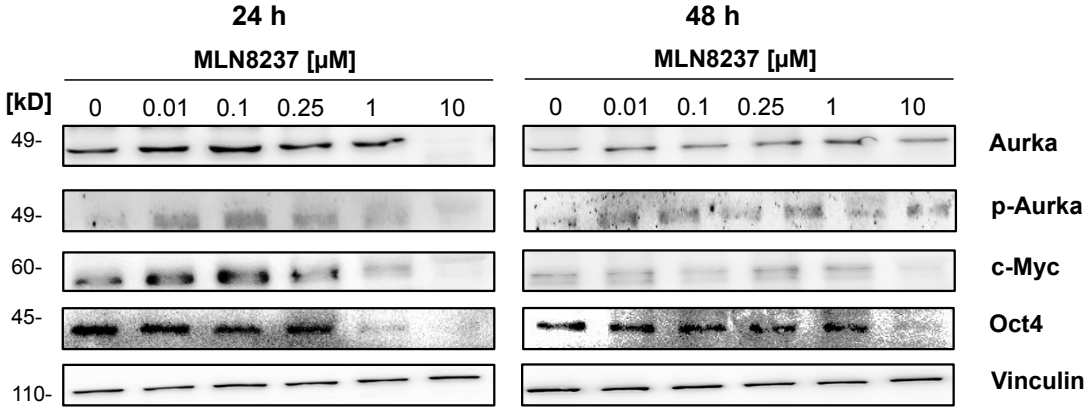

Figure 4.11: MLN8237 decreased Aurka, c-Myc and Oct4 protein levels in mESCs

Western blot of mESCs treated with the indicated concentrations of MLN8237. Cells were treated 24 h after seeding. 24 and 48 h after inhibitor treatment, the cells were harvested, lysed, sonicated and subjected to immunoblotting using the indicated antibodies. Vinculin was used as a reference protein in this experiment.

We performed an extensive study on the effect of MLN8237 in mESCs. Concentrations ranging from 0.01 to 10 µM were tested. After 24 h of treatment, low concentrations of MLN8237 (0.01-0.1 µM) led to higher Aurka protein levels as analyzed by western blot. The same effect was noticed for the activated phosphorylated form of Aurka (p-Aurka) as well. Remarkably, c-Myc levels correlated with Aurka levels. After 48 h, Aurka, c-Myc and Oct4 protein levels returned to the basal level (Figure 4.11).

Higher concentrations of MLN8237 (0.25-1 µM) led to lower protein levels of Aurka, c-Myc and Oct4 and 10 µM of MLN8237 caused complete abrogation of Aurka, p-Aurka, c-Myc and Oct4 protein bands 24 h after treatment. After 48 h, in the cells treated with 10 µM, Aurka and p-Aurka bands were restored to the basal level. However, c-Myc and Oct4 bands remained downregulated (Figure 4.11).

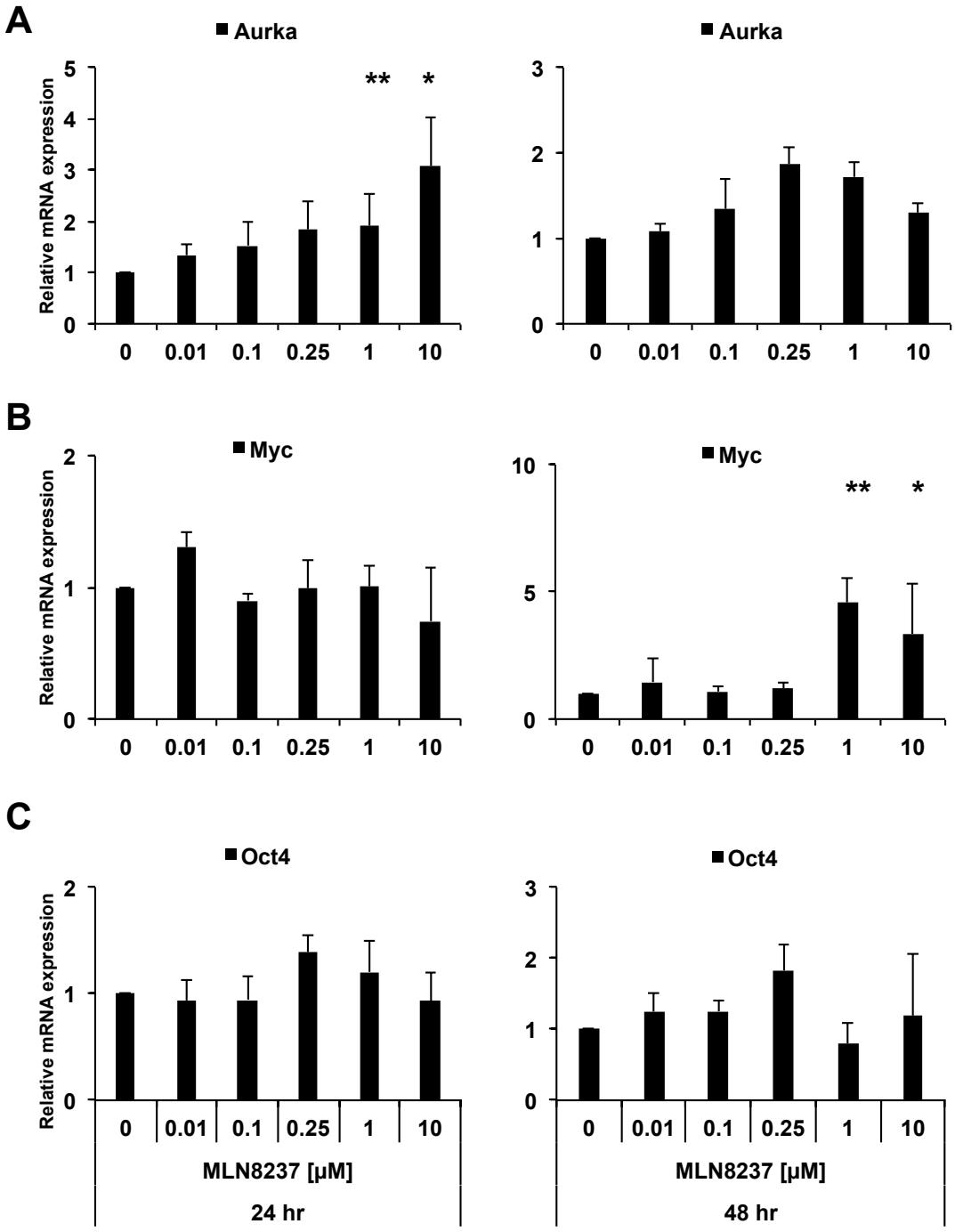

Figure 4.12: MLN8237 activated the transcription of Aurka, c-Myc and Oct4 mRNA in mESCs

mRNA expression analysis of mESCs treated with the indicated concentrations of MLN8237. Cells were treated 24 h after seeding. 24 and 48 h after inhibitor treatment, cells were harvested, lysed and RNA was isolated, reverse transcribed and subjected to qRT-PCR using the following primers:(**A**) Aurka, (**B**) Myc and (**C**) Oct4. n=3, results are normalized to the geometric mean of Gapdh and Actb and to DMSO control (0 µM) and expressed as mean + SD. * $p < 0.05$, ** $p < 0.01$.

mRNA expression levels of Aurka, c-Myc and Oct4 were analyzed after treatment with the same concentrations of MLN8237 (0.01-10 µM). MLN8237 increased Aurka expression in a concentration-dependent manner 24 h after treatment. The same effect was observed 48 h after treatment with the exception that in the cells treated with 10 µM concentration, Aurka level returned to the basal level (Figure 4.12 A). No significant changes were observed in c-Myc mRNA levels 24 h after treatment. However, after 48 h, higher concentrations of MLN8237 (1-10 µM) greatly activated its expression (Figure 4.12 B). MLN8237 slightly increased the expression of Oct4 but no concentration dependence was observed (Figure 4.12 C).

4.3.5. MLN8237 reduced the reprogramming efficiency of MEFs

c-Myc and Oct4 play a crucial role in reprogramming of MEFs to iPSCs and any changes in their regulation can alter the reprogramming efficiency (Takahashi and Yamanaka, 2006)

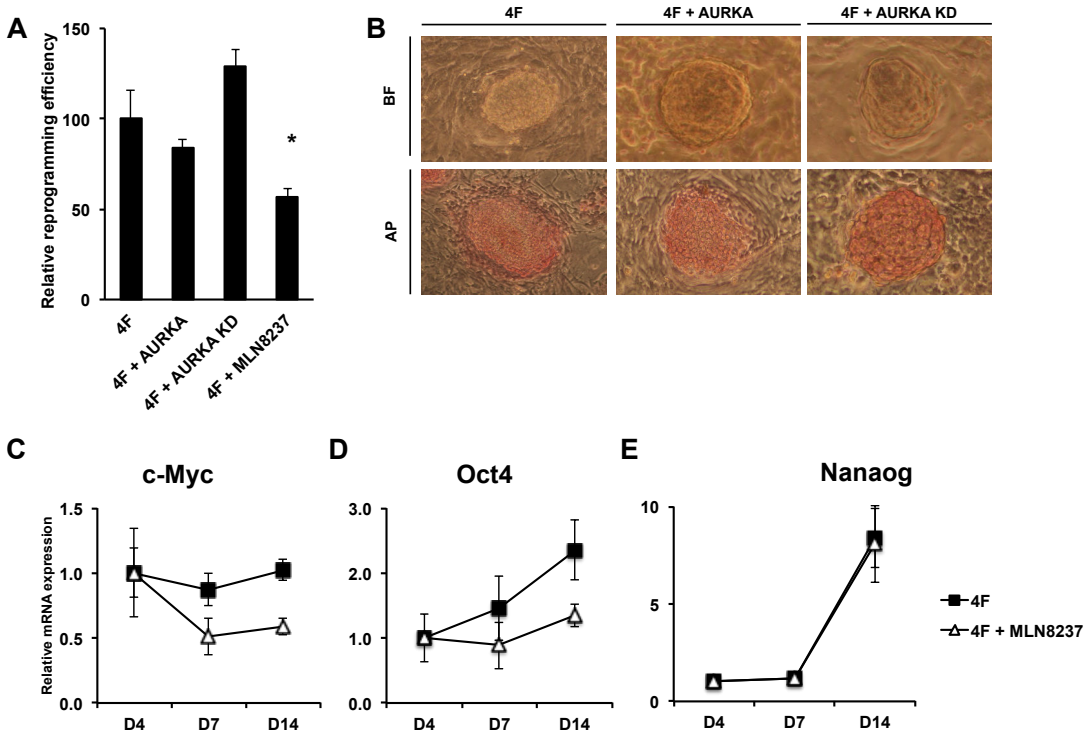

Figure 4.13: MLN8237 reduced the reprogramming efficiency of MEFs infected with the four factors OSKM (4F)

(**A**) Reprogramming efficiency of MEFs to iPSCs. MEFs were transduced with the retroviruses encoding for the indicated genes. MEFs were treated with MLN8237 24 h after transduction. Colonies were counted 14 days after infection and the results were normalized

on the number of colonies of the cells infected with the 4F and expressed as the relative reprogramming percentage. Results from triplicates were expressed as mean + SD, * p< 0.05. (**B**) Microscopic pictures of iPSCs generated from the reprogrammed MEFs. Bright field (BF) are shown in the upper panel and the alkaline phosphatase staining (AP) is shown in the lower panel (Magnification 200X). (**C-E**) mRNA expression analysis of the infected MEFs 4, 7 and 14 days after infection (D4, D7 and D14). Cells were harvested at the indicated time points, lysed and RNA was isolated, reverse transcribed and subjected to qRT-PCR analysis using the following primers: (**C**) c-Myc and (**D**) Oct4 and (**E**) Nanog. Results from triplicates were normalized to the geometric mean of Alas1/Actb and to D4 samples and expressed as mean ± SD. * p< 0.05.

Therefore, we tested the effect of AURKA overexpression and inhibition on the reprogramming process of MEFs infected with the 4F. AURKA or AURKA overexpression did not cause significant change in the reprogramming efficiency (Figure 4.13 A). Furthermore, the colonies from MEFs infected with the 4F together with AURKA or AURKA KD showed sharp borders and positive alkaline phosphatase staining indicating a fully reprogrammed state (Figure 4.13 B)

The use of MLN8237 in reprogramming has been a matter of debate in the field of reprogramming. Li and Rana reported that MLN8237 enhances the reprogramming efficiency of MEFs due to inhibition of Gsk3-β in an Akt-dependent pathway (Li and Rana, 2012). However, Lee et al. reported in the same year that MLN8237 reduced the reprogramming efficiency in a p53-dependent pathway (Lee et al., 2012a).

Consistent with Lee et al., we found that Aurka inhibition with MLN8237 reduced the reprogramming efficiency significantly (Figure 4.13 A). We explored the mRNA expression of three important genes during the reprogramming process, namely, c-Myc, Oct4 and Nanog. Moreover, we tracked the gene expression of these three genes over 14 days. In the 4F-infected MEFs, the expression of Oct4 and Nanog increased from day 4 to day 14 confirming a successful reprogramming. MLN8234 treatment reduced the expression of c-Myc and to a lesser extent the expression of Oct4. However, the expression of Nanog did not change upon MLN8237 treatment (Figure 4.11 C, D and E).

4.4. Biodegradable chitosan nanoparticles for OCT4 nuclear delivery

4.4.1. Small and large nanoparticles (S and L-NPs) showed homogeneous size and charge distribution

Using the ionotropic gelation method, we formulated two types of chitosan NPs as described previously (Tammam et al., 2015a). Scanning electron microscopy revealed that the generated chitosan NPs were spherical with no apparent aggregation (Figure 4.14).

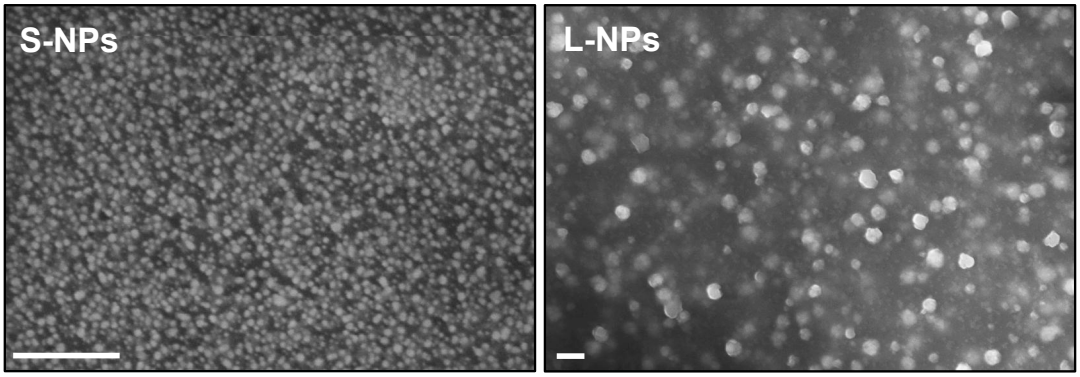

Figure 4.14: Small and large nanoparticles (S and L-NPs) exhibited homogeneous size distribution

Scanning electron micrographs from S-NPs (left) and L-NPs (right). Bars = 200 nm.

The average hydrodynamic diameter of S-NPs and L-NPs was 25 nm and 150 nm, respectively. Both NPs had a positive zeta potential which was higher in L-NPs compared to S-NPs (Table 1). The encapsulation of HRP did not significantly change the hydrodynamic diameter of the NPs. Neither did it affect HRP activity, since encapsulation efficiency (EE) determined by either protein content or enzyme activity did not significantly differ (Table 1)

Table 1: Characterization of chitosan S-NPs and L-NPs

NP	Cargo	HD (nm)	ZP (mV)	EE% (% Activity)	EE (% Protein)
S-NP	w/o	25 ± 2	35 ± 2	-,-	-,-
	HRP	26 ± 2	22 ± 2	56.2 ± 0.0	58.7 ± 2.9
L-NP	w/o	147 ± 3	50 ± 5	-,-	-,-
	HRP	143 ± 1	45 ± 2	97.6 ± 0.4	94.3 ± 3.4

EE: encapsulation efficiency; HD: hydrodynamic diameter; HRP: horseradish peroxidase; ZP: zeta potential

4.4.2. S-NPs preserved OCT4 activity *in vitro* more than L-NPs

Recombinant OCT4 has been shown to become rapidly degraded under cell culture conditions (Bosnali et al., 2008). We therefore tested the OCT4 DNA-binding activity by electrophoretic mobility shift assays using an oligonucleotide an octamer-binding site from the Ig heavy chain enhancer. Soluble OCT4 as well as OCT4 encapsulated in S-NPs induced the appearance of specific DNA/protein complex, which was not detectable with the negative control BSA (Figure 4.15 A) or in the presence of 50-fold excess of unlabeled oligonucleotide (data not shown).

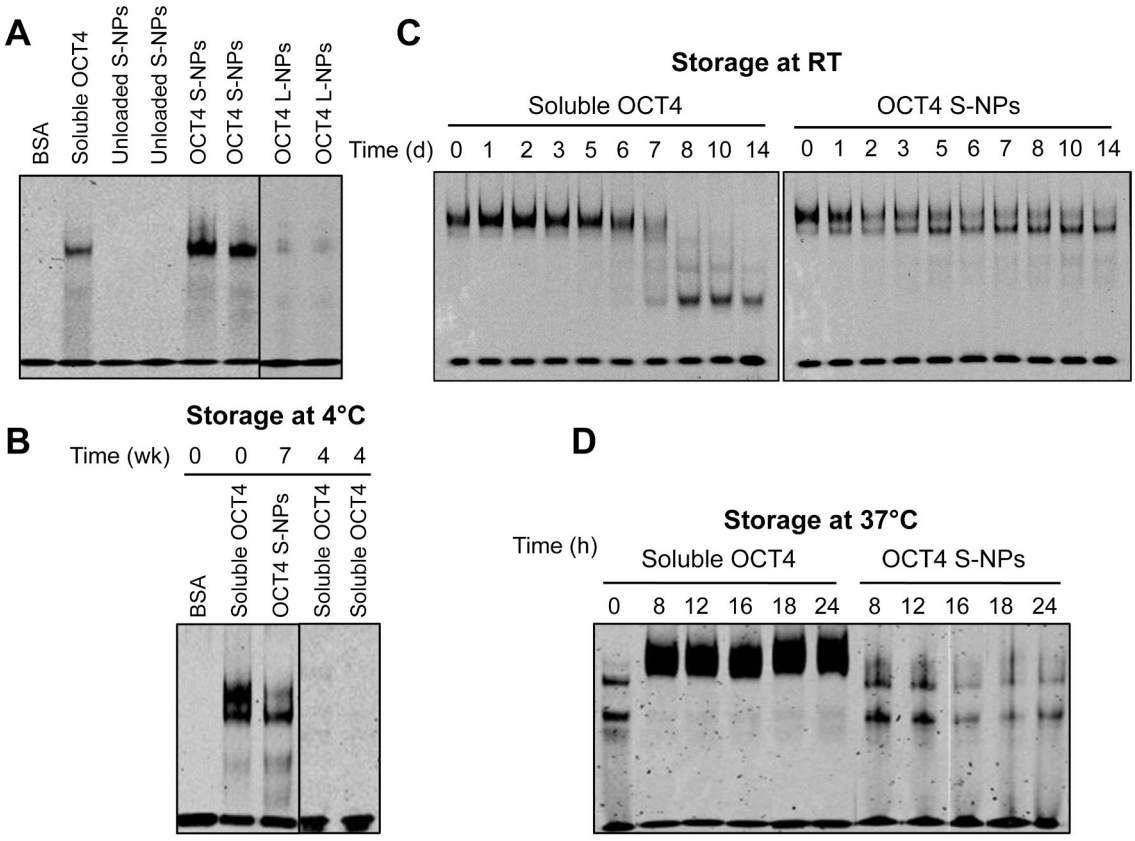

Figure 4.15: S-NPs preserved the activity of OCT4 protein under different conditions

(**A**) EMSA analysis showing OCT4 stabilization by S-NPs but not L-NPs. Unloaded S-NPs, soluble OCT4 protein as well as OCT4 encapsulated in S-NPs and L-NPs were subjected to EMSA analysis. The DNA-binding activity of OCT4 was analyzed using an oligonucleotide containing the OCT4 consensus motif. BSA was used as a negative control. (**B-D**) OCT4-loaded S-NPs stabilize OCT4 DNA-binding activity for 7 weeks at 4°C (**B**), for 14 days at RT (**C**), and for 24 h under cell culture conditions at 37°C in the presence of serum (**D**), whereas the DNA-binding activity of soluble OCT4 is rapidly lost under these conditions. The slowly migrating protein/DNA complex of soluble OCT4 shown in (**D**) is presumably caused by aggregation of the OCT4 protein under cell culture conditions. The protein amount used per lane for the EMSAs corresponds to 30 ng (**A**), 100 ng (**B**) and 250 ng (**C, D**)

In comparison to S-NPs, OCT4-loaded L-NPs induced a much weaker electrophoretic shift (Figure 4.15 A). Similar results obtained with higher L-NP concentrations (data not shown), indicating a less efficient release of OCT4 from L-NPs. Further experiments were therefore only conducted with OCT4-loaded S-NPs.

We next tested several storage conditions of the NPs for OCT4 DNA-binding. Whereas the long-term storage of OCT4-loaded NPs still retained DNA-binding activity even after 7 weeks, no DNA-binding activity could be retained with soluble OCT4 protein (Figure 4.15 B). Furthermore, at RT DNA binding of soluble OCT4 was lost within 7 days, whereas OCT4-loaded S-NPs showed still DNA binding after 14 days (Figure 4.15 C). Importantly, S-NPs were able to maintain OCT4 DNA-binding activity even in cell culture conditions at 37°C (Figure 4.15 D). In contrast, at 37°C soluble OCT4 caused the appearance of high molecular weight complex with reduced mobility (Figure 4.15 D), which was presumably due to the reported precipitation and aggregation of OCT4 under the cell culture condition in the presence of serum (Bosnali and Edenhofer, 2008; Thier et al., 2010). Thus, encapsulation of OCT4 in S-NPs results in a considerable stabilization of OCT4 DNA-binding activity.

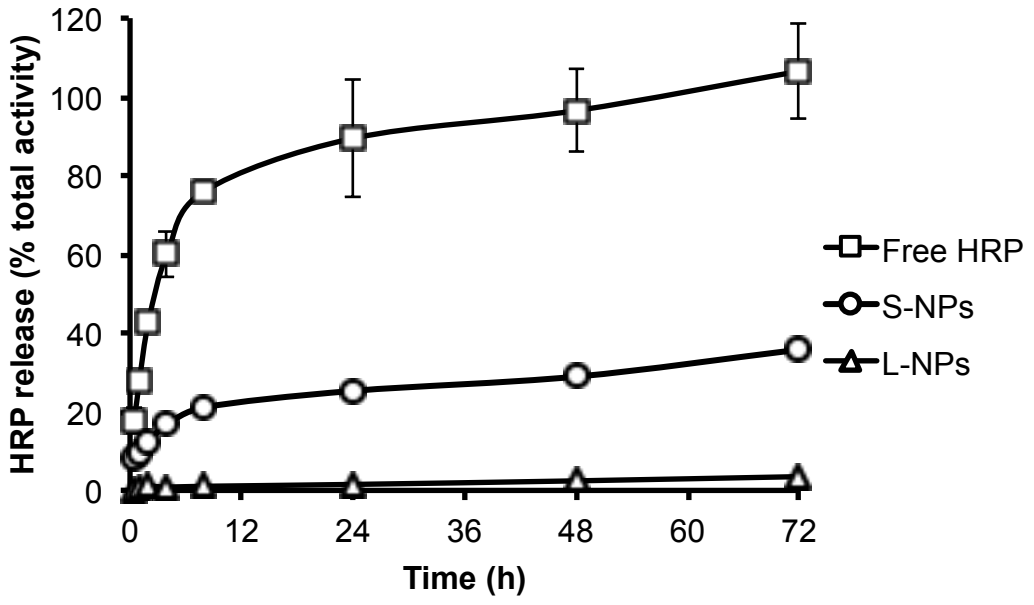

Figure 4.16: S-NPs provided a sustained release profile *in vitro*

Kinetics of HRP release from S-NPs and L-NPs in comparison to free HRP, as measured by enzyme activity. Results are given as mean ± SD from three experiments performed in triplicate. Similar release profiles were obtained by measuring protein content.

4.4.3. S-NPs provided a sustained release profile of HRP model protein

To demonstrate that chitosan NPs preserve protein activity we initially encapsulated horseradish peroxidase (HRP) as a model protein and investigated the encapsulation efficiency and release profile from small (S-NPs) and large (L-NPs) nanoparticles. Moreover, NPs of both sizes were able to release active HRP (Figure 4.16). S-NP showed an initial burst during the first 2 h when ≈12% of the loaded HRP activity was released. HRP release slowed down after that reaching ≈35% release in 72 h. The release of HRP from L-NPs was considerably weaker, and only ≈3.5% of the loaded HRP was released after 72 h.

4.4.4. NPs tagging with nuclear localization sequence (NLS) enhanced cell surface adsorption and uptake but reduced nuclear delivery

We next investigated whether tagging with an NLS could alter the cellular uptake and nuclear delivery of S-NPs. To this end, S-NPs with different NLS densities were generated and administered at different concentrations to human fibroblasts. Subsequent labeling of the NPs with WGA-FITC in permeabilized and non-permeabilized cells at different temperatures allowed the discrimination of cell-associated and internalized NPs. We found that increasing NP concentrations resulted in an increased cell association of the NP (Figure 4.17 A) as well an increased cell surface binding (Figure 4.17 B) and cellular uptake (Figure 4.17 C). Interestingly, the presence of an NLS dose-dependently increased the amount of cell surface-bound and internalized S-NPs. FRET spectroscopy with nuclear DNA dye Hoechst and FITC was then performed to quantify the nuclear delivery of S-NPs in human fibroblasts. Surprisingly and in contrast to the previous experiments, unmodified S-NPs revealed a higher FRET efficiency and hence an increased nuclear localization compared to NLS-modified NPs (Figure 4.17 D). Thus, even though NLS-tagging of S-NPs increased their cellular uptake, nuclear delivery was impaired. Since OCT4 exerts its cellular function in the nucleus, further tests were conducted with unmodified S-NPs, revealing the highest nuclear delivery.

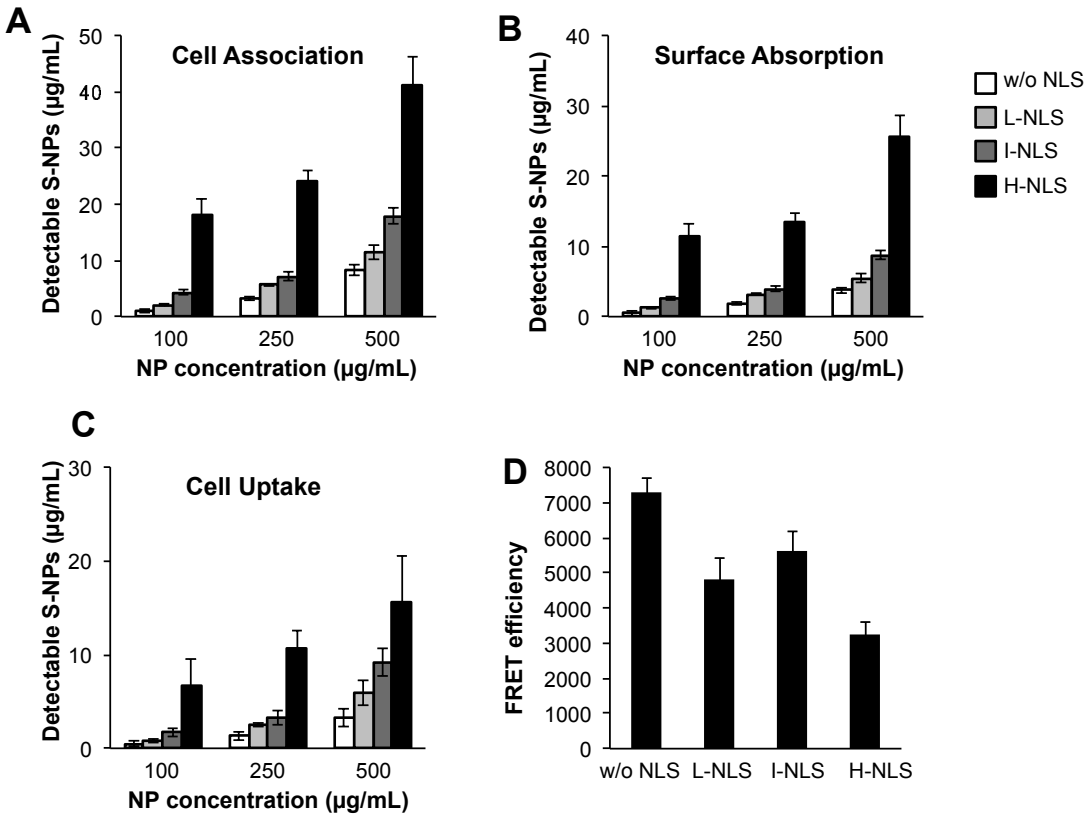

Figure 4.17: NLS density modulated association, surface adsorption, uptake and nuclear localization of S-NPs

(**A-C**) Non-modified S-NPs or S-NPs tagged with low (L), intermediate (I) or high (H) NLS densities were incubated at the indicated concentrations with human fibroblasts. After 24 h, chitosan NPs were stained as detailed in Material and Methods. The recovered amount of (**A**) cell-associated (i.e. surface-bound and internalized) NPs, (**B**) NPs bound to cell surface or (**C**) NPs taken up intracellularly was calculated from a standard curve by fluorometry. (**D**) Effects of NLS density on S-NP nuclear delivery as assessed by FRET fluoroscopy. Human fibroblasts were treated for 24 h with 250 µg/mL of the indicated versions of S-NPs. Measurement of FRET efficiency indicates the strongest colocalization of the nuclear DNA dye with SN-Ps lacking an NLS. Results are given as means ± SD.

4.4.5. S-NPs delivered OCT4 to the nucleus of hFFn

We next investigated the cellular distribution of OCT4-loaded S-NPs by confocal laser scanning microscopy. To this end, human fibroblasts were treated with equal protein amounts of either soluble OCT4 or OCT4-loaded S-NPs. Soluble OCT4 was exclusively found at the cell membrane but unable to enter the cells (Figure 4.18 A). In contrast, OCT4 encapsulated in NPs was efficiently imported into the fibroblasts, as revealed by co-staining for OCT4 using an OCT4 antibody and for chitosan using WGA-Alexafluor 488 (Figure 4.18 D-E).

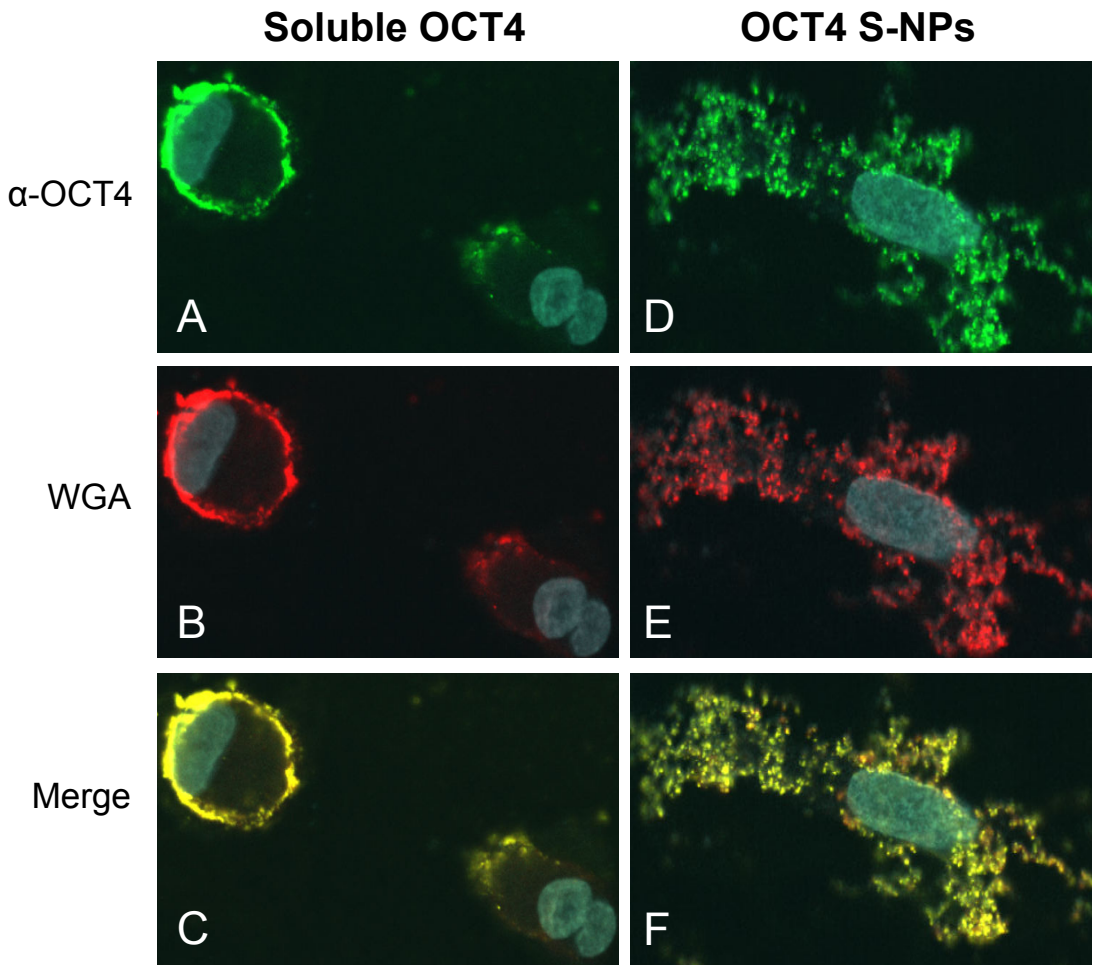

Figure 4.18: OCT4-loaded S-NPs but not soluble OCT4 protein were imported into cells and partially localized in the cell nucleus

Human primary fibroblasts were treated with 50 µg of each recombinant soluble OCT4 (**A-C**) or OCT4 encapsulated in S-NPs (**D-F**). After 24 h, cells were stained with OCT4 antibodies (green) or for chitosan NPs using WGA-Alexafluor 488 (red). Nuclear DNA was stained with Hoechst 33258 (blue). Merged images demonstrate that exogenous soluble OCT4 is excluded from cells and adheres to the cell membrane. In contrast, OCT4-loaded S-NPs are localized intracellularly, showing a partial overlap with Hoechst nuclear staining.

Moreover, this intracellular distribution partially overlapped with nuclear Hoechst staining, indicating a potential nuclear delivery of OCT4 (Figure 4.18 F). To further analyze a nuclear delivery of the OCT4-loaded NPs in different layers of cell nucleus, confocal Z-stack images were collected at 1-µm steps (Figure 4.19). Visualization of a Z-stack indeed indicated that OCT4 encapsulated in NPs was detectable in both perinuclear and intranuclear regions of the fibroblasts.

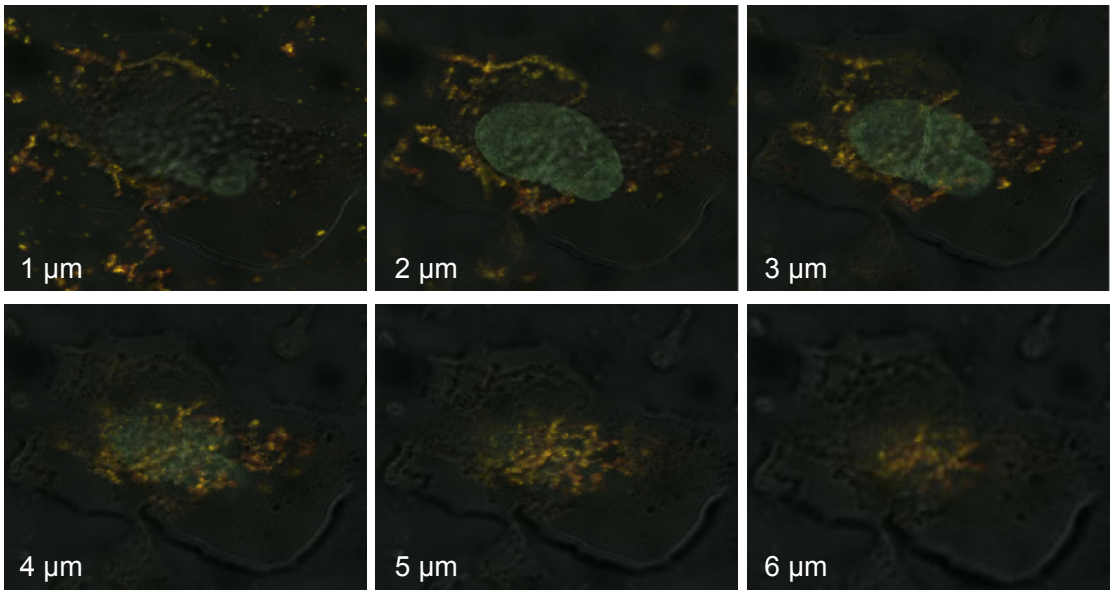

Figure 4.19: S-NPs delivered OCT4 protein to the nucleus

Z-stack imaging series of human fibroblasts treated with OCT4-loaded S-NPs. Cells were treated for 24 h with 50 µg of the SN-Ps and then stained with OCT4-antibody (green), WGA-Alexafluor 488 (red) and Hoechst 33258 (blue). Z-stack images through cell nucleus were collected at 1-µm steps by confocal laser scanning microscopy. The yellow fluorescence of the merged imaging indicates the colocalization of OCT4 and S-NPs in perinuclear and nuclear regions. The depth in micrometers at which images were taken is indicated.

5. Discussion

5.1. Novel AKT phosphorylation sites

The self-renewal of pluripotent stem cells is dependent on a coordinated network of a key set of transcription factors, which require a tight regulation of their expression to maintain pluripotency. OSKM factors have not only attracted increased interest for their role in stemness and embryonic pluripotency pathways but also have been implicated in tumorigenesis. So far, the mechanisms that regulate the levels of OSKM factors are poorly understood and only partially controlled by transcriptional events. For instance, SOX2 and OCT4 promote their own transcription by cooperative binding to adjacent DNA sites in the promoter regions of their genes (Chew et al., 2005). Recent evidence highlights an important role of post-translational modifications in regulating the levels and activity of pluripotency factors (Cai et al., 2012). However, although the transcriptional targets of these factors have been extensively studied, very little is known about how the proteins are regulated at the post-translational level.

The main intention or the present work was to establish an efficient *in vitro* system to study post-translational modifications of the OSKM factors. To this end, we employed a baculovirus expression system for GST fusion proteins in Sf9 insect cells. We demonstrate that, with the exception of c-MYC, all OSKM factors were localized in the nuclear compartment and could be therefore efficiently enriched from nuclear fractions of Sf9 cells. In contrast to our study, previous *in vitro* phosphorylation studies used recombinant transcription factors expressed in bacteria (Brumbaugh et al., 2012; Lin et al., 2012b). Bacterial expression systems exhibit several limitations because the recombinant proteins are mostly localized in inclusion bodies, requiring protein denaturation and an often inefficient refolding (Singh and Panda, 2005). In line with this notion, we found that several commercial preparations of bacterially expressed OSKM factors lacked robust DNA-binding activity. In contrast, consistent with their function as transcription factors, the baculovirally expressed OSKM factors revealed strong DNA-binding activity to their consensus sequences.

We chose to study AKT-mediated phosphorylation of the OSKM factors, because, in addition to its established function as a survival factor, AKT is regarded as an important regulator of stemness (Lin et al., 2012b; Watanabe et al., 2006). It is involved in many important cellular activities like cell-cycle progression and

metabolism (Figure 5.1). Moreover, increasing evidence indicates that AKT exerts an essential function in cancer stem cell biology (Martini et al., 2014; Merz et al., 2015). By combining *in vitro* phosphorylation and phosphoproteomic analyses, we were able to identify several novel putative AKT phosphorylation sites in the OSKM factors with the exception of c-MYC. For OCT4 we confirmed not only the previously reported AKT phosphorylation site T235 (Brumbaugh et al., 2012; Lin et al., 2012b), but also found new phosphorylation sites at S136, T159, T225 and S236. Likewise, for KLF4, we identified the reported AKT target site at S429 (Chen et al., 2013) as well as novel phosphorylation sites at S19, T33, S234 and S326. Despite several attempts, however, we were unable to verify the reported T116 site (equivalent to T118 in mouse) on SOX2 (Jeong et al., 2010), but identified a novel SOX2 phosphorylation site at S83.

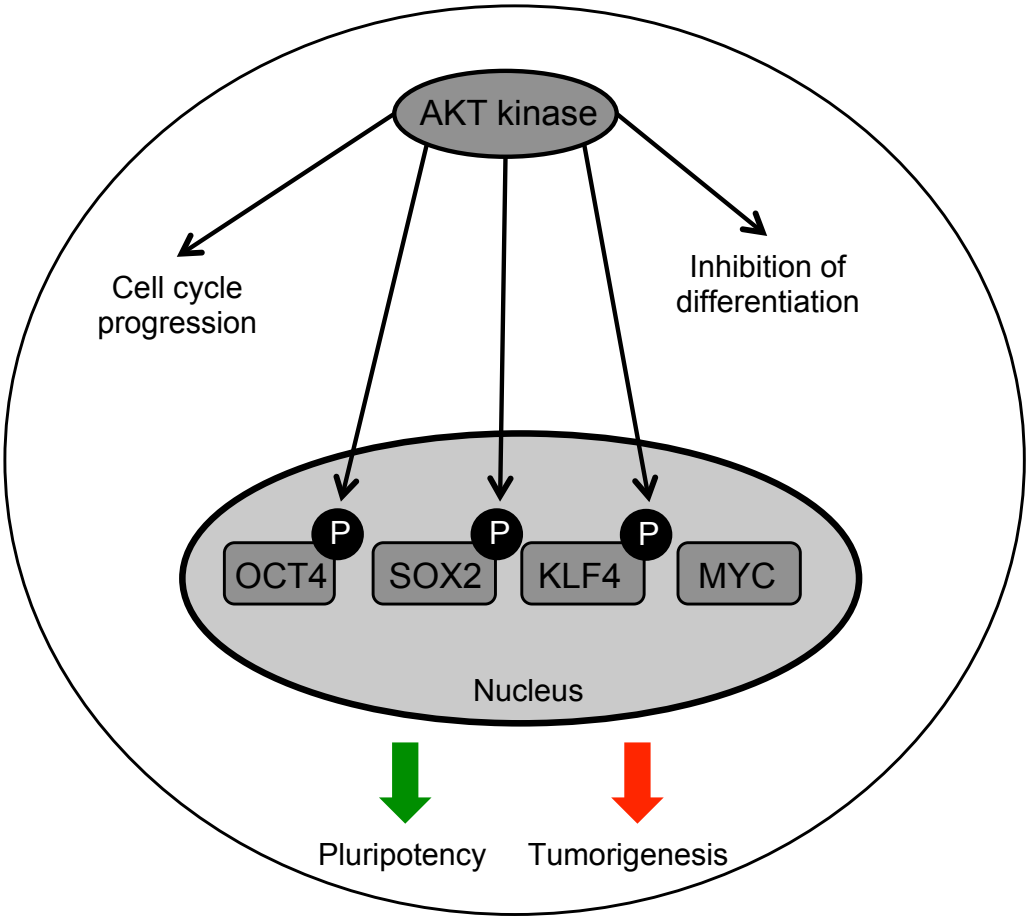

Figure 5.1: AKT-mediated cellular processes

AKT has an essential role in many cellular activities in the cytoplasm as well as in the nucleus. It mediates cell-cycle progression and inhibition of differentiation. The newly discovered AKT-mediated phosphorylation sites in OCT4, SOX2 and KLF4 can have significant effects on their nuclear localization and transcriptional activity, which certainly will affect the pluripotency and differentiation potential of stem cells.

It was reported that AKT-mediated phosphorylation of OCT4 at T235 promotes self-renewal, survival and the tumorigenic potential of embryonal carcinoma cells (Lin et al., 2012b). Mechanistically, AKT-mediated phosphorylation prevents its nuclear export and subsequent cytosolic degradation, resulting in increased stability and transcriptional activity of OCT4. Similarly, phosphorylation of OCT4 at the adjacent S236 site is likely to influence OCT4 activity (Saxe et al., 2009). Interestingly, the newly discovered site T225 in OCT4 is localized in POU DNA-binding domain, suggesting that phosphorylation at T225 might influence the DNA-binding and transcriptional activity of OCT4. Similar to OCT4, also the novel phosphorylation site of SOX2 at S83 is located within the DNA-binding domain as well as in one of the two nuclear localization sequences of SOX2. This might hint at the possibility that AKT-mediated phosphorylation of SOX2 might influence its nuclear import and DNA-binding activity. It should be noted that SOX2 can be also phosphorylated at T118 by AKT which not only promotes SOX2 stability in mouse embryonic stem cells, but its activity to reprogram mouse embryonic fibroblasts (Jeong et al., 2010).

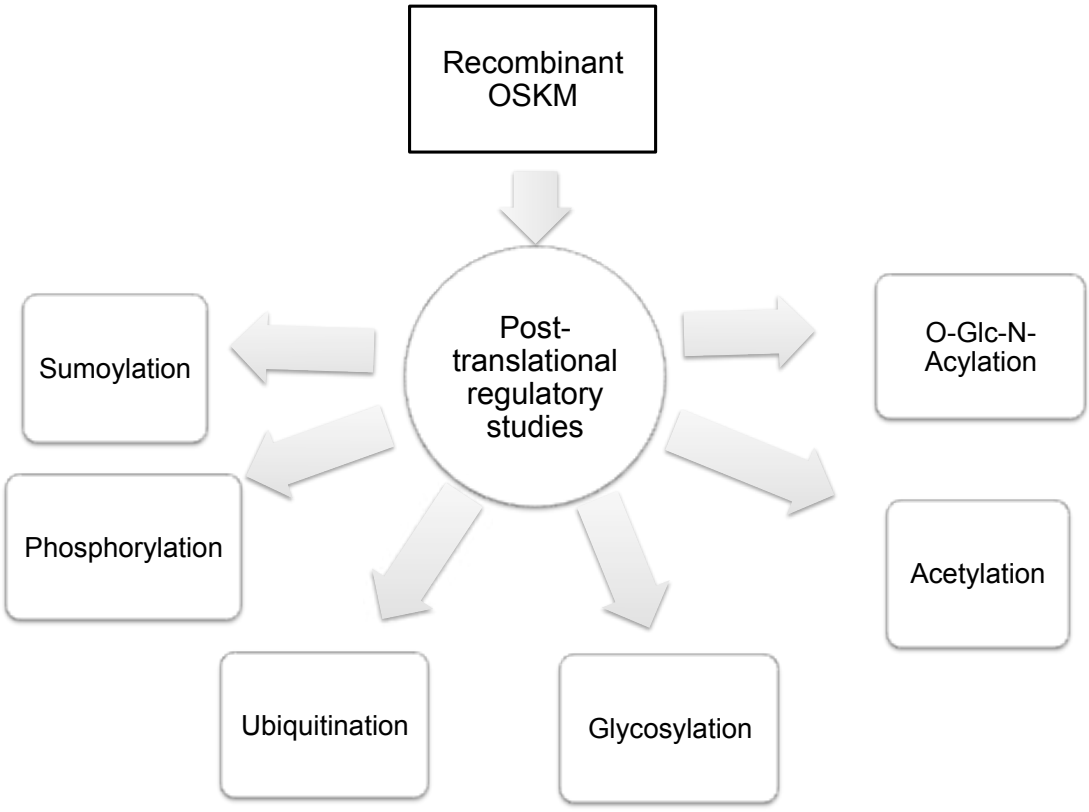

Figure 5.2: Post-translational regulatory studies that can be done using the recombinant OSKM

Recombinant transcription factors OSKM presented in this study can be used for further post-translational regulatory studies.

How the AKT-mediated phosphorylation of KLF4 affects nuclear localization or transcriptional activity remains unknown. Interestingly, both the reported phosphorylation site at T429, which is equivalent to mouse T399 (Chen et al., 2013), as well as the newly identified T33 site are located in one of the two nuclear localization sequences of KLF4.

All phosphorylation sites that we identified in OCT4, SOX2 and KLF4 are also present in the mouse proteins with one exception: S326 in human KLF4 is not present in mouse Klf4. The novel sites discovered in this study are therefore valuable candidates for *in vivo* validation and further functional analyses. Recent evidence demonstrates that, in addition to phosphorylation events, further post-translational modifications, including ubiquitination, sumoylation, methylation, acetylation or O-GlcNAcylation, may regulate the levels and activity of pluripotency factors (Cai et al., 2012). Our *in vitro* system will be also useful to study these post-translational modifications as well as their potential crosstalk in the OSKM factors (Figure 5.2).

5.2. Chitosan nanoparticles for efficient nuclear delivery of proteins

Since the introduction of the iPSC technology various strategies have been suggested to accomplish transgene-free derivation of iPSCs, including the use of non-integrating viruses, site-specific recombinases for transgene excision after reprogramming, plasmids or RNA transfection (Kaji et al., 2009; Okita et al., 2010; Sommer et al., 2010; Stadtfeld et al., 2008; VandenDriessche et al., 2009; Warren et al., 2010; Yu et al., 2009). Although these methods significantly reduce the risk of genome alterations, a nucleic acid-free system is generally preferred. Chitosan NPs are increasingly used as efficient protein delivery vehicles due to their mild formulation conditions in aqueous solvents. Several *in vitro* and *in vivo* tests have been performed with active proteins encapsulated in chitosan NPs (Agnihotri et al., 2004; Enríquez de Salamanca et al., 2006; Pan et al., 2002; Vila et al., 2004). To demonstrate that chitosan NPs preserve protein activity we initially encapsulated HRP as a model protein and investigated the encapsulation efficiency and release profile from S-NPs and L-NPs. Both S-NPs and L-NPs were able to release HRP activity in its active form. Since S-NPs, however, revealed a more efficient release and better preservation of OCT4 DNA-binding activity, further experiments were solely conducted with S-NPs.

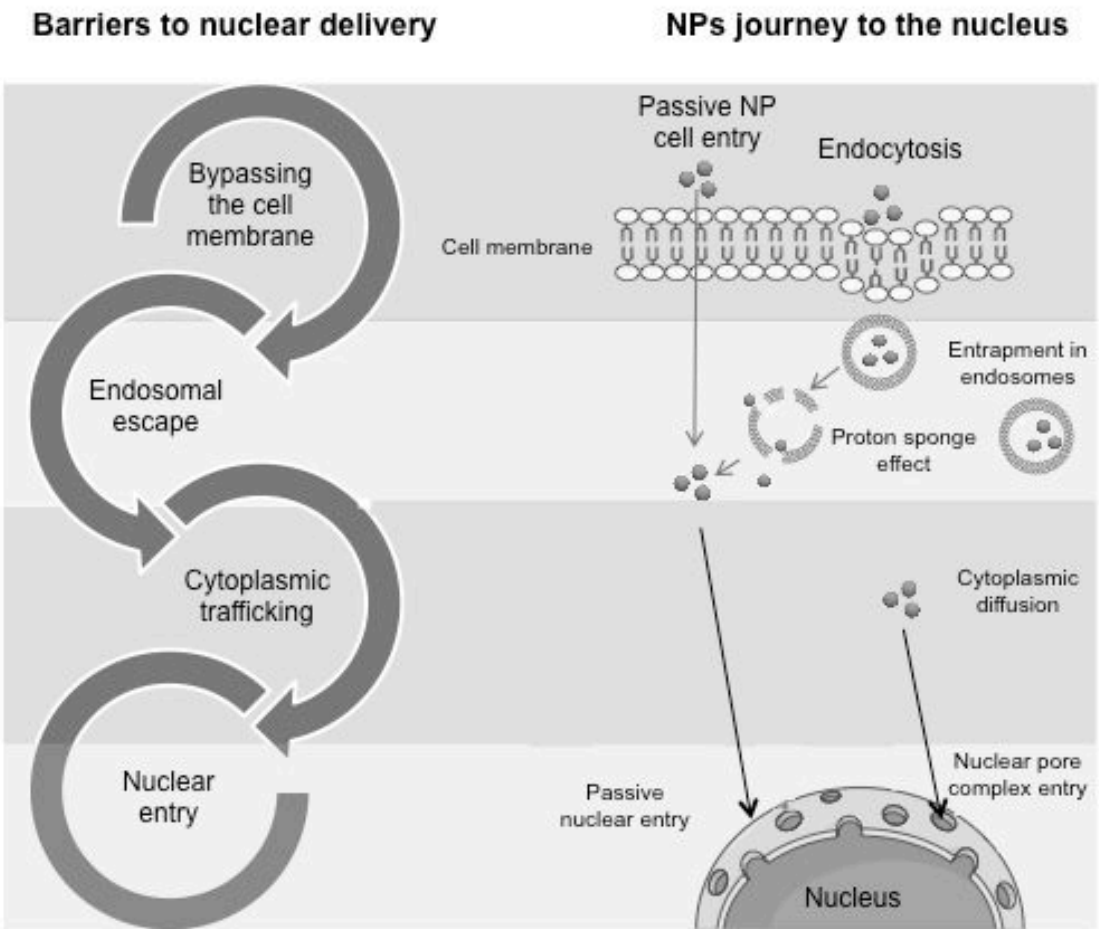

Figure 5.3: Barriers to nuclear delivery and mechanisms of NP nuclear delivery

Cell membrane, endosomal entrapment and nuclear membrane present the major barriers to NP nuclear delivery. However, chitosan NPs circumvent these hindrances via different mechanisms. The figure was adapted and modified from Tammam et al., 2016b.

An ideal protein transduction method has to fulfill a number of criteria and (1) stabilize the recombinant protein, (2) facilitate cellular entry and endosomal escape, (3) allow cell treatment with sufficient protein concentrations and (4) provide sustained protein levels that are required for iPSCs reprogramming without the need for repeated treatments. Compared to L-NPs, S-NPs showed a higher sustained release of active HRP over a 72-h incubation period and were able to increase OCT4 stability at 4°C (up to 7 weeks), at room temperature (up to two weeks) and more importantly in cell culture at 37°C. Under cell culture conditions the DNA-binding activity of OCT4 protein was lost within 1 h, whereas NP-encapsulated OCT4 preserved activity throughout the 24-h period tested. Also Bonsali *et al.* reported that a rapid loss of TAT-OCT4 activity under cell culture conditions (Bosnali and

Edenhofer, 2008). The presence of serum could stabilize both TAT fusion proteins but at the same time reduced their cellular uptake (Thier et al., 2010). Protein concentration was also reported to be limiting factor when working with non-purified HEK cell lysates containing recombinant OSKM factors (Kim et al., 2009a). Lastly, while a combination of serum and serum replacement containing lipid-rich BSA improved the stability and cellular uptake of TAT-OCT4, serum replacement was cytotoxic to fibroblasts that are mostly used in reprogramming experiments (Thier et al., 2010, 2012).

There are many barriers that NPs have to cross to reach the cell nucleus (Figure 5.3). It has been repeatedly reported that chitosan NPs can associate with cells (Enríquez de Salamanca et al., 2006; Huang et al., 2002). S-NPs can cross the cell membrane passively or via caveoli mediated endocytosis circumventing the endosomal/ lysosomal destruction pathway (Tammam et al., 2015a). Moreover, due to their positively charged surface (≈35 mV), S-NPs can escape the endosomal entrapment via the proton-sponge effect (Richard et al., 2013). Nuclear entry is achieved either by passive entry due to the small NP size (25 nm) or by interaction of the NLS with the nuclear pore complex (Fagotto et al., 1998).

Only a few studies differentiated between cell surface-bound and internalized NPs (Braun et al., 2014; Cho et al., 2009; Gottstein et al., 2013). Since soluble OCT4 is incapable of cell entry, we validated that chitosan NPs are capable of cellular entry rather than adhering to the cell surface. To this end, we employed a method that exploits the preferential affinity of WGA to chitosan and thereby allows the quantification of cell surface-bound and internalized chitosan NPs. In non-permeabilized cells at 4°C WGA-FITC was not internalized in cells and labeled only extracellular chitosan NPs, whereas in permeabilized cells at RT WGA-FITC labeled both surface-bound and internalized NPs, making it possible to quantify NPs that had been internalized and those that were only adsorbed on the surface (Tammam et al., 2015b).

For its function as a transcription factor, OCT4 requires its delivery into the nucleus. Employing a FRET-based assay to evaluate the nuclear targeting of NPs in intact fibroblasts, we surprisingly found that the presence of an NLS even reduced nuclear targeting of OCT4. Further experiments were therefore conducted with unmodified NPs. Confocal microscopy confirmed the cellular and nuclear entry of intact OCT4-NPs. Prior to microscopy, we treated the permeabilized cells with WGA-Alexafluor

488 to demonstrate that the green fluorescence seen was due to OCT4-NPs rather than free OCT4. Since WGA preferentially binds to chitosan NPs (Tammam et al., 2015b), the detectable yellow fluorescence indicated a co-localization of OCT4 and WGA, which further implied that the signal was due to intracellular OCT4-NPs rather than to soluble OCT4.

Apart from stabilizing OCT4 and delivering it to its site of action, NPs enable the use of high concentrations of reprogramming factors. In the case of OCT4, an encapsulation efficiency of ≈75% was achieved, which allowed cell treatment with a concentration of 100 µg/mL (≈2.6 µM) of OCT4. At this concentration (corresponding to 1 mg/mL chitosan) OCT4 was neither degraded, precipitated nor were the target cells affected. In line, we have previously demonstrated that S-NPs do not affect cell viability up to concentrations of 1 mg/mL (Tammam et al., 2015b).

So far, only two recent studies attempted to employ nanocarriers in protein-induced reprogramming. Cho *et al.* used TiO_2 nanotubes with electrostatically adsorbed Oct4, Sox2, Klf4 and Nanog for reprogramming of neural stem cells (Cho et al., 2013). While the authors observed stem cell-like morphological changes, fully reprogrammed iPSCs were not obtained. It is possible that the electrostatic binding, unlike chitosan encapsulation of proteins used in our study, hindered the release of the reprogramming factors. It is noteworthy that TiO_2 nanotubes are not biodegradable, and therefore additional studies are required to exclude their long-term toxicity.

Khan *et al.* successfully obtained iPSCs colonies from human fibroblasts using synthetic surfactants, known as bolaamphiphiles, which were complexed with KLF4, SOX2 and NR5A2 (Khan et al., 2013). The authors demonstrated that fully reprogrammed iPSCs could be obtained following three rounds of protein transduction. In addition, there are several other possibilities to enhance the efficiency of iPSC generation.
For instance, it was recently demonstrated that activation of toll-like receptor-3 enhances the reprogramming efficiency of cell-permeant OSKM fusion proteins, presumably by facilitating epigenetic alterations (Lee et al., 2012b). Similarly, histone deacetylase inhibitors, such as valproic acid, have been shown to improve protein-based iPSC generation (Zhou et al., 2009).

Low efficiencies could generally be attributed to the poor stability and solubility of recombinant factors, their low cellular entry or their poor endosomal release (Bosnali and Edenhofer, 2008; Kim et al., 2009b; Thier et al., 2010). Indeed, a major drawback of PTD fusion proteins is that their release from endosomal vesicles into the cytosol is inefficient. Interestingly, cell permeabilization with streptolysin O has been reported to enhance protein-induced reprogramming, presumably by avoiding entrapment and degradation of the OSKM factors in lysosomes (Cho et al., 2010). Similarly, sucrose, which also acts as a lysomotrophic agent, can increase the reprogramming efficiency of OCT4-TAT (Thier et al., 2010).

Although cell-permeant PTD-fused OKSM factors enhance the cellular uptake, they do not provide a sustained supply of the pluripotency factors, unless protein treatment is repeated several times. A sustained supply of the OSKM factor is required for reprogramming and a major reason for the high reprogramming efficiency of retroviral expression systems. In this context, NP-encapsulated OSKM factors might provide a more sustained supply compared to soluble proteins. Further studies are therefore ongoing to generate NPs for SOX2, c-MYC and KLF4 and to evaluate their utility in protein-based iPSC generation.

In conclusion, protein transduction techniques are still poorly developed and highly inefficient for the protein-based generation of iPSCs with recombinant reprogramming factors. Although protein-based techniques are regarded as safe and, unlike retroviral approaches, devoid of potential mutagenic side effects, the limited solubility, weak stability under cell culture conditions, the low cellular entry as well as the poor endosomal release of the recombinant factors together with a lack of their sustained expression are major bottlenecks for successful reprogramming approaches. Therefore, further developments of protein delivery systems are required to enhance the efficiency of cellular reprogramming to iPSCs.

In the present study we developed a NP-based delivery system for the transcription factor OCT4 as the most important reprogramming factor. Following its baculoviral expression, recombinant OCT4 was encapsuled in chitosan NPs. Our results demonstrate that, compared to soluble OCT4, NP encapsulation of OCT4 stabilized its activity and resulted in increased DNA binding as well as in its efficient cellular delivery into human fibroblasts. Our study therefore demonstrates a proof-of-concept for a DNA-free protein transduction system and suggests that chitosan NPs provide are promising tools for the generation of transgene-free iPSCs.

5.3. Aurora Kinase A: Kinase function not needed?

Aurka is of absolute importance for normal embryonic development. Aurka knockout mice die early before reaching the 16-cell stage due to mitotic defects, in particular, due to defects in spindle assembly (Lu et al., 2008). However, there is growing evidence that Aurka immense importance is not only due to its kinase function (Kress and Gotta, 2011). Intriguingly, Toya et al. showed that the kinase function of the Aurora kinase A homologue (AIR-1) in *C. elegans* is dispensable in microtubule spindle assembly (Toya et al., 2011).

Aurka has been described as a major regulator of self-renewal and pluripotency in mESCs. Upon its knockdown, Oct4 was downregulated and cells started differentiation in the ectodermal and mesodermal lineages. This has been mainly attributed to Aurka-p53 interaction (Lee et al., 2012a).

Our results confirmed the importance of Aurka in pluripotency maintenance, however, due to another mechanism of action. AURKA overexpression led to enhanced OCT4 and c-MYC transcriptional activity of the Ig µE4 luciferase reporter, where the E-box and octamer-binding motif were nearby. Interestingly, this effect was kinase-independent, because, upon the overexpression of the kinase-dead mutant (AURKA KD), the same enhancement was observed. However, AURKA's effect on c-MYC and OCT4 transcriptional activity could not be observed in two further reporters (Appendix figure 11.1 and 11.2) where either the E-box or octamer binding-motif was present but not both, indicating that the interaction depends on the presence of the three proteins and their binding sites. Notably, AURKA overexpression in mESC stabilized c-Myc protein as well as the KD mutant. However, knockdown of Aurka reduced Oct4 protein, which has been described to be a major trigger for mESC differentiation (Wagner and Cooney, 2009)

Lee et al. observed that Aurka inhibition with its specific inhibitor MLN8237 or its knockdown reduced reprogramming efficiency of MEFs to iPSCs due to increased p53 activity. We confirmed this observation. Nevertheless, we attribute the reduced reprogramming efficiency mainly due to reduced c-Myc and Oct4 activation on the transcriptional level. These results are opposing to the report published by Li and Rana (2012). They defined Aurka as a barrier kinase to reprogramming and showed that upon Aurka inhibition with MLN8237 or Aurka depletion with siRNA, the reprogramming efficiency was diminished (Li and Rana, 2012).

MLN8237 is a potent and selective AURKA inhibitor, which is currently in phase II clinical trials as a treatment for many solid tumors (Cheung et al., 2009; Manfredi et al., 2011). MLN8237 has been described to have diverse effects on AURKA and its interaction partners in stem cells. In one report, MLN8237 inhibited Aurka but, as a feedback, it increased its protein expression in a concentration dependent manner. Moreover, MLN8237 did not affect the pluripotency and self-renewal potential of mESCs (Li and Rana, 2012). However, in another report, MLN8237 completely abrogates the self-renewal potential of mESCs and initiates differentiation to ectodermal and mesodermal lineages (Lee et al., 2012a).

Due to the discrepancy of the published reports concerning MLN8237, we performed an extensive study on the effects of MLN8237 in mESCs. Remarkably, low concentrations (1-10 nM) of MLN8237 did not inhibit Aurka, however, it increased its protein level and its activity as observed by p-Aurka antibody. This increase in Aurka levels was accompanied by an increase in c-Myc protein level. Higher concentrations (1-10 μM) of MLN8237 inhibited Aurka and decreased its protein level. This decrease was however accompanied with a decrease in c-Myc and Oct4 proteins.

In summary, Aurora kinase A plays a critical role in the regulation of stem cell transcription factors c-Myc and Oct4, however, mainly in a kinase-independent manner. In our study, overexpression of the active kinase and the kinase-dead mutant increased the transcriptional activity of c-Myc and Oct4 in luciferase assays and stabilized c-Myc in mESCs. We confirmed that inhibition of Aurka reduced the reprogramming efficiency of MEFs to iPSCs. High concentrations of MLN8237 destabilize Aurka, c-Myc and Oct4 impairing the self-renewal and pluripotency of stem cells. Moreover, we shed the light on the effects of MLN8237 in the reprogramming process. MLN8237 decreased the mRNA levels of c-Myc and Oct4 during the reprogramming process diminishing the reprogramming efficiency of MEFs to iPSCs.

6. Summary

Stem cells possess intricate regulatory networks governed by the key transcription factors OCT4, SOX2, KLF4 and c-MYC (OSKM). OSKM transcriptional activity and stability are regulated by different post-translational modifications (PTMs), especially by phosphorylation. AKT (also known as Protein Kinase B) is essential for self-renewal and pluripotency maintenance of stem cells. It phosphorylates OCT4, SOX2 and KLF4 on several sites. However, the comprehensive phosphorylation pattern remains elusive. In the first project of this study, we established an *in vitro* tool to explore PTMs in the transcription factors OSKM, especially, phosphorylation by AKT kinase. For this purpose, OSKM were expressed in Sf9 insect cells using the Baculovirus Expression Vector System (BEVS). BEVS ensured high yield of properly folded proteins harboring PTMs similar to their mammalian counterparts. Recombinant OSKM were confirmed for purity, nuclear localization and biological activity. Furthermore, by combining *in vitro* kinase assays with mass spectrometry-based phosphoproteomic analyses, novel AKT phosphorylation sites were identified in OCT4, SOX2 and KLF4 *in vitro*.

c-MYC and OCT4 have been identified in a previous study in our lab as putative phosphorylation substrates to Aurora kinase A (AURKA). AURKA is an essential kinase in cell cycle and has various implications in cancer and stem cells. In the second project of this study, we investigated the interaction between AURKA, c-MYC and OCT4. Remarkably, AURKA increased the transcriptional activity of c-MYC and OCT4 in a kinase-independent manner. MLN8237, a specific Aurora kinase A inhibitor regulated the transcription and the protein stability of c-Myc and Oct4 in mouse embryonic stem cells and during reprogramming of mouse embryonic fibroblasts. Taken together, we showed that Aurka stabilized c-Myc and Oct4 and its kinase function was not needed in stem cells.

Ectopic overexpression of OSKM has been shown to reprogram terminally differentiated cells to become induced pluripotent stem cells. Conventionally, viral vectors are used for transduction increasing the risk of genetic manipulations by viral integrations in the host genome. Therefore, in the third project of this study, we established an integration-free, protein-based reprogramming method using biodegradable chitosan nanoparticles (NPs) loaded with recombinant OCT4 protein. NPs delivered OCT4 to the nucleus of human dermal fibroblasts and provided a sustained release profile to its cargo. Moreover, NPs stabilized OCT4 activity *in vitro*.

7. Zusammenfassung

Stammzellen besitzen komplexe regulatorische Netzwerke, die von den Transkriptionsfaktoren OCT4, SOX2, KLF4 und c-MYC (OSKM) gesteuert werden. Die transkriptionelle Aktivität und die Stabilität der OSKM Faktoren werden durch verschiedene posttranslationale Modifikationen (PTMs) geregelt, insbesondere, durch die Phosphorylierung. AKT, auch Protein-Kinase B genannt, ist für die Selbsterneuerung und die Erhaltung der Pluripotenz von Stammzellen unentbehrlich. Sie phosphoryliert OCT4, SOX2 und KLF4 an mehreren Stellen. Allerdings ist das Phosphorylierungsmuster noch unbekannt. Im ersten Projekt dieser Studie haben wir ein *in vitro* Werkzeug entwickelt, um die PTMs in den Transkriptionsfaktoren OSKM, vor allem die Phosphorylierung durch die AKT Kinase zu erforschen. Die OSKM wurden in Sf9 Insektenzellen mit Hilfe des Baculovirus-Expressionsvektor-Systems (BEVS) exprimiert. Der Einsatz von BEVS erlaubte eine hohe Expression von richtig gefalteten Proteinen, die ähnliche PTMs wie Säugerzellen besitzen. Die rekombinanten OSKM Proteine wurden auf ihre Reinheit, nukleäre Lokalisation und biologische Aktivität getestet. Darüber hinaus wurden durch Massenspektrometrie-basierte Phosphoproteom-Analysen neue AKT-Phosphorylierungsstellen in OCT4, SOX2 und KLF4 identifiziert.

C-MYC und OCT4 wurden in unserem Labor als putative Phosphorylierung-Substrate der Aurora-Kinase A (AURKA) identifiziert. AURKA spielt eine wichtige Rolle im Zellzyklus und hat verschiedene Auswirkungen auf Krebs und Stammzellen. Im zweiten Projekt dieser Studie untersuchten wir die Interaktion zwischen AURKA, c-MYC und OCT4. Interessanterweise erhöhte AURKA die transkriptionelle Aktivität von c-MYC und OCT4, in einer Kinase–unabhängigen Regulation. MLN8237, ein spezifischer AURKA Inhibitor, regulierte die Transkription und die Proteinstabilität von c-MYC und OCT4 in murinen embryonalen Stammzellen, aber auch bei der Reprogrammierung von murinen embryonalen Fibroblasten. Zusammengenommen haben wir gezeigt, dass Aurka c-Myc und OCT4 stabilisiert und dass ihre Kinasefunktion in Stammzellen hierfür nicht benötigt wird.

Es wurde gezeigt dass die ektopische Überexpression von OSKM die Reprogrammierung von differenzierten Zellen zu pluripotenten Stammzellen, induziert. Üblicherweise werden virale Vektoren zur Transduktion verwendet, was die Gefahr von genetischen Manipulationen durch die virale Integration in das

Wirtsgenom, erhöht. Im dritten Projekt dieser Studie haben wir eine integrationsfreie, proteinbasierte Reprogrammierungsmethode durch Verwendung von biologisch abbaubaren Chitosan-Nanopartikeln (NPs) entwickelt, die mit OCT4 rekombinanten Proteinen beladen waren. NPs beförderten OCT4 zum Zellkern von humanen dermalen Fibroblasten und erlaubten eine anhaltende Freisetzung von OCT4. Darüber hinaus stabilisierten die NPs *in vitro* die OCT4 Aktivität.

8. List of publications

Malak, P.N., Dannenmann, B., Hirth, A., Rothfuss, O.C., and Schulze-Osthoff, K. (2015). Novel AKT phosphorylation sites identified in the pluripotency factors OCT4, SOX2 and KLF4. Cell Cycle *14*, 3748–3754.

Tammam, S.*, **Malak, P.***, Correa, D., Rothfuss, O., Azzazy, H.M., Lamprecht, A., and Schulze-Osthoff, K. (2016a). Nuclear delivery of recombinant OCT4 by chitosan nanoparticles for transgene-free generation of protein-induced pluripotent stem cells. Oncotarget.
* Equal contribution

Merz, B., **Malak, P.N.**, and Rothfuss, O. (2015). Nuclear Akt: target for breast cancer therapy? Cell Cycle *14*, 2000.

Lehle, S., Hildebrand, D.G., Merz, B., **Malak, P.N.**, Becker, M.S., Schmezer, P., Essmann, F., Schulze-Osthoff, K., and Rothfuss, O. (2014). LORD-Q: a long-run real-time PCR-based DNA-damage quantification method for nuclear and mitochondrial genome analysis. Nucleic Acids Res. 42, e41.

9. Personal contribution

The concept of this study and the experimental planning were established by me in discussions with Prof. Schulze-Osthoff and Dr. Oliver Rothfuss. Execution of experiments was accomplished by me or by students under my supervision.

The thesis presents three projects. The first project was published in *Cell Cycle* namely, Novel Akt phosphorylation sites identified in the pluripotency factors OCT4, SOX2 and KLF4 (Malak et al., 2015). The protein expression, purification and activity confirmation work was done by me and by two bachelor students, Benjamin Dannenmann and Alexander Hirth under my supervision. The *in vitro* kinase assays were performed by Dr. Oliver Rothfuss, Benjamin Dannenmann and me. The phosphoproteomics analyses were performed by Dr. Boris Macek and Dr. Anna Velic from the Proteomics Center in Tuebingen. All data analysis and manuscript writing were performed by me.

The second project, namely, Aurka regulates c-Myc and Oct4 in stem cells in a kinase-independent manner, was accomplished in Tuebingen by me and three students, Benjamin Dannenmann, Franziska Herster and Julia Günter under my supervision. The luciferase assays in 6W-th-Luc reporters were performed by Benjamin Dannenmann as a part of his master thesis. The luciferase assays in E-box and octamer reporters, the mRNA and protein analyses using MLN8237 were performed by Franziska Herster as a part of her master thesis. Overexpression and knockdown of AURKA in mESCs were accomplished by Julia Günter.

The third project, namely, Nuclear delivery of recombinant OCT4 by chitosan nanoparticles for transgene-free generation of protein-induced pluripotent stem cells was published in *Oncotarget* (Tammam et al., 2016a). The project was performed in collaboration with the Pharmaceutical Institute in Bonn and the American University in Cairo. The concept was developed by Salma and me after discussion with Prof. Hassan Azzazy, Alf Lamprecht, Klaus Schulze-Osthoff and Dr. Oliver Rothfuss. The OCT4 protein expression and purification were done by me. The electrophoretic mobility shift assays were performed by Daphne Correa and me. The nanoparticle formulation and characterization were performed by Salma Tammam. The manuscript was written by Salma and me.

10. References

Agnihotri, S.A., Mallikarjuna, N.N., and Aminabhavi, T.M. (2004). Recent advances on chitosan-based micro- and nanoparticles in drug delivery.. J. Control. Release Soc. *100*, 5–28.

Akaogi, K., Nakajima, Y., Ito, I., Kawasaki, S., Oie, S.–., Murayama, A., Kimura, K., and Yanagisawa, J. (2009). KLF4 suppresses estrogen-dependent breast cancer growth by inhibiting the transcriptional activity of ERα. Oncogene *28*, 2894–2902.

Altomare, D.A., and Testa, J.R. (2005). Perturbations of the AKT signaling pathway in human cancer. Oncogene *24*, 7455–7464.

Baltus, G.A., Kowalski, M.P., Zhai, H., Tutter, A.V., Quinn, D., Wall, D., and Kadam, S. (2009). Acetylation of Sox2 Induces its Nuclear Export in Embryonic Stem Cells. STEM CELLS *27*, 2175–2184.

Barr, A.R., and Gergely, F. (2007). Aurora-A: the maker and breaker of spindle poles. J. Cell Sci. *120*, 2987–2996.

Bischoff, J.R., Anderson, L., Zhu, Y., Mossie, K., Ng, L., Souza, B., Schryver, B., Flanagan, P., Clairvoyant, F., Ginther, C., et al. (1998). A homologue of Drosophila aurora kinase is oncogenic and amplified in human colorectal cancers. EMBO J. *17*, 3052–3065.

Bosnali, M., and Edenhofer, F. (2008). Generation of transducible versions of transcription factors Oct4 and Sox2. Biol. Chem. *389*, 851–861.

Boyer, L.A., Lee, T.I., Cole, M.F., Johnstone, S.E., Levine, S.S., Zucker, J.P., Guenther, M.G., Kumar, R.M., Murray, H.L., Jenner, R.G., et al. (2005). Core Transcriptional Regulatory Circuitry in Human Embryonic Stem Cells. Cell *122*, 947–956.

Braun, G.B., Friman, T., Pang, H.-B., Pallaoro, A., Hurtado de Mendoza, T., Willmore, A.-M.A., Kotamraju, V.R., Mann, A.P., She, Z.-G., Sugahara, K.N., et al. (2014). Etchable plasmonic nanoparticle probes to image and quantify cellular internalization. Nat. Mater. *13*, 904–911.

Briassouli, P., Chan, F., Savage, K., Reis-Filho, J.S., and Linardopoulos, S. (2007). Aurora-A regulation of nuclear factor-kappaB signaling by phosphorylation of IkappaBalpha. Cancer Res. *67*, 1689–1695.

Brumbaugh, J., Hou, Z., Russell, J.D., Howden, S.E., Yu, P., Ledvina, A.R., Coon, J.J., and Thomson, J.A. (2012). Phosphorylation regulates human OCT4. Proceedings of the National Academy of Sciences *109*, 7162–7168.

Cai, N., Li, M., Qu, J., Liu, G.-H., and Belmonte, J.C.I. (2012). Post-translational modulation of pluripotency. J. Mol. Cell Biol. *4*, 262–265.

Campbell, P.A., and Rudnicki, M.A. (2013). Oct4 Interaction with Hmgb2 Regulates Akt Signaling and Pluripotency. STEM CELLS *31*, 1107–1120.

Chen, B., Xue, Z., Yang, G., Shi, B., Yang, B., Yan, Y., Wang, X., Han, D., Huang, Y., and Dong, W. (2013). Akt-Signal Integration Is Involved in the Differentiation of Embryonal Carcinoma Cells. PLoS ONE *8*, e64877.

Cheung, C.H.A., Coumar, M.S., Hsieh, H.-P., and Chang, J.-Y. (2009). Aurora kinase inhibitors in preclinical and clinical testing. Expert Opin. Investig. Drugs *18*, 379–398.

Chew, J.-L., Loh, Y.-H., Zhang, W., Chen, X., Tam, W.-L., Yeap, L.-S., Li, P., Ang, Y.-S., Lim, B., Robson, P., et al. (2005). Reciprocal Transcriptional Regulation of Pou5f1 and Sox2 via the Oct4/Sox2 Complex in Embryonic Stem Cells. Mol. Cell. Biol. *25*, 6031–6046.

Cho, E.C., Xie, J., Wurm, P.A., and Xia, Y. (2009). Understanding the role of surface charges in cellular adsorption versus internalization by selectively removing gold nanoparticles on the cell surface with a I2/KI etchant. Nano Lett. *9*, 1080–1084.

Cho, H.-J., Lee, C.-S., Kwon, Y.-W., Paek, J.S., Lee, S.-H., Hur, J., Lee, E.J., Roh, T.-Y., Chu, I.-S., Leem, S.-H., et al. (2010). Induction of pluripotent stem cells from adult somatic cells by protein-based reprogramming without genetic manipulation. Blood *116*, 386–395.

Cho, S.J., Choi, H.W., Cho, J., Jung, S., Seo, H.G., and Do, J.T. (2013). Activation of pluripotency genes by a nanotube-mediated protein delivery system. Mol. Reprod. Dev. *80*, 1000–1008.

Cox, J., Matic, I., Hilger, M., Nagaraj, N., Selbach, M., Olsen, J.V., and Mann, M. (2009). A practical guide to the MaxQuant computational platform for SILAC-based quantitative proteomics. Nat. Protoc. *4*, 698–705.

Crane, R., Kloepfer, A., and Ruderman, J.V. (2004). Requirements for the destruction of human Aurora-A. J. Cell Sci. *117*, 5975–5983.

Dutertre, S., Cazales, M., Quaranta, M., Froment, C., Trabut, V., Dozier, C., Mirey, G., Bouché, J.-P., Theis-Febvre, N., Schmitt, E., et al. (2004). Phosphorylation of CDC25B by Aurora-A at the centrosome contributes to the G2-M transition. J. Cell Sci. *117*, 2523–2531.

Enríquez de Salamanca, A., Diebold, Y., Calonge, M., García-Vazquez, C., Callejo, S., Vila, A., and Alonso, M.J. (2006). Chitosan nanoparticles as a potential drug delivery system for the ocular surface: toxicity, uptake mechanism and in vivo tolerance. Invest. Ophthalmol. Vis. Sci. *47*, 1416–1425.

Eyers, P.A., Erikson, E., Chen, L.G., and Maller, J.L. (2003). A novel mechanism for activation of the protein kinase Aurora A. Curr. Biol.*13*, 691–697.

Fagotto, F., Glück, U., and Gumbiner, B.M. (1998). Nuclear localization signal-independent and importin/karyopherin-independent nuclear import of beta-catenin. Curr. Biol. *8*, 181–190.

Franz-Wachtel, M., Eisler, S.A., Krug, K., Wahl, S., Carpy, A., Nordheim, A., Pfizenmaier, K., Hausser, A., and Macek, B. (2012). Global detection of protein kinase D-dependent phosphorylation events in nocodazole-treated human cells. Mol. Cell. Proteomics *11*, 160–170.

Fu, J., Bian, M., Jiang, Q., and Zhang, C. (2007). Roles of Aurora kinases in mitosis and tumorigenesis. Mol. Cancer Res. *5*, 1–10.

Glover, D.M., Leibowitz, M.H., McLean, D.A., and Parry, H. (1995). Mutations in aurora prevent centrosome separation leading to the formation of monopolar spindles. Cell *81*, 95–105.

Gottstein, C., Wu, G., Wong, B.J., and Zasadzinski, J.A. (2013). Precise quantification of nanoparticle internalization. ACS Nano *7*, 4933–4945.

Harush-Frenkel, O., Debotton, N., Benita, S., and Altschuler, Y. (2007). Targeting of nanoparticles to the clathrin-mediated endocytic pathway. Biochem. Biophys. Res. Commun. *353*, 26–32.

Herreros-Villanueva, M., Zhang, J.-S., Koenig, A., Abel, E.V., Smyrk, T.C., Bamlet, W.R., de Narvajas, A.A.-M., Gomez, T.S., Simeone, D.M., Bujanda, L., et al. (2013). SOX2 promotes dedifferentiation and imparts stem cell-like features to pancreatic cancer cells. Oncogenesis *2*, e61.

Huang, M., Ma, Z., Khor, E., and Lim, L.-Y. (2002). Uptake of FITC-chitosan nanoparticles by A549 cells. Pharm. Res. *19*, 1488–1494.

Jaenisch, R., and Young, R. (2008). Stem Cells, the Molecular Circuitry of Pluripotency and Nuclear Reprogramming. Cell *132*, 567–582.

Jeong, C.-H., Cho, Y.-Y., Kim, M.-O., Kim, S.-H., Cho, E.-J., Lee, S.-Y., Jeon, Y.-J., Yeong Lee, K., Yao, K., Keum, Y.-S., et al. (2010). Phosphorylation of Sox2 Cooperates in Reprogramming to Pluripotent Stem Cells. STEM CELLS *28*, 2141–2150.

Jerabek, S., Merino, F., Schöler, H.R., and Cojocaru, V. (2014). OCT4: dynamic DNA binding pioneers stem cell pluripotency. Biochim. Biophys. Acta *1839*, 138–154.

Kaji, K., Norrby, K., Paca, A., Mileikovsky, M., Mohseni, P., and Woltjen, K. (2009). Virus-free induction of pluripotency and subsequent excision of reprogramming factors. Nature *458*, 771–775.

Katayama, H., Sasai, K., Kawai, H., Yuan, Z.-M., Bondaruk, J., Suzuki, F., Fujii, S., Arlinghaus, R.B., Czerniak, B.A., and Sen, S. (2004). Phosphorylation by aurora kinase A induces Mdm2-mediated destabilization and inhibition of p53. Nat. Genet. *36*, 55–62.

Khan, M., Narayanan, K., Lu, H., Choo, Y., Du, C., Wiradharma, N., Yang, Y.-Y., and Wan, A.C.A. (2013). Delivery of reprogramming factors into fibroblasts for generation of non-genetic induced pluripotent stem cells using a cationic bolaamphiphile as a non-viral vector. Biomaterials *34*, 5336–5343.

Kim, D., Kim, C.-H., Moon, J.-I., Chung, Y.-G., Chang, M.-Y., Han, B.-S., Ko, S., Yang, E., Cha, K.Y., Lanza, R., et al. (2009a). Generation of human induced pluripotent stem cells by direct delivery of reprogramming proteins. Cell Stem Cell *4*, 472–476.

Kim, J.B., Sebastiano, V., Wu, G., Araúzo-Bravo, M.J., Sasse, P., Gentile, L., Ko, K., Ruau, D., Ehrich, M., van den Boom, D., et al. (2009b). Oct4-induced pluripotency in adult neural stem cells. Cell *136*, 411–419.

Klenk, H.-D. (1996). Post-translational modifications in insect cells. Cytotechnology *20*, 139–144.

Kress, E., and Gotta, M. (2011). Aurora A in cell division: kinase activity not required. Nat. Cell Biol. *13*, 638–639.

Kufer, T.A., Silljé, H.H.W., Körner, R., Gruss, O.J., Meraldi, P., and Nigg, E.A. (2002). Human TPX2 is required for targeting Aurora-A kinase to the spindle. J. Cell Biol. *158*, 617–623.

Lee, D.-F., Su, J., Ang, Y.-S., Carvajal-Vergara, X., Mulero-Navarro, S., Pereira, C.F., Gingold, J., Wang, H.-L., Zhao, R., Sevilla, A., et al. (2012a). Regulation of Embryonic and Induced Pluripotency by Aurora Kinase-p53 Signaling. Cell Stem Cell *11*, 179–194.

Lee, J., Sayed, N., Hunter, A., Au, K.F., Wong, W.H., Mocarski, E.S., Pera, R.R., Yakubov, E., and Cooke, J.P. (2012b). Activation of innate immunity is required for efficient nuclear reprogramming. Cell *151*, 547–558.

Li, Z., and Rana, T.M. (2012). A kinase inhibitor screen identifies small-molecule enhancers of reprogramming and iPS cell generation. Nat. Commun. *3*, 1085.

Lin, C.Y., Lovén, J., Rahl, P.B., Paranal, R.M., Burge, C.B., Bradner, J.E., Lee, T.I., and Young, R.A. (2012a). Transcriptional Amplification in Tumor Cells with Elevated c-Myc. Cell *151*, 56–67.

Lin, Y., Yang, Y., Li, W., Chen, Q., Li, J., Pan, X., Zhou, L., Liu, C., Chen, C., He, J., et al. (2012b). Reciprocal Regulation of Akt and Oct4 Promotes the Self-Renewal and Survival of Embryonal Carcinoma Cells. Mol. Cell *48*, 627–640.

Liu, Q., Kaneko, S., Yang, L., Feldman, R.I., Nicosia, S.V., Chen, J., and Cheng, J.Q. (2004). Aurora-A abrogation of p53 DNA binding and transactivation activity by phosphorylation of serine 215. J. Biol. Chem. *279*, 52175–52182.

Liu, X., Huang, J., Chen, T., Wang, Y., Xin, S., Li, J., Pei, G., and Kang, J. (2008). Yamanaka factors critically regulate the developmental signaling network in mouse embryonic stem cells. Cell Res. *18*, 1177–1189.

Livak, K.J., and Schmittgen, T.D. (2001). Analysis of relative gene expression data using real-time quantitative PCR and the 2(-Delta Delta C(T)) Method. Methods San Diego Calif *25*, 402–408.

Lu, L., Han, H., Tian, Y., Li, W., Zhang, J., Feng, M., and Li, Y. (2015). Aurora kinase A mediates c-Myc's oncogenic effects in hepatocellular carcinoma. Mol. Carcinog. *54*, 1467–1479.

Lu, L.-Y., Wood, J.L., Ye, L., Minter-Dykhouse, K., Saunders, T.L., Yu, X., and Chen, J. (2008). Aurora A Is Essential for Early Embryonic Development and Tumor Suppression. J. Biol. Chem. *283*, 31785–31790.

Malak, P.N., Dannenmann, B., Hirth, A., Rothfuss, O.C., and Schulze-Osthoff, K. (2015). Novel AKT phosphorylation sites identified in the pluripotency factors OCT4, SOX2 and KLF4. Cell Cycle *14*, 3748–3754.

Manfredi, M.G., Ecsedy, J.A., Chakravarty, A., Silverman, L., Zhang, M., Hoar, K.M., Stroud, S.G., Chen, W., Shinde, V., Huck, J.J., et al. (2011). Characterization of Alisertib (MLN8237), an investigational small-molecule inhibitor of aurora A kinase using novel in vivo pharmacodynamic assays. Clin. Cancer Res. *17*, 7614–7624.

Martini, M., De Santis, M.C., Braccini, L., Gulluni, F., and Hirsch, E. (2014). PI3K/AKT signaling pathway and cancer: an updated review. Ann. Med. *46*, 372–383.

Marumoto, T., Zhang, D., and Saya, H. (2005). Aurora-A — A guardian of poles. Nat. Rev. Cancer *5*, 42–50.

Mehra, R., Serebriiskii, I.G., Burtness, B., Astsaturov, I., and Golemis, E.A. (2013). Aurora kinases in head and neck cancer. Lancet Oncol. *14*, e425–e435.

Meraldi, P., Honda, R., and Nigg, E.A. (2002). Aurora-A overexpression reveals tetraploidization as a major route to centrosome amplification in p53-/- cells. EMBO J. *21*, 483–492.

Merz, B., Malak, P.N., and Rothfuss, O. (2015). Nuclear Akt: target for breast cancer therapy? Cell Cycle *14*, 2000–2000.

Nemes, C., Varga, E., Polgar, Z., Klincumhom, N., Pirity, M.K., and Dinnyes, A. (2014). Generation of mouse induced pluripotent stem cells by protein transduction. Tissue Eng. Part C Methods *20*, 383–392.

Nikonova, A.S., Astsaturov, I., Serebriiskii, I.G., Dunbrack, R.L., and Golemis, E.A. (2013). Aurora-A kinase (AURKA) in normal and pathological cell growth. Cell. Mol. Life Sci. *70*, 661–687.

Okita, K., and Yamanaka, S. (2011). Induced pluripotent stem cells: opportunities and challenges. Philos. Trans. R. Soc. Lond. B. Biol. Sci. *366*, 2198–2207.

Okita, K., Hong, H., Takahashi, K., and Yamanaka, S. (2010). Generation of mouse-induced pluripotent stem cells with plasmid vectors. Nat. Protoc. *5*, 418–428.

Olsen, J.V., and Macek, B. (2009). High accuracy mass spectrometry in large-scale analysis of protein phosphorylation. Methods Mol. Biol. *492*, 131–142.

Otto, T., Horn, S., Brockmann, M., Eilers, U., Schüttrumpf, L., Popov, N., Kenney, A.M., Schulte, J.H., Beijersbergen, R., Christiansen, H., et al. (2009). Stabilization of N-Myc Is a Critical Function of Aurora A in Human Neuroblastoma. Cancer Cell *15*, 67–78.

Pan, Y., Li, Y., Zhao, H., Zheng, J., Xu, H., Wei, G., Hao, J., and Cui, F. (2002). Bioadhesive polysaccharide in protein delivery system: chitosan nanoparticles improve the intestinal absorption of insulin in vivo. Int. J. Pharm. *249*, 139–147.

Peng, X., Draney, D.R., Volcheck, W.M., Bashford, G.R., Lamb, D.T., Grone, D.L., Zhang, Y., and Johnson, C.M. (2006). Phthalocyanine dye as an extremely photostable and highly fluorescent near-infrared labeling reagent. p. 60970E–60970E–12.

Radzisheuskaya, A., and Silva, J.C.R. (2014). Do all roads lead to Oct4? the emerging concepts of induced pluripotency. Trends Cell Biol. *24*, 275–284.

Radzisheuskaya, A., Le Bin Chia, G., dos Santos, R.L., Theunissen, T.W., Castro, L.F.C., Nichols, J., and Silva, J.C.R. (2013). A defined Oct4 level governs cell state transitions of pluripotency entry and differentiation into all embryonic lineages. Nat. Cell Biol. *15*, 579–590.

Reed, L.J., and Muench, H. (1938). A Simple Method of Estimating Fifty Per Cent Endpoints. Am. J. Epidemiol. *27*, 493–497.

Richard, I., Thibault, M., De Crescenzo, G., Buschmann, M.D., and Lavertu, M. (2013). Ionization behavior of chitosan and chitosan-DNA polyplexes indicate that chitosan has a similar capability to induce a proton-sponge effect as PEI. Biomacromolecules *14*, 1732–1740.

Robinton, D.A., and Daley, G.Q. (2012). The promise of induced pluripotent stem cells in research and therapy. Nature *481*, 295–305.

Ruchaud, S., Carmena, M., and Earnshaw, W.C. (2007). Chromosomal passengers: conducting cell division. Nat. Rev. Mol. Cell Biol. *8*, 798–812.

Sasai, K., Katayama, H., Stenoien, D.L., Fujii, S., Honda, R., Kimura, M., Okano, Y., Tatsuka, M., Suzuki, F., Nigg, E.A., et al. (2004). Aurora-C kinase is a novel chromosomal passenger protein that can complement Aurora-B kinase function in mitotic cells. Cell Motil. Cytoskeleton *59*, 249–263.

Saxe, J.P., Tomilin, A., Schöler, H.R., Plath, K., and Huang, J. (2009). Post-Translational Regulation of Oct4 Transcriptional Activity. PLoS ONE *4*, e4467.

Schaefer, T., and Lengerke, C. (2015). AKT-driven phospho-patterns of pluripotency. Cell Cycle *14*, 3784–3785.

Schöler, H.R., Dressler, G.R., Balling, R., Rohdewohld, H., and Gruss, P. (1990). Oct-4: a germline-specific transcription factor mapping to the mouse t-complex. EMBO J. *9*, 2185–2195.

Seki, A., Coppinger, J.A., Jang, C.-Y., Yates, J.R., and Fang, G. (2008). Bora and the kinase Aurora a cooperatively activate the kinase Plk1 and control mitotic entry. Science *320*, 1655–1658.

Shao, S., Wang, Y., Jin, S., Song, Y., Wang, X., Fan, W., Zhao, Z., Fu, M., Tong, T., Dong, L., et al. (2006). Gadd45a Interacts with Aurora-A and Inhibits Its Kinase Activity. J. Biol. Chem. *281*, 28943–28950.

Singh, S.M., and Panda, A.K. (2005). Solubilization and refolding of bacterial inclusion body proteins. J. Biosci. Bioeng. *99*, 303–310.

Sommer, C.A., Sommer, A.G., Longmire, T.A., Christodoulou, C., Thomas, D.D., Gostissa, M., Alt, F.W., Murphy, G.J., Kotton, D.N., and Mostoslavsky, G. (2010). Excision of reprogramming transgenes improves the differentiation potential of iPS cells generated with a single excisable vector. Stem Cells *28*, 64–74.

Stadtfeld, M., Nagaya, M., Utikal, J., Weir, G., and Hochedlinger, K. (2008). Induced pluripotent stem cells generated without viral integration. Science *322*, 945–949.

Tachibana, M., Amato, P., Sparman, M., Gutierrez, N.M., Tippner-Hedges, R., Ma, H., Kang, E., Fulati, A., Lee, H.-S., Sritanaudomchai, H., et al. (2013). Human Embryonic Stem Cells Derived by Somatic Cell Nuclear Transfer. Cell *153*, 1228–1238.

Tahmasebi, S., Ghorbani, M., Savage, P., Yan, K., Gocevski, G., Xiao, L., You, L., and Yang, X.-J. (2013). Sumoylation of Krüppel-like factor 4 inhibits pluripotency induction but promotes adipocyte differentiation. J. Biol. Chem. *288*, 12791–12804.

Takahashi, K. (2007). Induction of pluripotent stem cells from adult human fibroblasts by defined factors. Cell *131*, 861–872.

Takahashi, K., and Yamanaka, S. (2006). Induction of pluripotent stem cells from mouse embryonic and adult fibroblast cultures by defined factors. Cell *126*, 663–676.

Takahashi, K., Tanabe, K., Ohnuki, M., Narita, M., Ichisaka, T., Tomoda, K., and Yamanaka, S. (2007). Induction of pluripotent stem cells from adult human fibroblasts by defined factors. Cell *131*, 861–872.

Tammam, S., Malak, P., Correa, D., Rothfuss, O., Azzazy, H.M., Lamprecht, A., Schulze-Osthoff, K. (2016a). Nuclear delivery of recombinant OCT4 by chitosan nanoparticles for transgene-free generation of protein-induced pluripotent stem cells. Oncotarget *7*, 37728–37739.

Tammam, S.N., Azzazy, H.M., Breitinger, H.G., and Lamprecht, A. (2015a). Chitosan Nanoparticles for Nuclear Targeting: The Effect of Nanoparticle Size and Nuclear Localization Sequence Density. Mol. Pharm. *12*, 4277–4289.

Tammam, S.N., Azzazy, H.M.E., and Lamprecht, A. (2015b). A high throughput method for quantification of cell surface bound and internalized chitosan nanoparticles. Int. J. Biol. Macromol. *81*, 858–866.

Tammam, S.N., Azzazy, H.M.E., and Lamprecht, A. (2016b). How successful is nuclear targeting by nanocarriers? J. Controlled Release *229*, 140–153.

Tatsuka, M., Sato, S., Kanda, A., Miki, T., Kamata, N., Kitajima, S., Kudo, Y., and Takata, T. (2009). Oncogenic role of nuclear accumulated Aurora-A. Mol. Carcinog. *48*, 810–820.

Thier, M., Münst, B., and Edenhofer, F. (2010). Exploring refined conditions for reprogramming cells by recombinant Oct4 protein. Int. J. Dev. Biol. *54*, 1713–1721.

Thier, M., Münst, B., Mielke, S., and Edenhofer, F. (2012). Cellular reprogramming employing recombinant sox2 protein. Stem Cells Int. *2012*, 549846.

Thomson, J.A., Itskovitz-Eldor, J., Shapiro, S.S., Waknitz, M.A., Swiergiel, J.J., Marshall, V.S., and Jones, J.M. (1998). Embryonic Stem Cell Lines Derived from Human Blastocysts. Science *282*, 1145–1147.

Toya, M., Terasawa, M., Nagata, K., Iida, Y., and Sugimoto, A. (2011). A kinase-independent role for Aurora A in the assembly of mitotic spindle microtubules in Caenorhabditis elegans embryos. Nat. Cell Biol. *13*, 708–714.

Trinder, P. (1969). Determination of blood glucose using an oxidase-peroxidase system with a non-carcinogenic chromogen. J. Clin. Pathol. *22*, 158–161.

Van Hoof, D., Muñoz, J., Braam, S.R., Pinkse, M.W.H., Linding, R., Heck, A.J.R., Mummery, C.L., and Krijgsveld, J. (2009). Phosphorylation dynamics during early differentiation of human embryonic stem cells. Cell Stem Cell *5*, 214–226.

VandenDriessche, T., Ivics, Z., Izsvák, Z., and Chuah, M.K.L. (2009). Emerging potential of transposons for gene therapy and generation of induced pluripotent stem cells. Blood *114*, 1461–1468.

Vila, A., Sánchez, A., Janes, K., Behrens, I., Kissel, T., Vila Jato, J.L., and Alonso, M.J. (2004). Low molecular weight chitosan nanoparticles as new carriers for nasal vaccine delivery in mice. Eur J Pharm Biopharm *57*, 123–131.

Wagner, R.T., and Cooney, A.J. (2009). OCT4: Less is more. Cell Res. *19*, 527–528.

Walter, A.O., Seghezzi, W., Korver, W., Sheung, J., and Lees, E. (2000). The mitotic serine/threonine kinase Aurora2/AIK is regulated by phosphorylation and degradation. Oncogene *19*, 4906–4916.

Wang, Y.-C., Peterson, S.E., and Loring, J.F. (2014). Protein post-translational modifications and regulation of pluripotency in human stem cells. Cell Res. *24*, 143–160.

Wang, Y.-D., Cai, N., Wu, X.-L., Cao, H.-Z., Xie, L.-L., and Zheng, P.-S. (2013). OCT4 promotes tumorigenesis and inhibits apoptosis of cervical cancer cells by miR-125b/BAK1 pathway. Cell Death Dis. *4*, e760.

Warren, L., Manos, P.D., Ahfeldt, T., Loh, Y.-H., Li, H., Lau, F., Ebina, W., Mandal, P.K., Smith, Z.D., Meissner, A., et al. (2010). Highly Efficient Reprogramming to Pluripotency and Directed Differentiation of Human Cells with Synthetic Modified mRNA. Cell Stem Cell *7*, 618–630.

Watanabe, S., Umehara, H., Murayama, K., Okabe, M., Kimura, T., and Nakano, T. (2006). Activation of Akt signaling is sufficient to maintain pluripotency in mouse and primate embryonic stem cells. Oncogene *25*, 2697–2707.

Wei, F., Schöler, H.R., and Atchison, M.L. (2007). Sumoylation of Oct4 Enhances Its Stability, DNA Binding, and Transactivation. J. Biol. Chem. *282*, 21551–21560.

Yang, S., He, S., Zhou, X., Liu, M., Zhu, H., Wang, Y., Zhang, W., Yan, S., Quan, L., Bai, J., et al. (2010). Suppression of Aurora-A oncogenic potential by c-Myc downregulation. Exp. Mol. Med. *42*, 759–767.

Yu, J., Hu, K., Smuga-Otto, K., Tian, S., Stewart, R., Slukvin, I.I., and Thomson, J.A. (2009). Human induced pluripotent stem cells free of vector and transgene sequences. Science *324*, 797–801.

Zhang, H., Ma, Y., Gu, J., Liao, B., Li, J., Wong, J., and Jin, Y. (2012). Reprogramming of somatic cells via TAT-mediated protein transduction of recombinant factors. Biomaterials *33*, 5047–5055.

Zhou, H., Kuang, J., Zhong, L., Kuo, W.L., Gray, J.W., Sahin, A., Brinkley, B.R., and Sen, S. (1998). Tumour amplified kinase STK15/BTAK induces centrosome amplification, aneuploidy and transformation. Nat. Genet. *20*, 189–193.

Zhou, H., Wu, S., Joo, J.Y., Zhu, S., Han, D.W., Lin, T., Trauger, S., Bien, G., Yao, S., Zhu, Y., et al. (2009). Generation of induced pluripotent stem cells using recombinant proteins. Cell Stem Cell *4*, 381–384.

11. Appendix

Two further firefly luciferase reporters were utilized to confirm the kinase-independent regulation between AURKA on one side and c-MYC and OCT4 on the other side. The first reporter: E-box luciferase reporter (Figure 11.1) encodes the firefly luciferase gene under the control of a minimal (m) CMV promoter and tandem repeats of the c-Myc responsive element (E-box consensus CACGTG). The second reporter: Octamer luciferase reporter (Figure 11.2), likewise, encodes for firefly luciferase gene under the control of mCMV promoter but with tandem repeats of OCT4 responsive element (Octamer motif ATTTGCAT).

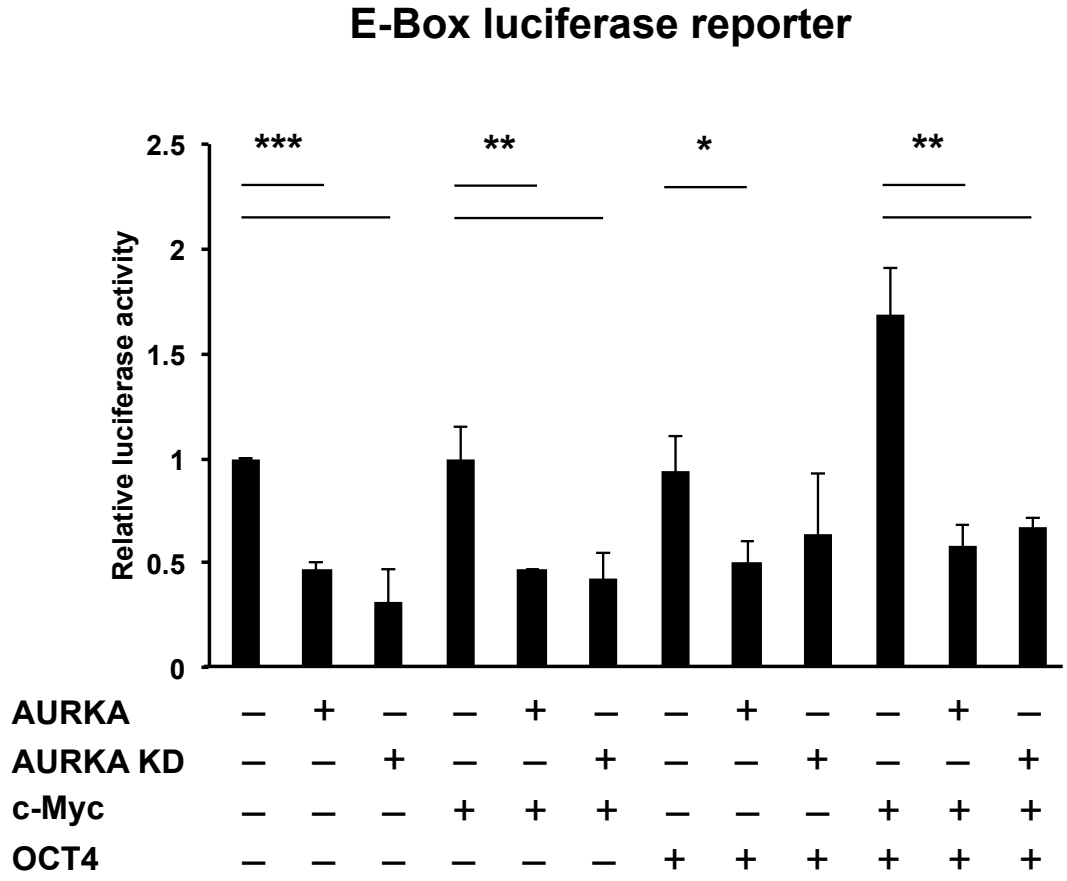

Figure 11.1: AURKA reduces c-MYC transcriptional activity on E-box reporter

Luciferase assay in HEK293 FT cells upon overexpression of c-MYC, OCT4, AURKA or AURKA kinase dead mutant (KD) using a firefly reporter coding for E-box binding site CACGTG. Cells were transfected with the indicated DNA, E-box firefly luciferase reporter and a constitutively expressing renilla construct as a transfection control. Cells were harvested 48 h after transfection. Luminescence values were normalized on renilla and GFP controls. n=3, results are expressed as mean ± sd. * p< 0.05, ** p< 0.01, *** p< 0.001.

In E-box reporter, upon overexpression of AURKA, the transcriptional activity of c-MYC in the luciferase assay decreased. Surprisingly, the same decrease was noticed upon overexpression of AURKA KD mutant (Figure 11.1). c-MYC overexpression did not increase the signal. This could be attributed to the prevalence of c-MYC in HEK293 FT cells. Therefore to confirm the specificity and sensitivity of the reporter towards c-MYC, luciferase assay with the same settings was performed in MEF cells, which have lower levels of c-MYC. In MEFs, c-MYC overexpression increased the relative luciferase activity 2 folds relative to the control (data not shown). OCT4 overexpression did not give any signal indicating the specificity of the reporter to c-MYC. However, overexpression of OCT4 together with c-MYC resulted in increase in the luciferase readout (Figure 11.1).

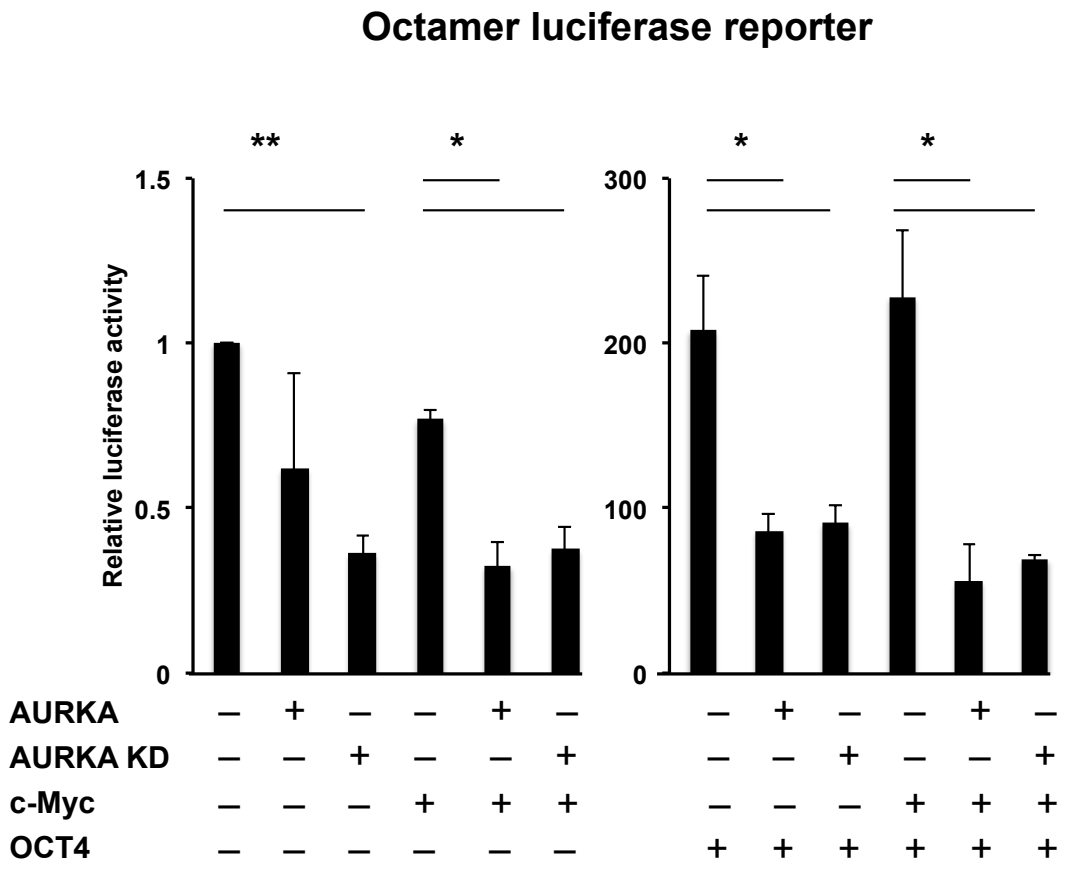

Figure 11.2: AURKA reduces OCT4 transcriptional activity on octamer motif

Luciferase assay in HEK293 FT cells upon overexpression of c-MYC, OCT4, AURKA or AURKA kinase dead mutant (KD) using a firefly reporter coding for octamer motif ATTTGCAT. Cells were transfected with the indicated DNA, octamer luciferase reporter and a constitutively expressing renilla construct as a transfection control. Cells were harvested 48 h after transfection. Luminescence values were normalized on renilla and GFP controls. n=3, results are expressed as mean ± sd. * $p < 0.05$, ** $p < 0.01$.

In Octamer reporter, similar results were observed, upon overexpression of AURKA or AURKA KD, the relative luciferase activity dropped in the absence of OCT4 or MYC or both. OCT4 overexpression highly activated the transcription of the luciferase gene increasing the signal to 200 folds. c-MYC did not have any effect indicating the specificity of the reporter to OCT4. However, AURKA or AURKA KD overexpression decreased the relative luciferase activity to the half when overexpressed with OCT4 or c-MYC or both (Figure 11.2).

Paper 1:

Novel AKT phosphorylation sites identified in the pluripotency factors OCT4, SOX2 and KLF4

Peter N Malak, Benjamin Dannenmann, Alexander Hirth, Oliver C Rothfuss, and Klaus Schulze-Osthoff

Cell Cycle 14:23, 3748–3754; December 1, 2015; © 2015 Taylor & Francis Group, LLC

Novel AKT phosphorylation sites identified in the pluripotency factors OCT4, SOX2 and KLF4

Peter N Malak[1], Benjamin Dannenmann[1], Alexander Hirth[1], Oliver C Rothfuss[1], and Klaus Schulze-Osthoff[1,2,*]

[1]Interfaculty Institute for Biochemistry; University of Tübingen; Tübingen, Germany; [2]German Cancer Consortium (DKTK) and German Cancer Research Center; Heidelberg, Germany

Keywords: AKT, c-MYC, KLF4, OCT4, phosphorylation, pluripotency, SOX2, stem cells

Abbreviations: BSA, bovine serum albumin; CV, column volume; GST, glutathione S-transferase; EMSA, electrophoretic mobility shift assay; MALDI, matrix-assisted laser desorption/ionization; MOI, multiplicity of infection; MS, mass spectrometry; OSKM, OCT4, SOX2, KLF4, c-MYC; UTF1, undifferentiated embryonic cell transcription factor 1

Downloaded by [Universitaetsbibliothek Tuebingen] at 23:33 17 December 2015

The four OSKM factors OCT4, SOX2, KLF4 and c-MYC are key transcription factors modulating pluripotency, self-renewal and tumorigenesis in stem cells. However, although their transcriptional targets have been extensively studied, little is known about how these factors are regulated at the posttranslational level. In this study, we established an *in vitro* system to identify phosphorylation patterns of the OSKM factors by AKT kinase. OCT4, SOX2, KLF4 and c-MYC were expressed in Sf9 insect cells employing the baculoviral expression system. OCT4, SOX2 and KLF4 were localized in the nucleus of insect cells, allowing their easy purification to near homogeneity upon nuclear fractionation. All transcription factors were isolated as biologically active DNA-binding proteins. Using *in vitro* phosphorylation and mass spectrometry-based phosphoproteome analyses several novel and known AKT phosphorylation sites could be identified in OCT4, SOX2 and KLF4.

Introduction

Stem cells require intricate regulatory networks governed by a limited number of key transcription factors in order to maintain self-renewal and pluripotency. Essential for these processes are the so-called OSKM factors including the transcription factors OCT4, SOX2, KLF4 and c-MYC.[1] The ectopic expression of solely OSKM factors is sufficient to reprogram terminally differentiated cells back to pluripotency in both human and mouse systems.[2,3] OSKM transcription factors are involved not only in pluripotency and differentiation of stem cells, but also in tumorigenesis.[4-11]

The expression of OSKM factors is controlled in a coordinated manner by several feedback loops and requires a tight regulation to maintain stem cell potential. A slight change in the amount of the proteins can lead to drastic alterations in cell fate that may eventually result in tumorigenesis. For instance, the level of OCT4, also known as POU5F1, is crucial for cell fate transitions and embryonic development.[12,13] If OCT4 protein is elevated more than 2-fold compared to normal conditions, stem cells loose their pluripotency and start differentiation into endoderm and mesoderm.[14] Moreover, a moderate increase of OCT4 is sufficient to cause to tumorigenesis e.g. of gonadal tumors.[15]

Both the expression levels and transcriptional activity of OSKM factors are fine-tuned by various posttranslational modifications, such as sumoylation, acetylation, methylation, O-GlcNAcylation and phosphorylation.[16-22] Recent evidence suggests that the serine/threonine kinase AKT plays a critical role not only in tumorigenesis, but is also required for self-renewal and pluripotency of normal cells.[23-25] AKT1 has been shown to directly phosphorylate OCT4, SOX2 and KLF4, modulating their nuclear localization, stability and transcriptional activity.[26-28] In particular, AKT phosphorylates OCT4 at T235 leading to enhanced apoptosis resistance and tumorigenic potential in mouse embryonic carcinoma cells.[29] Likewise, SOX2 phosphorylation at T118 by AKT results in decreased proteasomal degradation of SOX2 protein and enhanced self-renewal capacity of mouse embryonic stem cells.[27,30] In contrast, AKT-mediated phosphorylation of human KLF4 on T429 accelerates its degradation and thereby impairs stemness.[31] In addition to triggering posttranslational modifications, indirect links between AKT and certain OSKM factors, such SOX2, have been described. In mice, Akt has been suggested to repress *Sox2* transcription via a regulatory circuit involving FoxO1.[28] Moreover, AKT was reported to regulate *SOX2* transcriptional activity via p27 and miR-30a in nasopharyngeal cancers.[32] AKT mediates posttranslational modifications of the OSKM factors but, conversely,

*Correspondence to: Klaus Schulze-Osthoff; Email: kso@uni-tübingen.de
Submitted: 08/12/2015; Revised: 09/10/2015; Accepted: 09/29/2015
http://dx.doi.org/10.1080/15384101.2015.1104444
Revised Version Cell Cycle 2015CC6781

posttranslational modifications of OCT4 might also modulate AKT activity, thereby forming a positive feedback loop.[26,29] Thus, these data point to multiple mutual links between AKT and the OSKM factors, which might be critical for maintenance of stemness in malignant and non-malignant stem cells.

Despite the increasing evidence for the interaction of AKT with OSKM factors, the AKT-specific phosphorylation sites of the OSKM factors are still incompletely understood. Previous *in vitro* phosphorylation studies have been solely performed with recombinant OSKM proteins expressed in bacteria.[29,33] This approach exhibits several limitations, because the transcription factors are mostly expressed in inclusion bodies and need to be denatured and refolded *in vitro*. However, refolding of proteins from inclusion bodies is challenging and usually results in poor yields of natively folded, bioactive proteins.[34]

In the present study we developed a reliable *in vitro* tool to identify the AKT phosphorylation sites, based on the baculoviral expression of OCT4, SOX2, KLF4 and c-MYC in insect cells. This expression system is capable of performing most mammalian post-translational modifications, which are crucial for the regulation of transcriptions factors.[35] We show that all OSKM factors can be purified in a simple manner to near homogeneity as native proteins and – similar to their mammalian counterparts – retain essential activities, such as nuclear translocation and DNA binding. Using *in vitro* kinase assays coupled with mass spectrometry-based phosphoproteomics we could not only confirm previously reported phosphorylation sites, but were able to identify several new AKT phosphorylation sites within OCT4, SOX2 and KLF4. The described approach will be also suitable to explore additional posttranslational modifications of OSKM transcription factors.

Results

Recombinant OSKM factors translocate to the nucleus of Sf9 insect cells

A major advantage of the Sf9 baculovirus system is that, unlike bacterial expression systems, proteins can be produced in a native form retaining the correct subcellular compartmentalization and posttranslational modifications. To produce human OSKM proteins their cDNAs were cloned into the N-terminal glutathione S-transferase (GST) fusion plasmid pAcG2T. After cotransfection of the vector with linearized wildtype baculoviral DNA high-titer virus stocks were produced. To optimize protein production we first analyzed several multiplicities of infection (MOI) and incubation periods postinfection. In first fractionation experiments we noticed that OCT4, SOX2 and KLF4 were predominantly localized in the nucleus of Sf9 cells, whereas c-MYC was distributed both in cytoplasmic and nuclear fractions, as revealed by Coomassie staining and Western blotting (**Fig. 1A**). For the purification of OCT4, SOX2 and KLF4 we therefore developed a single-step nuclear extraction protocol, allowing an easy enrichment of the transcription factors by nuclear fractionation, whereas c-MYC was purified from whole cell lysates.

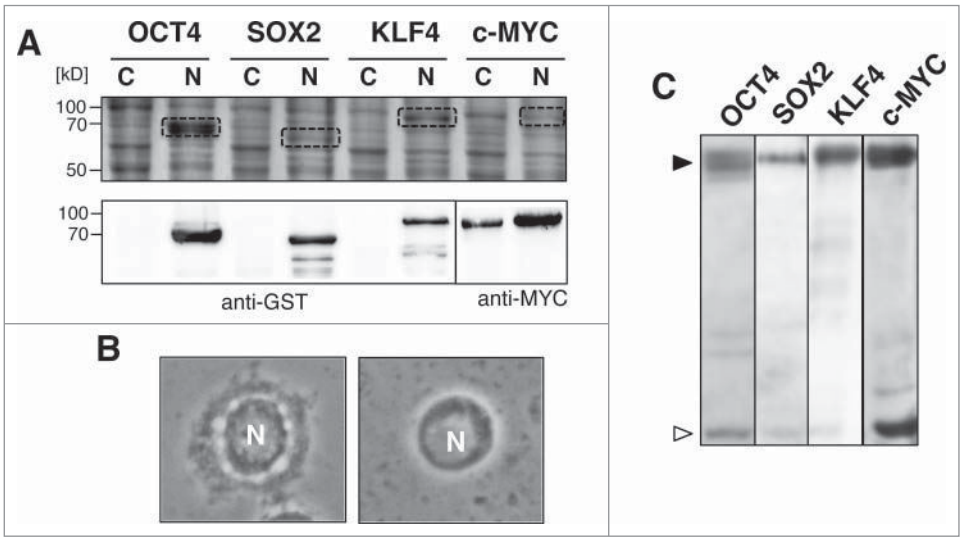

Figure 1. Recombinant OCT4, SOX2, and KLF4 are enriched in nuclear fractions of Sf9 insect cells. (**A**) Nuclear localization of OSKM factors: Sf9 cells were infected with baculoviruses encoding human OCT4, SOX2, KLF4 and c-MYC. Two days postinfection for SOX2, KLF4 and c-MYC, and 3 d postinfection for OCT4 cytosolic and nuclear fractions were prepared and subjected to SDS-PAGE. The upper panel shows a Coomassie blue staining of the gel with dotted boxes highlighting the protein of interest in the nuclear fractions. The lower panel shows an immunoblot using a GST antibody for the detection of OCT4, SOX2, and KLF4 and a MYC antibody for detection of c-MYC. (**B**) Representative microscopical pictures of the nuclear extraction. The nucleus (N) of Sf9 cells is shown before and after disruption of the cell membrane. 200x magnification. (**C**) SDS-PAGE of the purified OSKM factors following affinity chromatography on glutathione-coupled sepharose columns. The full-length proteins are marked with a close arrowhead, and the 27 kD GST fragment of the fusion proteins with an open arrowhead.

To prepare nuclear fractions Sf9 cells were swollen in hypotonic buffer and broken up with a Dounce homogenizer. Representative microscopic pictures show the successful nuclear extraction after disruption of the cell membrane (**Fig. 1B**). Following lysis of the nuclei for OCT4, SOX2 and KLF4 or of whole cells for c-MYC GST-affinity chromatography was performed. As revealed by silver staining, all transcription factors could be purified to near homogeneity (**Fig. 1C**). Purified KLF4 showed minor protein bands at 50 and 70 kDa, which were recognized by the KLF4 antibody and, as revealed by matrix-assisted laser desorption/ionization (MALDI) analysis, represented fragments of the transcription factor (data not shown). In addition, a minor GST band was found at 27 kDa, which was most pronounced for c-MYC, presumably due to its purification from cell lysates (**Fig. 1C**). Importantly, from

Downloaded by [Universitaetsbibliothek Tuebingen] at 23:33 17 December 2015

Sf9 suspension cultures considerable protein yields of the transcription factors could be obtained: i.e. OCT4: 6.1 mg/l; SOX2: 1.5 mg/l; c-MYC: 2.8 mg/l and KLF4: 3.8 mg/l.

Recombinant OSKM factors bind to their DNA consensus motifs in vitro

We next tested the DNA-binding activity of the purified factors using electrophoretic mobility shift assays (EMSAs) with different DNA consensus motifs (**Fig. 2**). Even a small amount (75 ng) of recombinant OCT4 was sufficient to reveal strong DNA binding to an octamer-binding site from the Ig heavy chain enhancer (1W motif). A slightly weaker DNA binding of OCT4 was detected to the OCT4-binding site from the enhancer of undifferentiated embryonic cell transcription factor 1 (UTF1) which contains an additional adjacent SOX2-binding site (**Fig. 2**). In addition, also DNA binding of recombinant SOX2 could be demonstrated to the classical DNA consensus site present in the miR-302 promoter as well as to the UTF1 site.[36]

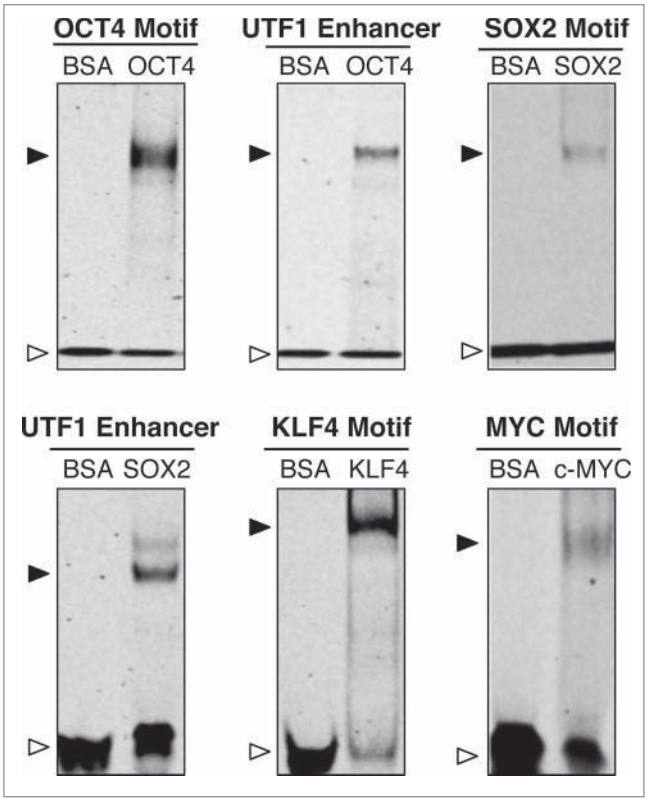

Figure 2. Recombinant OSKM factors retain DNA-binding activity. The purified OSKM factors were subjected to EMSA analysis. The DNA-binding activity of OCT4 was analyzed using oligonucleotides containing the OCT4 1W consensus motif or UTF1 enhancer sequence. SOX2 DNA binding was analyzed using oligonucleotides containing the SOX2 consensus motif or the UTF1 enhancer sequence. Similarly, the DNA-binding activity of KLF4 and c-MYC was tested with oligonucleotides containing the DNA consensus sequences of the transcription factors. Bovine serum albumin (BSA) was used as a negative control. The closed arrowheads indicate the specific protein-DNA complexes and the open arrowheads the unbound oligonucleotides.

Moreover, KLF4 bound efficiently to the typical DNA consensus sequence of the Nanog promoter. DNA binding of recombinant c-MYC to the classical E-box element was somewhat weaker but clearly detectable. For all transcription factors DNA-binding was abolished by competition with unlabeled oligonucleotides (data not shown). These results therefore suggest that recombinant OSKM factors retain not only their typical nuclear localization, but also their DNA-binding activity.

Identification of novel AKT phosphorylation sites in OCT4, SOX2 and KLF4

In order to investigate AKT phosphorylation sites of the different transcription factors, we incubated all 4 OSKM factors with active baculovirus-derived recombinant AKT1 in an *in-vitro* kinase assay. Subsequent immunoblotting of the reactions mixtures with an anti–phospho-(Ser/Thr) AKT substrate antibody, which recognizes AKT phosphorylation motif sequences, revealed that OCT4, SOX2 and KLF4 were efficiently phosphorylated by AKT (**Fig. 3A**). OCT4 showed several degradation products that were strongly phosphorylated by AKT, whereas no phosphorylation of c-MYC could be detected.

To identify the AKT phosphorylation sites of the different transcription factors we subjected *in vitro* phosphorylated as well the control OSKM factors to mass spectrometry (MS)-based phosphoproteomic analysis. As expected, we identified several intrinsic phosphorylation sites on OCT4 and KLF4 that were phosphorylated in the absence of ATP and AKT, indicating that the proteins were modified by the intrinsic phosphorylation machinery of Sf9 cells. Most phosphorylation sites however were dependent on AKT and their MS/MS spectra are depicted in Supplemental **Figures 1–9**. A representative spectrum of phosphorylation at of OCT4 at T225 is shown in **Figure 3B**. As published previously,[29] OCT4 was found to be further phosphorylated by AKT at T235. Importantly, our phosphoproteomic analysis identified 4 further unreported sites in OCT4 that were phosphorylated by AKT, namely, S136, T159, T225 and S236 (**Fig. 4**). In addition to OCT4, we found that AKT phosphorylated SOX2 at S83, which has been also yet not described. KLF4 was phosphorylated by AKT at 5 different sites: the already known residue T429, which is homologous to T399 in mouse,[31] and 4 further novel sites, namely, S19, T33, S234 and S326 (**Fig. 4**, Supplemental Figures 6–9).

Discussion

The self-renewal of pluripotent stem cells is dependent on a coordinated network of a key set of transcription factors, which require a tight regulation of their expression to maintain pluripotency. OSKM factors have not only attracted increased interest for their role in stemness and embryonic pathways, but have been also implicated in tumorigenesis. So far, the mechanisms that regulate the levels of OSKM factors are poorly understood and only partially controlled by transcriptional events. For instance, SOX2 and OCT4 promote their own transcription by cooperative binding to adjacent DNA sites in the promoter

Downloaded by [Universitaetsbibliothek Tuebingen] at 23:33 17 December 2015

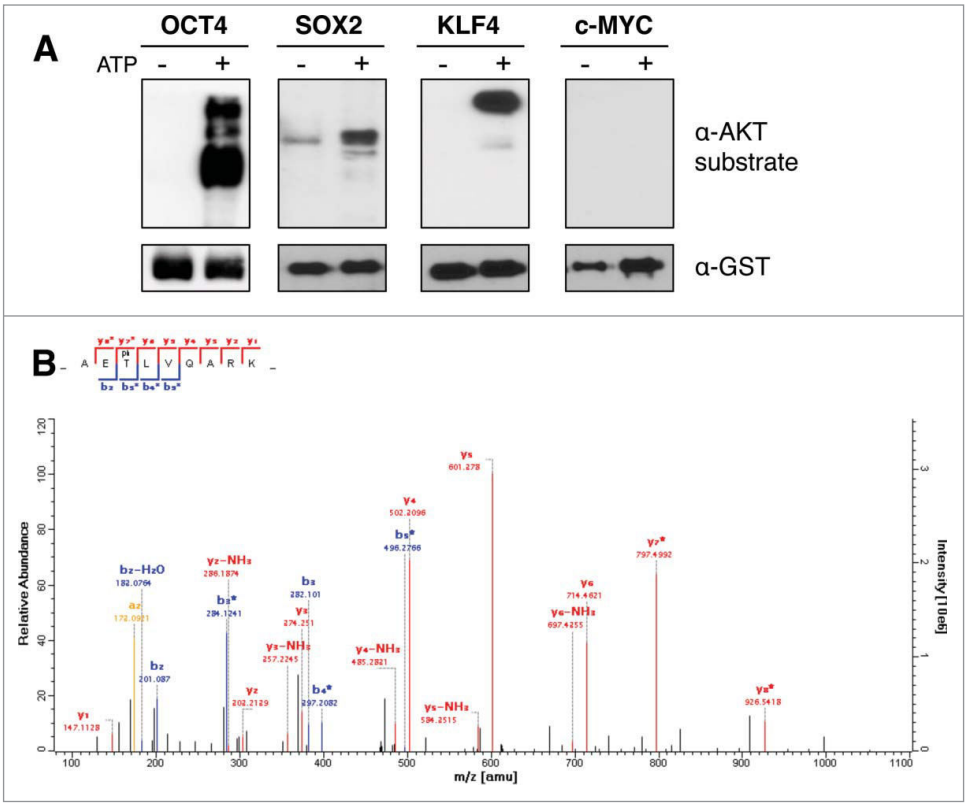

Figure 3. OCT4, SOX2 and KLF4, but not c-MYC are phosphorylated by AKT *in vitro*. (**A**) *In vitro* kinase assay: The purified OSKM factors were incubated with active AKT1 protein in the absence or presence of ATP, and immunoblotted with the indicated antibodies. (**B**) Representative mass spectrum demonstrating AKT-mediated phosphorylation of OCT4 at T225 following digestion with LysC.

regions of their genes.[37] Recent evidence highlights an important role of posttranslational modifications in regulating the levels and activity of pluripotency factors.[38] However, although the transcriptional targets of these factors have been extensively studied, very little is known about how the proteins are regulated at the posttranslational level.

The main intention of the present work was to establish an efficient *in vitro* system to study posttranslational modifications of the OSKM factors. To this end, we employed a baculoviral expression system for GST fusion proteins. We demonstrate that, with the exception of c-MYC, all OSKM factors were localized in the nuclear compartment and could be therefore efficiently enriched from nuclear fractions of Sf9 cells. In contrast to our study, previous *in vitro* phosphorylation studies used recombinant transcription factors expressed in bacteria.[29,33] Bacterial expression systems exhibit several limitations, because the recombinant proteins are mostly localized in inclusion bodies, requiring protein denaturation and an often inefficient refolding.[34] In line with this notion, we found that several commercial preparations of bacterially expressed OSKM factors lacked robust DNA-binding activity. In contrast, consistent with their function as transcription factors, the baculovirally expressed OSKM factors revealed strong DNA-binding activity to their consensus sequences.

We chose to study AKT-mediated phosphorylation of the OSKM factors, because, in addition to its established function as a survival factor, AKT is regarded as an important regulator of stemness.[25,29] Moreover, increasing evidence indicates that AKT exerts an essential function in cancer stem cell biology.[39,40] By combining *in vitro* phosphorylation and phosphoproteomic analyses, we were able to identify several novel putative AKT phosphorylation sites in the OSKM factors with the exception of c-MYC. For OCT4 we confirmed not only the previously reported AKT phosphorylation site T235,[29,33] but also found new phosphorylation sites at S136, T159, T225 and S236. Likewise, for KLF4 we identified the reported AKT target site at S429 [31] as well as novel phosphorylation sites at S19, T33, S234 and S326. Despite several attempts, however, we were unable to verify the reported T116 site of SOX2 (equivalent to T118 in the murine protein),[27] but identified a novel SOX2 phosphorylation site at S83.

It was reported that AKT-mediated phosphorylation of OCT4 at T235 promotes self-renewal, survival and the tumorigenic potential of embryonal carcinoma cells.[29] Mechanistically, AKT-mediated phosphorylation prevents its nuclear export and subsequent cytosolic degradation, resulting in increased stability and transcriptional activity of OCT4. Similarly, phosphorylation of OCT4 at the adjacent S236 site is likely to influence OCT4 activity.[41] Interestingly, the newly discovered site T225 in OCT4 is localized in POU DNA-binding domain, suggesting that phosphorylation at T225 might influence the DNA-binding and transcriptional activity of OCT4. Similar to OCT4, also the novel phosphorylation site of SOX2 at S83 is located within the DNA-binding domain as well as in one of the 2 nuclear localization sequences of SOX2. This might hint at the possibility that AKT-mediated phosphorylation of SOX2 might influence its nuclear import and DNA-binding activity. It should be noted that murine Sox2 can be also phosphorylated at T118 by AKT which not only promotes its stability, but also its activity to reprogram mouse embryonic fibroblasts.[27] How the AKT-mediated phosphorylation of KLF4 affects nuclear localization or transcriptional activity remains unknown. Interestingly, both the reported phosphorylation site at T429, which is equivalent to mouse T399,[31] as well as the newly identified T33 site are located in one of the 2 nuclear localization sequences of KLF4.

Downloaded by [Universitaetsbibliothek Tuebingen] at 23:33 17 December 2015

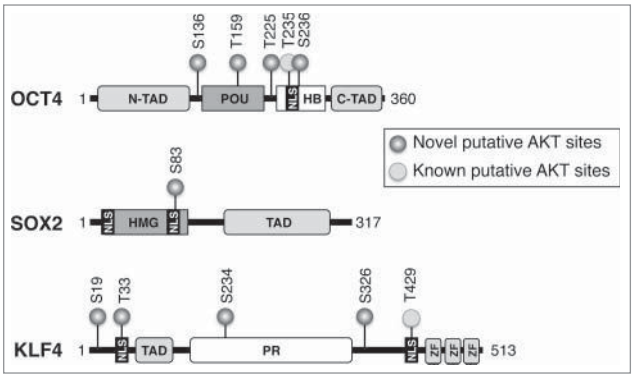

Figure 4. AKT phosphorylation sites in OCT4, SOX2 and KLF4. The scheme shows the novel and previously reported AKT phosphorylation sites with the functional domains of OCT4, SOX2 and KLF4. OCT4 contains POU-specific and homeodomain (HD) DNA-binding domains as well as transactivation domains located at the N-terminus (N-TAD) and C-terminus (C-TAD). SOX2 has a high mobility group (HMG) DNA-binding domain and a transactivation domain (TAD). KLF4 contains a single N-terminal TAD, a central proline-rich region (PR) and 3 zinc-finger (ZF) DNA-binding domains. NLS marks the nuclear localization sequences of the transcription factors.

With the exception of S326 in human KLF4, all phosphorylation sites that we identified in OCT4, SOX2 and KLF4 are also present in the mouse proteins. The novel sites discovered in this study are therefore valuable candidates for *in vivo* validation and further functional analyses. Recent evidence demonstrates that, in addition to phosphorylation events, further posttranslational modifications, including ubiquitination, sumoylation, methylation, acetylation or O-GlcNAcylation, may regulate the levels and activity of pluripotency factors.[38] Our *in vitro* system will be also useful to study these posttranslational modifications as well as their potential crosstalk in the OSKM factors. All constructs used in this study will be therefore made available to the scientific community.

Material and Methods

Recombinant protein expression in Sf9 cells

The cDNAs of human OCT4, SOX2, KLF4 and c-MYC were amplified using Pfx polymerase (Life Technologies) and flanked with a flag tag and BamH1 site from the 5′ end and EcoR1 site from the 3′ end. After digestion with EcoR1 and BamH1 (Thermo Scientific) and ligation with T4 ligase, the DNA amplicons were cloned into the insect cell transfer vector pAcG2T (BD Biosciences) encoding N-terminal GST fusion proteins. Following transformation of competent NEB 5-α *E. coli* the correct cloning of the inserts was verified by restriction analysis using PvuII. Sf9 insect cells were cultured at 27°C in Excell 420 medium (Sigma-Aldrich) supplemented with 10% fetal calf serum (PAA Laboratories). Recombinant baculoviruses were generated through homologous recombination after calcium phosphate transfection of the recombinant pAcG2T transfer vector and Baculogold Bright Linearized DNA (BD Biosciences). After virus amplification and production of high-titer virus stocks protein production of the transcription factors was performed in Sf9 cell suspension cultures. Different multiplicities of infections (MOIs) and incubation times postinfection were explored for each transcription factor to optimize protein production.

Purification of recombinant OSKM factors

Sf9 cells were harvested 2 d postinfection for SOX2, KLF4 and c-MYC, and 3 d postinfection for OCT4 at 2500 g for 10 min. OCT4, SOX2 and KLF4 were isolated from purified Sf9 cell nuclei. To this end, the cell pellet was washed with PBS and resuspended in a hypotonic buffer containing 10 mM Na-HEPES, pH 7.9, 10 mM KCl, 0.1 mM EDTA, 0.1 mM EGTA, 1 mM dithiothreitol and 0.5 mM PMSF. After incubation on ice for 15 min, cells were homogenized with 25 strokes in a Dounce homogenizer. After centrifugation at 7000 g for 10 min at 4°C, the nuclear pellet was resuspended in 5 pellet volumes of extraction buffer (20 mM Na-HEPES, pH 7.9, 400 mM KCl, 1 mM EDTA, 1 mM EGTA, 10% glycerol, 1 mM dithiothreitol, 10 nM aprotinin, 10 μM leupeptin, 0.5 μg/ml pepstatin and 0.5 mM PMSF), and incubated for 30 min at 4°C with rotation. For c-MYC, whole cell extraction was performed by incubating the cells for 45 min in ice-cold RIPA lysis buffer (25 mM Tris-HCl, pH 7.6, 150 mM NaCl, 1% NP-40, 1% sodium deoxycholate, 0.1% SDS) containing protease inhibitors. Both the nuclear and whole cell lysates were centrifuged at 50,000 g for 15 min at 4°C to remove cellular debris and filtered through a 0.45 μm filter. Protein purification was performed using GSTrap FF 1-ml columns (GE Healthcare) coupled to a peristaltic pump. The column was equilibrated with 5 column volumes (CV) of PBS, before the lysates were loaded with a flow-rate of 1 ml/min. After sample application, the column was washed with 10 CV PBS and proteins were eluted in 0.5 ml fractions with 5 CV glutathione elution buffer (10 mM GSH, 50 mM Tris-HCl, pH 8.0) at a flow rate of 0.2 ml/min. All steps were performed at 4°C.

Coomassie/silver staining and immunoblotting

The recombinant proteins were separated by 10% SDS-PAGE. For Coomassie staining, gels were stained for 1 h in staining solution (0.1% Coomassie brilliant blue R-250, 50% methanol and 10% acetic acid) and destained overnight in 10% acetic acid, 10% isopropanol and 10% methanol. For silver staining, gels were fixed for 30 min in 10% acetic acid and 40% ethanol, sensitized for 30 min in 40% ethanol, 8 mM $Na_2S_2O_3$ x 5 H_2O, 500 mM sodium acetate, and washed thrice for 5 min in H_2O. After staining in 30 mM silver nitrate solution for 30 min gels were washed in H_2O and developed in 100 ml of a solution containing 235 mM Na_2CO_3, 50 μl 37% formaldehyde and 25 μl 10% $Na_2S_2O_3$ x 5 H_2O. For Western blot analysis proteins were transferred onto polyvinylidenedifluoride membranes (Amersham Biosciences).[42,43] Membranes were blocked in PBS containing 4% BSA and 0.05% Tween-20 for 1 h, followed by an overnight incubation with the primary antibodies in

Downloaded by [Universitaetsbibliothek Tuebingen] at 23:33 17 December 2015

blocking buffer at 4°C. The following antibodies were used: mouse anti-GST (Santa Cruz, clone 1E5, 1:1000), mouse anti-c-MYC (Santa Cruz, clone A-14, 1:1000) and rabbit anti-phospho-(Ser/Thr) AKT substrate (RxRxxS/T) antibody (Cell Signaling, 1:1000). After washing the membrane in TBS/0.05% Tween and incubation with peroxidase-coupled secondary antibodies for 1 h proteins were visualized using ECL reagents (Amersham Biosciences).

Electrophoretic mobility shift assay (EMSA)

EMSA was performed using Odyssey® Infrared EMSA Kit (LI-COR Bioscience) according to the manufacturer's instructions. Briefly, the recombinant proteins were incubated with 1 μl of IRDye® 700 infrared dye-labeled double-stranded oligonucleotides, 2 μl of 10 × binding buffer, 2.5 mM DTT, 0.25% Tween-20 and 1 μg of poly(dI-dC) in a total volume of 20 μl for 20 min at room temperature in the dark. Samples were separated on 4% native polyacrylamide gels in 0.5 × Tris-borate-EDTA buffer. The gel was scanned by direct infrared fluorescence detection on the Odyssey® imaging system. The following oligonucleotides with high-affinity binding sites for the transcription factors were labeled from both 5′ and 3′ ends with IRDye 700: OCT4 (GCCGAA**TTTGCA**TATTTGCATGGCTG), UTF1 (CTGAAAGATGAGAGCCCT**CATTGTT***ATGCTAGT*GAAGTGCCAAGCTGA), SOX2 (CAGATAGAAAC**ACAATG**CCTTTCTCGGC), KLF4 (GTAGGGGGTGTGCCCGCCAGGAGGG**GTGGG**TCTAAGGTGATAGAGCCTTC) and c-MYC (GTGTTAATTGGGAG**CACGTG**TAGGTC). The DNA-binding sites are written in bold. In the UTF1 enhancer element, the OCT4-binding site is written in bold italic and the SOX2-binding site in bold.

Kinase Assays

Kinase assays were carried out essentially as described [44,45] in kinase buffer containing 25 mM Tris-HCl, pH 7.5, 5 mM β-glycerophosphate, 2 mM DTT, 0.1 mM sodium orthovanadate and 10 mM $MgCl_2$ with or without 200 μM ATP. Three μg of the recombinant substrates and 0.5 μg of active human AKT1 protein (Millipore) were incubated for 2 h at 30°C.

Mass spectrometry and data analysis

After the kinase assays proteins were processed for MS analyses as described [46] with the following changes: In-solution digestion was performed with endoproteinases Lys-C, trypsin or AspN. LC-MS/MS analyses were performed on an EasyLC nano-HPLC (Proxeon Biosystems) coupled to an LTQ Orbitrap Elite mass spectrometer (Thermo Scientific) as described.[47] For the analyses, 15 most intense precursor ions were sequentially fragmented in each scan cycle (90 min, HCD, top15). The MS data of all experiments were processed using default parameters of the MaxQuant software version 1.2.2.9.[48] Peak lists were searched against a human target-decoy database (taxonomy id 9606), containing 84946 forward protein sequences and 248 common contaminants, and GST-tagged versions of OCT4, SOX2 and KLF4. The following criteria were applied for the database search: Endoproteinases Lys-C, trypsin or AspN were defined as proteases and 2 missed cleavages were allowed. Carbamidomethylation of cysteine was set as fixed modification; N-terminal acetylation, oxidation of methionine, and phosphorylation of serine, threonine and tyrosine were set as variable modifications. Initial precursor mass tolerance was set to 7 ppm and 20 ppm at the fragment ion level. Identified MS/MS spectra were further processed by MaxQuant for statistical validation and quantification of peptides and protein groups. A false discovery rate of 1% was set at the peptide, protein and phosphorylation site level.

Disclosure of Potential Conflicts of Interest

No potential conflicts of interest were disclosed.

Acknowledgments

We thank Boris Maček and Ana Velic for the proteome analyses.

Funding

This study was supported by the Baden-Württemberg Foundation (Adult Stem Cells II Program), the Deutsche Forschungsgemeinschaft (GRK1302, SFB665) and the German Ministry for Education and Research (AID-NET; 01FP09104B).

References

1. Loh YH, Ng JH, Ng HH. Molecular framework underlying pluripotency. Cell Cycle 2008; 7:885-91; PMID:18414030; http://dx.doi.org/10.4161/cc.7.7.5636
2. Takahashi K, Yamanaka S. Induction of pluripotent stem cells from mouse embryonic and adult fibroblast cultures by defined factors. Cell 2006; 126:663-76; PMID:16904174; http://dx.doi.org/10.1016/j.cell.2006.07.024
3. Li Y, Shen Z, Shelat H, Geng YJ. Reprogramming somatic cells to pluripotency: a fresh look at Yamanaka's model. Cell Cycle 2013; 12:3594-8; PMID:24189530; http://dx.doi.org/10.4161/cc.26952
4. Ben-Porath I, Thomson MW, Carey VJ, Ge R, Bell GW, Regev A, Weinberg RA. An embryonic stem cell-like gene expression signature in poorly differentiated aggressive human tumors. Nat Genet 2008; 40:499-507; PMID:18443585; http://dx.doi.org/10.1038/ng.127
5. Bass AJ, Watanabe H, Mermel CH, Yu S, Perner S, Verhaak RG, Kim SY, Wardwell L, Tamayo P, Gat-Viks I, et al. SOX2 is an amplified lineage-survival oncogene in lung and esophageal squamous cell carcinomas. Nat Genet 2009; 41:1238-42; PMID:19801978; http://dx.doi.org/10.1038/ng.465
6. Corominas-Faja B, Cufí S, Oliveras-Ferraros C, Cuyàs E, López-Bonet E, Lupu R, Alarcón T, Vellon L, Iglesias JM, Leis O, et al. Nuclear reprogramming of luminal-like breast cancer cells generates SOX2-overexpressing cancer stem-like cellular states harboring transcriptional activation of the mTOR pathway. Cell Cycle 2013; 12:3109-24; PMID:23974095; http://dx.doi.org/10.4161/cc.26173
7. Vazquez-Martin A, Cufí S, López-Bonet E, Corominas-Faja B, Cuyàs E, Vellon L, Iglesias JM, Leis O, Martín AG, Menendez JA. Reprogramming of non-genomic estrogen signaling by the stemness factor SOX2 enhances the tumor-initiating capacity of breast cancer cells. Cell Cycle 2013; 12:3471-7; PMID:24107627; http://dx.doi.org/10.4161/cc.26692
8. Marzi I, Cipolleschi MG, D'Amico M, Stivarou T, Rovida E, Vinci MC, Pandolfi S, Dello Sbarba P, Stecca B, Olivotto M. The involvement of a Nanog, KLF4 and c-MYC transcriptional circuitry in the intertwining between neoplastic progression and reprogramming. Cell Cycle 2013; 12:353-64; PMID:23287475; http://dx.doi.org/10.4161/cc.23200
9. Hussenet T, du Manoir S. SOX2 in squamous cell carcinoma: amplifying a pleiotropic oncogene along carcinogenesis. Cell Cycle 2010; 9:1480-6; PMID:20372069; http://dx.doi.org/10.4161/cc.9.8.11203
10. Bareiss PM, Paczulla A, Wang H, Schairer R, Wiehr S, Kohlhofer U, Rothfuss OC, Fischer A, Perner S,

Downloaded by [Universitaetsbibliothek Tuebingen] at 23:33 17 December 2015

Downloaded by [Universitaetsbibliothek Tuebingen] at 23:33 17 December 2015

Staebler A, et al. SOX2 expression associates with stem cell state in human ovarian carcinoma. Cancer Res 2013; 73:5544-55; PMID:23867475; http://dx.doi.org/10.1158/0008-5472.CAN-12-4177

11. Boumahdi S, Driessens G, Lapouge G, Rorive S, Nassar D, Le Mercier M, Delatte B, Caauwe A, Lenglez S, Nkusi E, et al. SOX2 controls tumour initiation and cancer stem-cell functions in squamous-cell carcinoma. Nature 2014; 511:246-50; PMID:24909994; http://dx.doi.org/10.1038/nature13305
12. Stefanovic S, Pucéat M. Oct-3/4: not just a gatekeeper of pluripotency for embryonic stem cell, a cell fate instructor through a gene dosage effect. Cell Cycle 2007; 6:8-10; PMID:17245123; http://dx.doi.org/10.4161/cc.6.1.3633
13. Radzisheuskaya A, Chia Gle B, dos Santos RL, Theunissen TW, Castro LF, Nichols J, Silva JC. A defined OCT4 level governs cell state transitions of pluripotency entry and differentiation into all embryonic lineages. Nat Cell Biol 2013; 15:579-90; PMID:23629142; http://dx.doi.org/10.1038/ncb2742
14. Niwa H, Miyazaki J, Smith AG. Quantitative expression of Oct-3/4 defines differentiation, dedifferentiation or self-renewal of ES cells. Nat Genet 2000; 24:372-6; PMID:10742100; http://dx.doi.org/10.1038/74199
15. Ovitt CE, Schöler HR. The molecular biology of Oct-4 in the early mouse embryo. Mol Hum Reprod 1998; 4:1021-31; PMID:9835353; http://dx.doi.org/10.1093/molehr/4.11.1021
16. Tahmasebi S, Ghorbani M, Savage P, Yan K, Gocevski G, Xiao L, You L, Yang XJ. Sumoylation of Krüppel-like factor 4 inhibits pluripotency induction but promotes adipocyte differentiation. J Biol Chem 2013; 288:12791-804; PMID:23515309; http://dx.doi.org/10.1074/jbc.M113.465443
17. Wei F, Schöler HR, Atchison ML. Sumoylation of OCT4 enhances its stability, DNA binding, and transactivation. J Biol Chem 2007; 282:21551-60; PMID:17525163; http://dx.doi.org/10.1074/jbc.M611041200
18. González-Prieto R, Cuijpers SA, Kumar R, Hendriks IA, Vertegaal AC. c-MYC is targeted to the proteasome for degradation in a SUMOylation-dependent manner, regulated by PIAS1, SENP7 and RNF4. Cell Cycle 2015; 14:1859-72; http://dx.doi.org/10.1080/15384101.2015.1040965
19. Baltus GA1, Kowalski MP, Zhai H, Tutter AV, Quinn D, Wall D, Kadam S. Acetylation of SOX2 induces its nuclear export in embryonic stem cells. Stem Cells 2009; 27:2175-84; PMID:19591226; http://dx.doi.org/10.1002/stem.168
20. Van Hoof D, Muñoz J, Braam SR, Pinkse MW, Linding R, Heck AJ, Mummery CL, Krijgsveld J. Phosphorylation dynamics during early differentiation of human embryonic stem cells. Cell Stem Cell 2009; 5:214-26; PMID:19664995; http://dx.doi.org/10.1016/j.stem.2009.05.021
21. Swaney DL, Wenger CD, Thomson JA, Coon JJ. Human embryonic stem cell phosphoproteome revealed by electron transfer dissociation tandem mass spectrometry. Proc Natl Acad Sci USA 2009; 106:995-1000; PMID:19144917; http://dx.doi.org/10.1073/pnas.0811964106
22. Jang H, Kim TW, Yoon S, Choi SY, Kang TW, Kim SY, Kwon YW, Cho EJ, Youn HD. O-GlcNAc regulates pluripotency and reprogramming by directly acting on core components of the pluripotency network. Cell Stem Cell 2012; 11:62-74; PMID:22608532; http://dx.doi.org/10.1016/j.stem.2012.03.001
23. Altomare DA, Testa JR. Perturbations of the AKT signaling pathway in human cancer. Oncogene 2005; 24:7455-64; PMID:16288292; http://dx.doi.org/10.1038/sj.onc.1209085
24. Gonzalez E, McGraw TE. The AKT kinases: isoform specificity in metabolism and cancer. Cell Cycle 2009; 8:2502-8; PMID:19597332; http://dx.doi.org/10.4161/cc.8.16.9335
25. Watanabe S, Umehara H, Murayama K, Okabe M, Kimura T, Nakano T. Activation of AKT signaling is sufficient to maintain pluripotency in mouse and primate embryonic stem cells. Oncogene 2006; 25:2697-707; PMID:16407845; http://dx.doi.org/10.1038/sj.onc.1209307
26. Campbell PA, Rudnicki MA. OCT4 interaction with Hmgb2 regulates AKT signaling and pluripotency. Stem Cells 2013; 31:1107-20; PMID:23495099; http://dx.doi.org/10.1002/stem.1365
27. Jeong CH, Cho YY, Kim MO, Kim SH, Cho EJ, Lee SY, Jeon YJ, Lee KY, Yao K, Keum YS, Bode AM, Dong Z. (2010). Phosphorylation of SOX2 cooperates in reprogramming to pluripotent stem cells. Stem Cells 2010; 28:2141-50; PMID:20945330; http://dx.doi.org/10.1002/stem.540
28. Ormsbee Golden BD, Wuebben EL, Rizzino A. SOX2 expression is regulated by a negative feedback loop in embryonic stem cells that involves AKT signaling and FoxO1. PLoS One 2013; 8:e76345; PMID:24116102; http://dx.doi.org/10.1371/journal.pone.0076345
29. Lin Y, Yang Y, Li W, Chen Q, Li J, Pan X, Zhou L, Liu C, Chen C, He J, et al. Reciprocal regulation of AKT and OCT4 promotes the self-renewal and survival of embryonal carcinoma cells. Mol Cell 2012; 48:627-40; PMID:23041284; http://dx.doi.org/10.1016/j.molcel.2012.08.030
30. Fang L, Zhang L, Wei W, Jin X, Wang P, Tong Y, Li J, Du JX, Wong J. A methylation-phosphorylation switch determines SOX2 stability and function in ESC maintenance or differentiation. Mol Cell 2014; 55:537-51; PMID:25042802; http://dx.doi.org/10.1016/j.molcel.2014.06.018
31. Chen B, Xue Z, Yang G, Shi B, Yang B, Yan Y, Wang X, Han D, Huang Y, Dong W. AKT-signal integration is involved in the differentiation of embryonal carcinoma cells. PLoS One 2013; 8:e64877; PMID:23762260; http://dx.doi.org/10.1371/journal.pone.0064877
32. Qin J, Ji J, Deng R, Tang J, Yang F, Feng GK, Chen WD, Wu XQ, Qian XJ, Ding K, Zhu XF. DC120, a novel AKT inhibitor, preferentially suppresses nasopharyngeal carcinoma cancer stem-like cells by downregulating Sox2. Oncotarget 2015; 6:6944-58; PMID:25749514; http://dx.doi.org/10.18632/oncotarget.3128
33. Brumbaugh J, Hou Z, Russell JD, Howden SE, Yu P, Ledvina AR, Coon JJ, Thomson JA. Phosphorylation regulates human OCT4. Proc Natl Acad Sci USA 2012; 109:7162-8; PMID:22474382; http://dx.doi.org/10.1073/pnas.1203874109
34. Singh SM, Panda AK. Solubilization and refolding of bacterial inclusion body proteins. J Biosci Bioeng 2005; 99:303-10; PMID:16233795; http://dx.doi.org/10.1263/jbb.99.303
35. Klenk HD. Post-translational modifications in insect cells. Cytotechnology 1996; 20:139-44; PMID:22358478; http://dx.doi.org/10.1007/BF00350394
36. Boyer LA, Lee TI, Cole MF, Johnstone SE, Levine SS, Zucker JP, Guenther MG, Kumar RM, Murray HL, Jenner RG, et al. Core transcriptional regulatory circuitry in human embryonic stem cells. Cell 2005; 122:947-56; PMID:16153702; http://dx.doi.org/10.1016/j.cell.2005.08.020
37. Chew JL1, Loh YH, Zhang W, Chen X, Tam WL, Yeap LS, Li P, Ang YS, Lim B, Robson P, Ng HH. Reciprocal transcriptional regulation of Pou5f1 and SOX2 via the OCT4/SOX2 complex in embryonic stem cells. Mol Cell Biol 2005; 25:6031-46; PMID:15988017; http://dx.doi.org/10.1128/MCB.25.14.6031-6046.2005
38. Cai N, Li M, Qu J, Liu GH, Izpisua Belmonte JC. Post-translational modulation of pluripotency. J Mol Cell Biol 2012; 4:262-5; PMID:22679102; http://dx.doi.org/10.1093/jmcb/mjs031
39. Martini M, De Santis MC, Braccini L, Gulluni F, Hirsch E. PI3K/AKT signaling pathway and cancer: an updated review. Ann Med 2014; 46:372-83; PMID:24897931; http://dx.doi.org/10.3109/07853890.2014.912836
40. Merz B, Malak PN, Rothfuss O. Nuclear AKT: target for breast cancer therapy? Cell Cycle 2015; 14:2000; PMID:25970831; http://dx.doi.org/10.1080/15384101.2015.1049089
41. Saxe JP, Tomilin A, Schöler HR, Plath K, Huang J. Post-translational regulation of Oct4 transcriptional activity. PLoS One 2009; 4:e4467; PMID:19221599; http://dx.doi.org/10.1371/journal.pone.0004467
42. Dannenmann B, Lehle S, Hildebrand DG, Kübler A, Grondona P, Schmid V, Holzer K, Fröschl M, Essmann F, Rothfuss O, Schulze-Osthoff K. High glutathione and glutathione peroxidase-2 levels mediate cell-type-specific DNA damage protection in human induced pluripotent stem cells. Stem Cell Reports 2015; 4:886-98; PMID:25937369; http://dx.doi.org/10.1016/j.stemcr.2015.04.004
43. Sohn D, Schulze-Osthoff K, Jänicke RU. Caspase-8 can be activated by interchain proteolysis without receptor-triggered dimerization during drug-induced apoptosis. J Biol Chem 2005; 280:5267-73; PMID:15611097; http://dx.doi.org/10.1074/jbc.M408585200
44. Keil E, Höcker R, Schuster M, Essmann F, Ueffing N, Hoffman B, Liebermann DA, Pfeffer K, Schulze-Osthoff K, Schmitz I. Phosphorylation of Atg5 by the Gadd45β-MEKK4-p38 pathway inhibits autophagy. Cell Death Differ 2013; 20:321-32; PMID:23059785; http://dx.doi.org/10.1038/cdd.2012.129
45. Belka C, Marini P, Lepple-Wienhues A, Budach W, Jekle A, Los M, Lang F, Schulze-Osthoff K, Gulbins E, Bamberg M. The tyrosine kinase lck is required for CD95-independent caspase-8 activation and apoptosis in response to ionizing radiation. Oncogene 1999; 18:4983-92; PMID:10490833; http://dx.doi.org/10.1038/sj.onc.1202878
46. Olsen JV, Macek B. High accuracy mass spectrometry in large-scale analysis of protein phosphorylation. Methods Mol Biol 2009; 492:131-42; PMID:19241030; http://dx.doi.org/10.1007/978-1-59745-493-3_7
47. Franz-Wachtel M, Eisler SA, Krug K, Wahl S, Carpy A, Nordheim A, Pfizenmaier K, Hausser A, Macek B. Global detection of protein kinase D-dependent phosphorylation events in nocodazole-treated human cells. Mol Cell Proteomics 2012; 11:160-70; PMID:22496350; http://dx.doi.org/10.1074/mcp.M111.016014
48. Cox J, Matic I, Hilger M, Nagaraj N, Selbach M, Olsen JV, Mann M. A practical guide to the MaxQuant computational platform for SILAC-based quantitative proteomics. Nat Protoc 2009; 4:698-705; PMID:19373234; http://dx.doi.org/10.1038/nprot.2009.36

Paper 2:

Nuclear delivery of recombinant OCT4 by chitosan nanoparticles for transgene-free generation of protein-induced pluripotent stem cells

Salma Tammam*, **Peter Malak***, Daphne Correa, Oliver Rothfuss, Hassan ME Azzazy, Alf Lamprecht1, Klaus Schulze-Osthoff

* Shared first authorship

Nuclear delivery of recombinant OCT4 by chitosan nanoparticles for transgene-free generation of protein-induced pluripotent stem cells

Salma Tammam[1,2,#], Peter Malak[3,#], Daphne Correa[3], Oliver Rothfuss[3], Hassan ME Azzazy[2], Alf Lamprecht[1,4,*], Klaus Schulze-Osthoff[3,5,*]

[1]Laboratory of Pharmaceutical Technology and Biopharmaceutics, University of Bonn, 53121 Bonn, Germany

[2]Department of Chemistry, The American University in Cairo, 11835 Cairo, Egypt

[3]Interfaculty Institute for Biochemistry, University of Tuebingen, 72076 Tuebingen, Germany

[4]Laboratory of Pharmaceutical Engineering, University of Franche-Comté, Besançon 25000, France

[5]German Cancer Consortium (DKTK) and German Cancer Research Center, 69120 Heidelberg, Germany

[#]Co-first authors, these authors contributed equally to this work

[*]These authors have contributed equally and share senior authorship

Correspondence to: Klaus Schulze-Osthoff, **e-mail:** kso@uni-tuebingen.de

Keywords: *induced pluripotent stem cells, OCT4, transgene-free stem cells, chitosan nanoparticles, reprogramming*

Received: *March 03, 2016* ***Accepted:*** *April 16, 2016* ***Published:*** *May 10, 2016*

ABSTRACT

Protein-based reprogramming of somatic cells is a non-genetic approach for the generation of induced pluripotent stem cells (iPSCs), whereby reprogramming factors, such as OCT4, SOX2, KLF4 and c-MYC, are delivered as functional proteins. The technique is considered safer than transgenic methods, but, unfortunately, most protein-based protocols provide very low reprogramming efficiencies. In this study, we developed exemplarily a nanoparticle (NP)-based delivery system for the reprogramming factor OCT4. To this end, we expressed human OCT4 in Sf9 insect cells using a baculoviral expression system. Recombinant OCT4 showed nuclear localization in Sf9 cells indicating proper protein folding. In comparison to soluble OCT4 protein, encapsulation of OCT4 in nuclear-targeted chitosan NPs strongly stabilized its DNA-binding activity even under cell culture conditions. OCT4-loaded NPs enabled cell treatment with high micromolar concentrations of OCT4 and successfully delivered active OCT4 into human fibroblasts. Chitosan NPs therefore provide a promising tool for the generation of transgene-free iPSCs.

INTRODUCTION

The generation of human induced pluripotent stem cells (iPSCs) from somatic cells represents a major advancement in stem cell biology, especially because of their many potential applications including patient-specific tissue replacement, drug screening and disease modeling [1, 2]. Human somatic cells can be reprogrammed to iPSCs by the ectopic expression of the four pluripotency-related transcription factors OCT4, SOX2, KLF4 and c-MYC, also known as the OSKM factors [3, 4].

In most cases the OSKM factors are introduced via retroviral transduction, which however bears the risk of insertional mutagenesis of the genome-integrating viruses [5, 6]. Indeed, retroviral vector DNAs can insert at a large number of sites in the host genome and promote the expression of oncogenes or disrupt tumor suppressor genes. Several protocols have been explored to circumvent the integration of foreign DNA into the genome. These include the transient expression of reprogramming factors using non-integrating adenoviruses, plasmids, RNA, episomal vectors or the excision of the transgenes after reprogramming by site-specific recombinases or transposases [7–13]. While such approaches reduce the risk of insertional mutagenesis, nucleic acid-free approaches by the direct delivery of reprogramming proteins represent presumably the safest methods with respect to future clinical applications of iPSCs. In addition,

the use of proteins also avoids the sustained expression of transgenes after reprogramming. Since pluripotency factors are not only crucial for stemness but also involved in tumorigenesis, their expression should be restricted to the reprogramming process [14–18].

A major hurdle for the intracellular delivery of proteins is their limited ability to cross the cell membrane. Small protein transduction domains (PTDs) from proteins (e.g., HIV-TAT) can be fused to proteins of interest to facilitate their delivery into host cells [19–21]. Nevertheless, reprogramming by PTD-bearing proteins is very slow (≈8 weeks) and inefficient (≈0.001% reprogramming rate) compared to retrovirus-based protocols (≈0.01% of input cells). The low success of protein-induced stem cell generation is presumably caused by the low stability and solubility of recombinant reprogramming factors as well as their poor endosomal release. Therefore, further developments in protein delivery systems are required to enhance the efficiency of reprogramming to iPSCs.

Polymeric nanoparticles (NPs), such as chitosan NPs, offer a more promising approach. Apart from their biocompatibility and biodegradability, their ability to encapsulate therapeutic biomolecules protects them from premature degradation [22–26]. Chitosan [poly(N-acetyl glucosamine)] is a biodegradable polysaccharide that can be used to formulate NPs by several methods. The ionotropic gelation method, which allows the incorporation of the therapeutic protein into the NPs, occurs via mild electrostatic interactions in aqueous, physiological conditions [22]. As cationic polymers chitosan NPs adhere to the negatively charged cell surface, facilitating their cellular uptake by endocytosis [27]. The presence of primary amine groups on the NP surface facilitates endosomal escape via the proton sponge effect. Moreover, tagging of nuclear localization sequences (NLS) to the chitosan NPs allows directing NPs to the cell nucleus [28].

Among the OSKM factors, the transcription factor OCT4 (POU5F1) is of particular importance for reprogramming and the self-renewal of stem cells [29]. OCT4 is highly expressed in pluripotent cells and becomes silenced upon differentiation. The precise expression level of OCT4 determines the fate of embryonic stem cells [30]. DNA binding of OCT4 to promoter regions initiates transcription of various genes involved in pluripotency or self-renewal, such as *NANOG* and *SOX2* [31–32]. OCT4 is therefore considered a master regulator for the maintenance of pluripotent cells and successful reprogramming with *OCT4* alone has been shown [33]. It was however reported that recombinant OCT4 protein has a limited solubility and stability under cell culture conditions. Furthermore, recombinant cell-permeant OCT4-TAT fusion proteins show a weak endosomal release after cellular uptake, which, in addition to their poor stability, represents another bottleneck for achieving robust reprogramming by protein transduction [34, 35].

Various expression systems are available for recombinant protein production. Several groups reported the expression of OCT4 in *E. coli* or mammalian cells [19–21, 36]. Bacterially expressed OCT4 is usually found in inclusion bodies and needs to be denatured and refolded *in vitro*. The refolding process is cumbersome and results in very poor yields of properly folded active proteins [37]. On the other hand, OCT4 expressed in mammalian cells can be purified in a native state, but production of large quantities of purified and active protein remains challenging. This limitation might be overcome by the baculoviral expression system in Sf9 insect cells, which can provide high yields of functional proteins [38].

In this study, we report the formulation of nuclear-targeted chitosan NPs for human OCT4. OCT4 was expressed in Sf9 insect cells, evaluated with respect to its activity and nuclear localization and encapsulated in chitosan NPs. Chitosan NPs were able to considerably stabilize the DNA-binding activity of recombinant OCT4 as well as to deliver the OCT4 cargo into nuclei of human fibroblasts. Our study therefore demonstrates a proof-of-concept for a DNA-free protein transduction system, making chitosan NPs a promising and safe tool for cellular reprogramming and derivation of transgene-free iPSCs.

RESULTS

Chitosan NP formulation and characterization

To demonstrate that chitosan NPs preserve protein activity we initially encapsulated horseradish peroxidase (HRP) as a model protein and investigated the encapsulation efficiency and release profile from small (S-NPs) and large (L-NPs) nanoparticles. Scanning electron microcopy revealed that the chitosan NPs were spherical with no apparent aggregation (Figure 1A). The average hydrodynamic diameter of S-NPs and L-NPs was 25 nm and 150 nm, respectively. Both NPs had a positive zeta potential, a surface parameter affecting the stability of dispersed NPs and their cellular adsorption (Table 1). The encapsulation of HRP did not significantly change the hydrodynamic diameter of the NPs. Neither did it affect HRP activity, since encapsulation efficiency determined by either protein content or enzyme activity did not significantly differ (Table 1). Moreover, NPs of both sizes were able to release active HRP (Figure 1B). S-NP showed an initial burst during the first 2 h when ≈12% of the loaded HRP activity was released. HRP release then slowed down reaching ≈35% release within 72 h. The release of HRP from L-NPs was considerably weaker, and only ≈3.5% was released after 72 h (Figure 1B).

Baculoviral OCT4 expression and purification

For encapsulation in NP, the pluripotency factor OCT4 was expressed as a glutathione-S-transferase (GST) fusion protein in Sf9 insect cells using the baculoviral expression system. Following homologous recombination of the *GST-OCT4* cDNA with linearized wildtype baculovirus DNA, high-titer virus stocks were produced. Infection of Sf9 cells with the recombinant viruses resulted in high infection efficiencies, as monitored by expression of the *GFP* gene on the baculoviral DNA (Figure 2A). Since recombinant OCT4 was mainly localized in the nucleus of Sf9 cells (Figure 2B), we first isolated the nuclei of Sf9 cells five days post-infection. After lysis of the nuclei GST-affinity chromatography was performed. As revealed by silver staining and immunoblotting (Figure 2B), OCT4 protein could be easily enriched by this protocol, yielding ≈6 mg/l of purified OCT4 from Sf9 cell suspension cultures.

Chitosan S-NPs stabilize OCT4 DNA-binding activity

Recombinant OCT4 has been shown to become rapidly degraded under cell culture conditions [34]. We therefore tested the OCT4 DNA-binding activity by electrophoretic mobility shift assays using an oligonucleotide with the octamer-binding site from the Ig heavy chain enhancer. Soluble OCT4 as well as OCT4 encapsulated in S-NPs induced the appearance of a specific DNA/protein complex, which was not detectable with bovine serum albumin (BSA) as the negative control (Figure 3A) or in the presence of a 50-fold excess of unlabeled oligonucleotide (data not shown). In comparison to S-NPs, OCT4-loaded L-NPs induced a much weaker electrophoretic shift (Figure 3A). Similar results were obtained with higher L-NP concentrations (data not shown), indicating a less efficient release of OCT4 from L-NPs. Further experiments were therefore only conducted with OCT4-loaded S-NPs.

We next tested several storage conditions of the NPs for OCT4 DNA-binding. Whereas the long-term storage of OCT4-loaded NPs at 4°C still retained DNA-binding activity even after 7 weeks, no DNA-binding activity could be retained with soluble OCT4 protein (Figure 3B). Furthermore, at room temperature (RT) DNA binding of soluble OCT4 was lost within 7 days, whereas OCT4-loaded NPs showed still DNA binding after 14 days (Figure 3C). Importantly, S-NPs were able to maintain OCT4 DNA-binding activity even under cell culture conditions at 37°C (Figure 3D). In contrast, at 37°C soluble OCT4 caused the appearance of a high-molecular weight complex with reduced mobility (Figure 3D), which

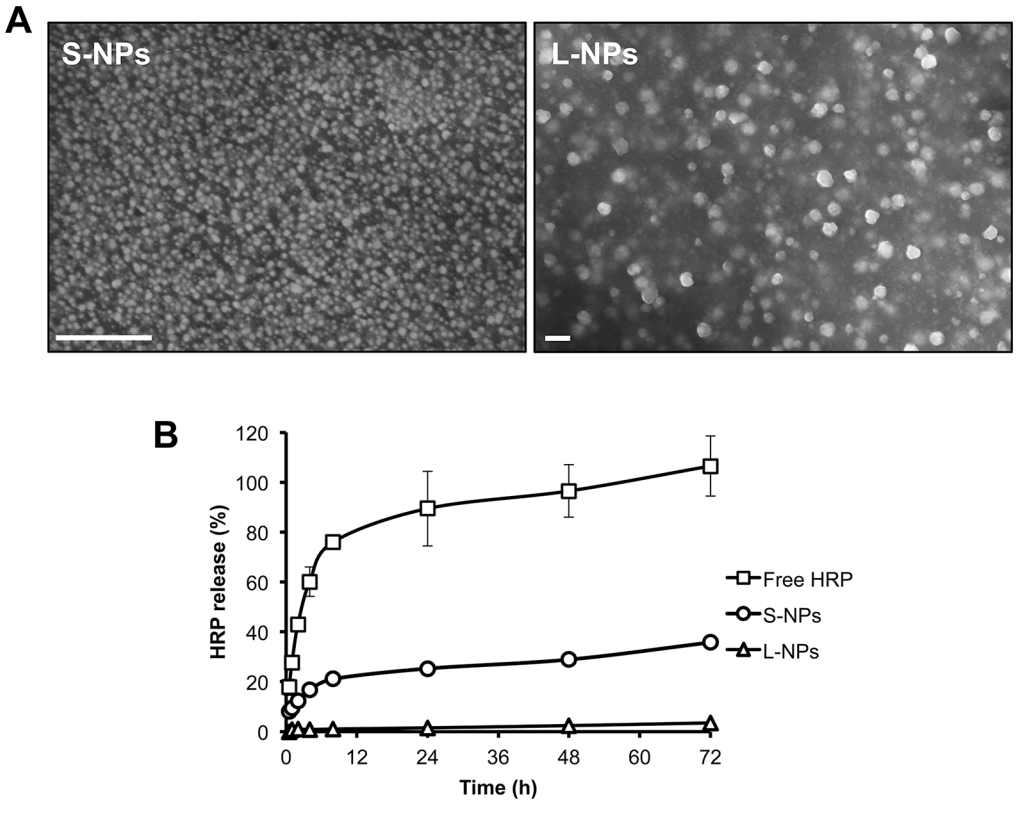

Figure 1: Characterization of chitosan NPs. (**A**) Scanning electron micrographs from S-NPs (left) and L-NPs (right). Bars = 200 nm. (**B**) Kinetics of HRP release from S-NPs and L-NPs in comparison to free HRP, as measured by enzyme activity. Results are given as mean ± SD from three experiments performed in triplicate. Similar release profiles were obtained by measuring protein content.

Table 1: Characterization of chitosan S-NPs and L-NPs

NP	Cargo	HD (nm)	ZP (mV)	EE % (% Activity)	EE (% Protein)
S-NP	w/o	25 ± 2	35 ± 2	-,-	-,-
	HRP	26 ± 2	22 ± 2	56.2 ± 0.0	58.7 ± 2.9
L-NP	w/o	147 ± 3	50 ± 5	-,-	-,-
	HRP	143 ± 1	45 ± 2	97.6 ± 0.4	94.3 ± 3.4

EE: encapsulation efficiency; HD: hydrodynamic diameter; HRP: horseradish peroxidase; ZP: zeta potential.

was presumably due to the reported precipitation and aggregation of OCT4 under cell culture conditions in the presence of serum [34, 35]. Thus, encapsulation of OCT4 in S-NPs results in a considerable stabilization of OCT4 DNA-binding activity.

Effects of NLS density on S-NP cell binding, uptake and nuclear delivery

We next investigated whether tagging with a nuclear localization sequence (NLS) could alter the cellular uptake and nuclear delivery of S-NPs. To this end, S-NPs with different NLS densities were generated and administered at different concentrations to human dermal fibroblasts. Subsequently, NPs were labeled with FITC-coupled wheat germ agglutinin (WGA) exhibiting a high affinity to chitosan. WGA labeling was performed in permeabilized and non-permeabilized cells at different temperatures to allow the discrimination of cell-associated and internalized NPs. We found that increasing NP concentrations resulted in an elevated cell association of the NPs (Figure 4A) as well as an increased cell surface binding (Figure 4B) and cellular uptake (Figure 4C). The presence of an NLS dose-dependently increased the amount of cell surface-bound and internalized S-NPs.

FRET spectroscopy with the nuclear DNA dye Hoechst and FITC was then performed to quantify the nuclear delivery of S-NPs in human fibroblasts.

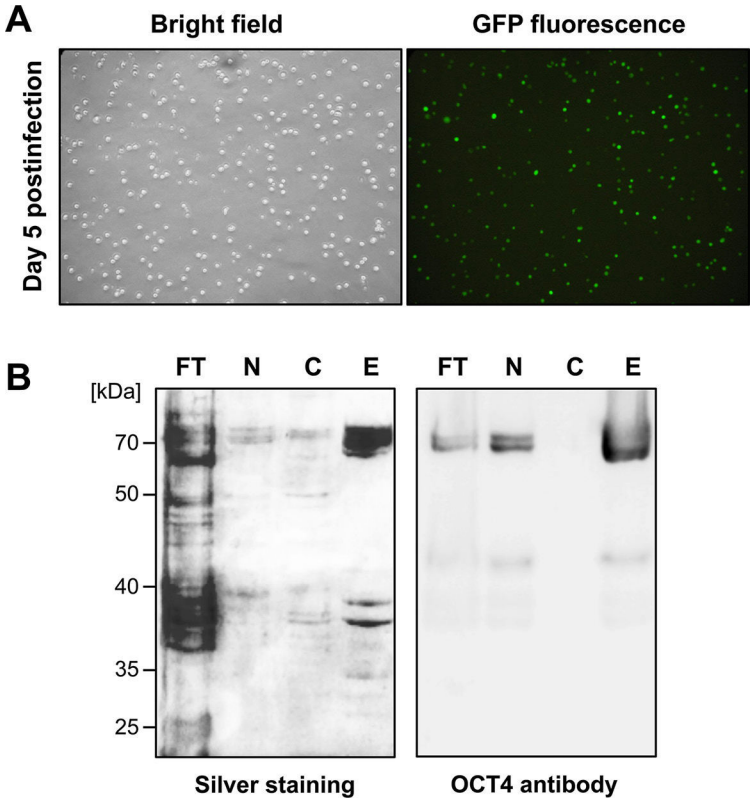

Figure 2: OCT4 expression and purification from Sf9 cells. (**A**) Efficient Sf9 cell infection with recombinant OCT4-encoding baculoviruses was monitored by expression of GFP five days post-infection. (**B**) Recombinant OCT4 is enriched in nuclear fractions of Sf9 cells and can be purified by GST affinity chromatography, as shown by silver staining (left) and immunoblot analysis using an OCT4 antibody (right). FT: column flow-through, N: nuclear fraction, C: cytosolic fraction, E: column eluates.

Surprisingly and in contrast to the previous experiments, unmodified S-NPs revealed a higher FRET efficiency and hence an increased nuclear localization compared to NLS-modified NPs (Figure 4D). Thus, even though NLS-tagging of S-NPs increased their cellular uptake, nuclear delivery was impaired. Since OCT4 exerts its cellular function in the nucleus, further tests were conducted with unmodified S-NPs, revealing the highest nuclear delivery.

Intracellular OCT4 delivery by S-NPs

We next investigated the cellular distribution of OCT4-loaded S-NPs by confocal laser scanning microscopy. To this end, human fibroblasts were treated with equal protein amounts of either soluble OCT4 or OCT4-loaded S-NPs. Soluble OCT4 was exclusively found at the cell membrane but was unable to enter the cells (Figure 5A–5C). In contrast, OCT4 encapsulated in NPs was efficiently imported into the fibroblasts, as revealed by costaining for OCT4 and chitosan using an OCT4 antibody and WGA-Alexafluor 488, respectively (Figure 5D–5E). Moreover, this intracellular distribution partially overlapped with nuclear Hoechst staining, indicating nuclear delivery of OCT4 (Figure 5F). To further analyze a nuclear delivery of the OCT4-loaded NPs in different layers of cell nucleus, confocal *Z*-stack images were collected at 1-µm steps (Figure 6). Visualization of a Z-stack indeed indicated that OCT4 encapsulated in NPs was detectable in both perinuclear and intranuclear regions of the fibroblasts.

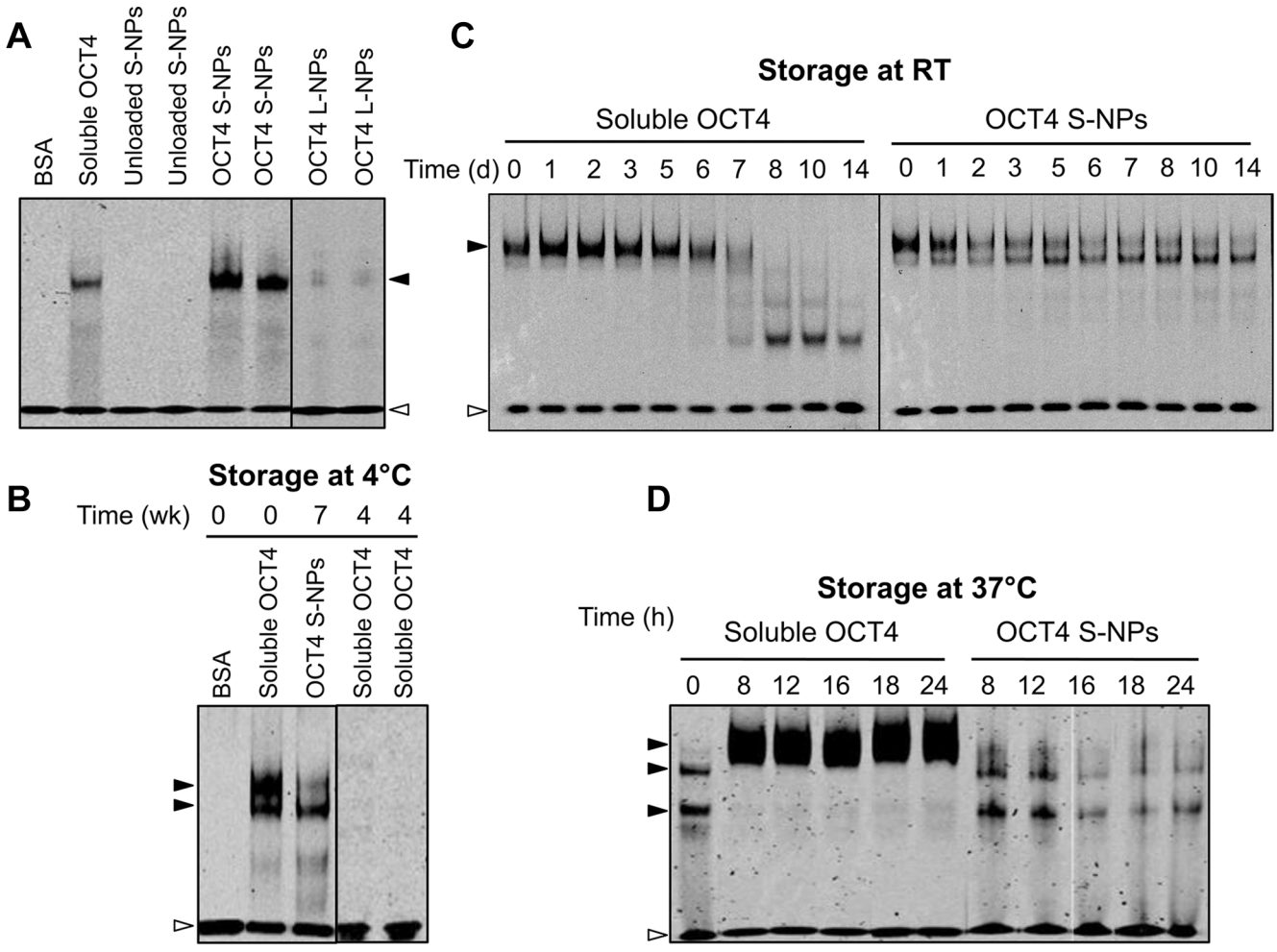

Figure 3: S-NP encapsulation stabilizes OCT4 DNA-binding activity. (**A**) EMSA analysis showing OCT4 stabilization by S-NPs but not L-NPs. Unloaded S-NPs, soluble OCT4 protein as well as OCT4 encapsulated in S-NPs and L-NPs were subjected to EMSA analysis. The DNA-binding activity of OCT4 was analyzed using an oligonucleotide containing the OCT4 consensus motif. BSA was used as a negative control. (**B**–**D**) OCT4-loaded S-NPs stabilize OCT4 DNA-binding activity for 7 weeks at 4°C (B), for 14 days at RT (C), and for 24 h under cell culture conditions at 37°C in the presence of serum (D), whereas the DNA-binding activity of soluble OCT4 is rapidly lost under these conditions. The slowly migrating protein/DNA complex of soluble OCT4 shown in (D) is presumably caused by aggregation of the OCT4 protein under cell culture conditions. The protein amount used per lane for the EMSAs corresponds to 30 ng (A), 100 ng (B) and 250 ng (C, D). The OCT4/DNA complexes and unbound oligonucleotide are marked by closed and open arrowheads, respectively.

DISCUSSION

Various strategies have been suggested to accomplish transgene-free derivation of iPSCs, including the use of non-integrating viruses, site-specific recombinases for transgene excision, plasmids or RNA transfection [7–13]. Although these methods significantly reduce the risk of genome alterations, a nucleic acid-free system is generally preferred. Chitosan NPs are increasingly used as protein delivery vehicles due to their mild formulation conditions [22–24]. To demonstrate that chitosan NPs preserve protein activity we initially encapsulated HRP as a model protein and investigated the encapsulation efficiency and release profile. Both S-NPs and L-NPs released HRP in its active form. Since S-NPs revealed a more efficient release and better preservation of OCT4 DNA-binding, further experiments were solely conducted with S-NPs.

Compared to L-NPs, S-NPs showed a higher sustained release of active HRP over a 72-h incubation period and were able to increase OCT4 stability at 4°C (up to 7 weeks), at room temperature (up to two weeks) and more importantly in cell culture at 37°C. Under cell culture conditions the DNA-binding activity of soluble OCT4 was lost within 1 h, whereas NP-encapsulated OCT4 preserved activity throughout the 24-h period tested. Also Bonsali *et al.* reported that a rapid loss of TAT-OCT4 activity under cell culture conditions [34]. The presence of serum stabilized the TAT fusion protein but at the same time reduced its cellular uptake [35]. Moreover, while a combination of serum and serum replacement containing lipid-rich BSA improved the stability and cellular uptake of TAT-OCT4, serum replacement was cytotoxic to fibroblasts [35, 39].

An ideal protein transduction method has to fulfill several criteria and (1) stabilize the recombinant protein, (2) facilitate its cellular entry and endosomal escape, (3) allow cell treatment with sufficient protein concentrations and (4) provide sustained protein levels without the need for repeated treatments. We found that chitosan NPs were able to considerably stabilize OCT4 in cell culture conditions. The ability of chitosan NPs to associate with cells has been

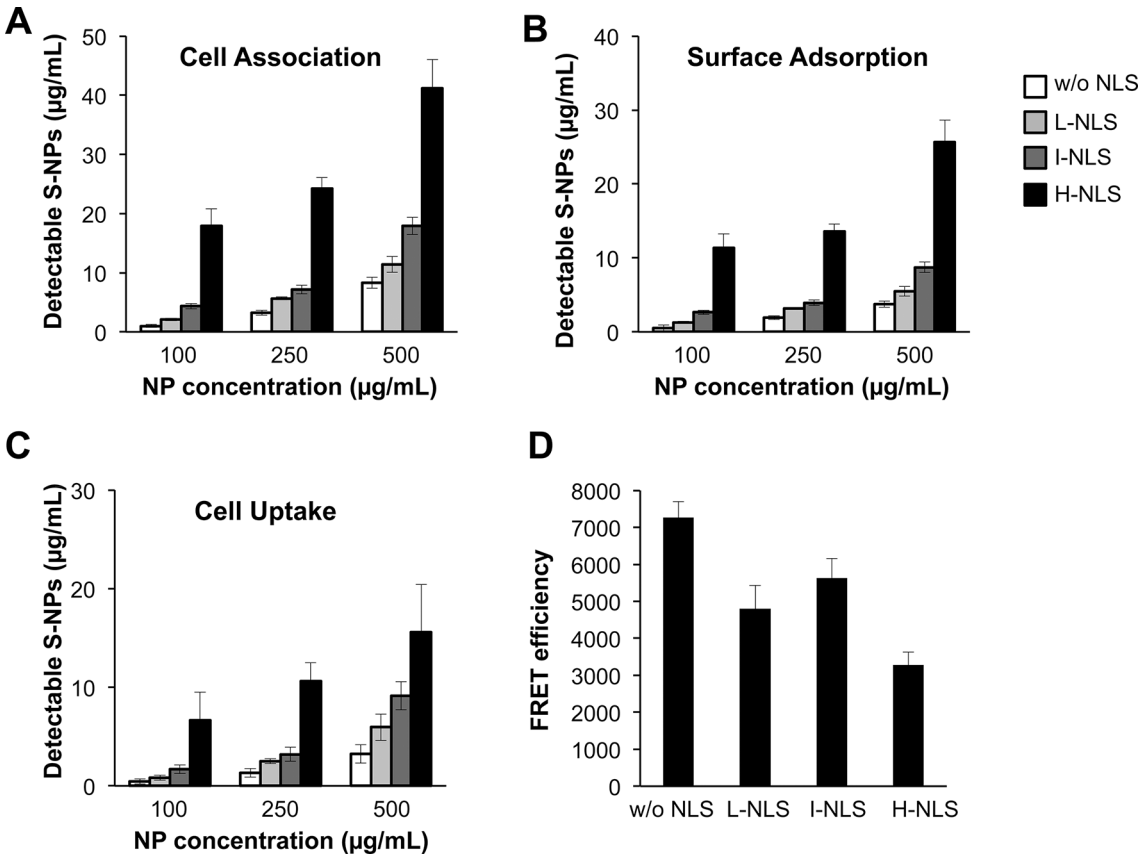

Figure 4: Effects of NLS density on S-NP cell surface binding, uptake and nuclear delivery. (**A**–**C**) Non-modified S-NPs or S-NPs tagged with low (L), intermediate (I) or high (H) NLS densities were incubated at the indicated concentrations with human fibroblasts. After 24 h chitosan NPs were stained as detailed in Material and Methods. The recovered amount of (A) cell-associated (i.e. surface-bound and internalized) NPs, (B) NPs bound to cell surface or (C) NPs taken up intracellularly was calculated from a standard curve by fluorometry. (**D**) Effects of NLS density on S-NP nuclear delivery as assessed by FRET fluoroscopy. Human fibroblasts were treated for 24 h with 250 µg/mL of the indicated versions of S-NPs. Measurement of FRET efficiency indicates the strongest colocalization of the nuclear DNA dye with SN-Ps lacking an NLS. Results are given as means ± SD.

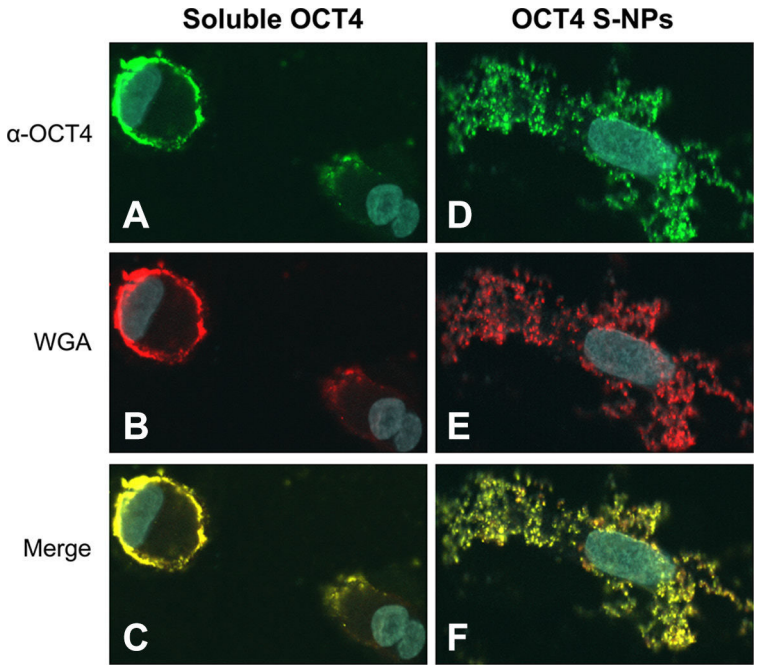

Figure 5: OCT4-loaded S-NPs but not soluble OCT4 protein are imported into cells and partially localize in the cell nucleus. Human primary fibroblasts were treated with 50 µg of each recombinant soluble OCT4 (**A**–**C**) or OCT4 encapsulated in S-NPs (**D**–**F**). After 24 h cells were stained with OCT4 antibodies (green) or for chitosan NPs using WGA-Alexafluor 488 (red). Nuclear DNA was stained with Hoechst 33258 (blue). Merged images demonstrate that exogenous soluble OCT4 is excluded from cells and adheres to the cell membrane. In contrast, OCT4-loaded S-NPs are localized intracellularly, showing a partial overlap with Hoechst nuclear staining.

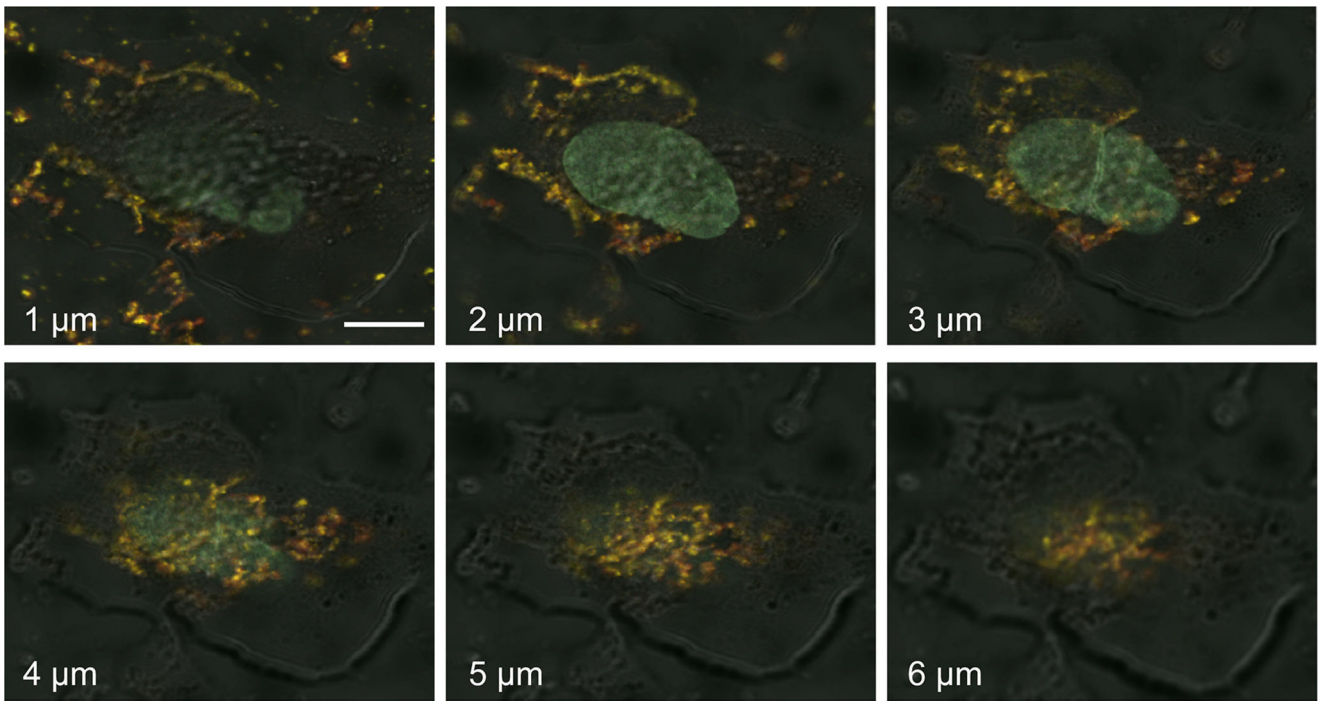

Figure 6: Z-stack imaging series of human fibroblasts treated with OCT4-loaded S-NPs. Cells were treated for 24 h with 50 µg of the SN-Ps and then stained with OCT4 antibody (green), WGA-Alexafluor 488 (red) and Hoechst 33258 (blue). Z-stack images through the cell nucleus were collected at 1-µm steps by confocal laser scanning microscopy. The yellow fluorescence of the merged images indicates the colocalization of OCT4 and S-NPs in perinuclear and nuclear regions. The depth in micrometers at which images were taken is indicated. Scale bar = 10 µM.

repeatedly reported [25, 40], however, only a few studies distinguished between cell surface-bound and internalized NPs [41–43]. Since soluble OCT4 is incapable of cell entry, we validated that chitosan NPs are capable of cellular entry rather than adhering to the cell surface. To this end, we employed a method that exploits the preferential affinity of WGA to chitosan and thereby allows the quantification of cell surface-bound and internalized chitosan NPs. In non-permeabilized cells at 4°C WGA-FITC was not internalized and labeled only extracellular chitosan NPs, whereas in permeabilized cells at RT WGA-FITC labeled both surface-bound and internalized NPs, making it possible to quantify NPs that had been internalized and those that were only adsorbed onto the surface [44].

As a transcription factor, OCT4 requires its delivery into the nucleus. Employing a FRET assay to evaluate the nuclear targeting of NPs, we surprisingly found that the presence of an NLS even reduced nuclear targeting of OCT4. Further experiments were therefore conducted with unmodified NPs. Confocal microscopy confirmed the cellular and nuclear entry of intact OCT4-NPs. Prior to microscopy, we treated the permeabilized cells with WGA-Alexafluor 488 to demonstrate that the green fluorescence was due to OCT4-NPs rather than free OCT4. Since WGA preferentially binds to chitosan NPs [44], the detectable yellow fluorescence indicated a co-localization of OCT4 and WGA, suggesting that the signal was due to intracellular rather than free OCT4.

Apart from stabilizing and delivering OCT4 to its site of action, NPs enable the use of high concentrations of reprogramming factors. In the case of OCT4 an encapsulation efficiency of ≈75% was achieved, which allowed cell treatment with a concentration of 100 µg/mL (≈2.6 µM) of OCT4. At this concentration (corresponding to 1 mg/mL chitosan) OCT4 was neither degraded, precipitated nor were the target cells affected.

So far, only two studies employed nanocarriers in protein-induced reprogramming. Cho *et al.* used TiO_2 nanotubes with electrostatically adsorbed Oct4, Sox2, Klf4 and Nanog for reprogramming of neural stem cells [45]. While the authors observed stem cell-like morphological changes, fully reprogrammed iPSCs were not obtained. It is possible that the electrostatic binding, unlike chitosan encapsulation of proteins, hindered the release of the reprogramming factors. Khan *et al.* obtained iPSC colonies using synthetic surfactants complexed with KLF4, SOX2 and NR5A2 following three rounds of protein transduction [46]. In addition, several other possibilities can enhance the efficiency of iPSC generation. For instance, histone deacetylase inhibitors or activation of toll-like receptor-3 were reported to enhance reprogramming by cell-permeant OSKM fusion proteins by facilitating epigenetic alterations [19, 47].

In contrast to the baculoviral expression yielding high amounts of active OCT4, most studies used bacterially expressed OSKM factors for protein-induced reprogramming attempts. The bacterially overexpressed transcription factors were found in inclusion bodies and had to be denatured and refolded *in vitro*, resulting in a partial loss of activity and reprogramming efficiency [19]. Low efficiencies could generally be attributed to the poor stability and solubility of recombinant factors, their low cellular entry or their poor endosomal release [33–35]. Indeed, a major drawback of PTD fusion proteins is their inefficient release from endosomal vesicles into the cytosol. Interestingly, cell permeabilization with streptolysin O has been reported to enhance protein-induced reprogramming, presumably by avoiding entrapment of OSKM factors in lysosomes [48]. Similarly, sucrose acting as a lysomotrophic agent can increase the reprogramming efficiency of OCT4-TAT [35].

Although cell-permeant PTD-fused OSKM factors enhance the cellular uptake, they do not provide a sustained supply, unless protein treatment is repeated several times. A sustained supply of the OSKM factors is required for reprogramming and a major reason for the high reprogramming efficiency of retroviral expression systems. In this context NP-encapsulated OSKM factors might provide a more sustained supply compared to soluble proteins. Further studies are therefore ongoing to generate NPs for SOX2, c-MYC and KLF4 and to evaluate their utility in protein-based iPSC generation.

MATERIALS AND METHODS

Chitosan nanoparticle formulation and characterization

Small and large chitosan NPs were formulated by the inotropic gelation method using low-molecular weight chitosan (50–190 kDa; Sigma-Aldrich, St. Louis, MO) and tripolyphosphate (TPP; Mistral Chemicals, Antrim, UK) [28]. NP average hydrodynamic diameter and zeta potential were determined using a Zetasizer Nano ZS90 device (Malvern Instruments, Herrenberg, Germany). After dilution of the NP suspension with de-ionized water samples were measured in triplicate at 25°C and calculated as means ± SD. For morphological analysis, a drop of the diluted NP suspension was spread on glass slides and subjected to field-emission scanning electron microscopy using a LEO SUPRA 55 microscope (Carl Zeiss, Reutlingen, Germany).

Horseradish peroxidase (HRP; ~150 U/mg; Sigma-Aldrich) was used as a model protein to study protein encapsulation. HRP-loaded chitosan NPs were formulated by dissolving HRP in TPP solution. To exclude that the NP encapsulation of proteins by inotropic gelation did affect protein activity, encapsulation efficiency (EE) was determined based on enzyme activity and protein content. To this end, L-NPs were centrifuged at 14000 g for 30 min, before un-entrapped protein was quantified in the supernatant. S-NPs were centrifuged in Roti®-Spin

centrifugal filters (molecular weight cut-off 100 kDa; Carl Roth GmbH, Karlsruhe Germany) for 20 min at 4000 g, before the non-entrapped protein was quantified in the flow-through. EE based on total protein content was determined by Coomassie Plus (Pierce Biotechnology, Rockford, IL) following removal of excess chitosan. HRP L-NPs and S-NPs were purified as described above. To 1 mL of L-NP supernatant and S-NP flow-through 20 µL of 20% NaOH were added. Samples were then centrifuged at 14000 g for 5 min, before chitosan-free supernatants were used to quantify un-entrapped protein using Coomassie dye.

Activity-based quantification of HRP was performed as described [49]. Briefly, 1.5 mL of 1.7 mM of hydrogen peroxide in 0.2 M potassium phosphate buffer was mixed with 1.4 mL of 2.5 M 4-aminoantipyrine-phenol (Acros Organics, Geel, Belgium). Increase in absorbance at 510 nm was recorded using a UV–Vis spectrophotometer every 30 sec for 5 min upon addition of 100 µL enzyme-containing test solution (L-NP supernatant or S-NP flow through). Rate of reaction was determined and used to calculate the enzyme concentration from a HRP standard calibration curve.

To determine the ability of NPs to release proteins, HRP-loaded NPs were purified, reconstituted in 1 mL de-ionized water and placed in spectra/por float-A-lyzers (molecular weight cut-off 100 kDa; Spectrum Labs, Breda, The Netherlands). NP-loaded float-A-lyzers were submerged in 6 mL PBS and maintained at 37°C in a shaking water bath. At predetermined time intervals, 200 µL of the samples were removed, replaced with fresh buffer and analyzed for active HRP. All samples were analyzed in triplicate and results are given as means ± SD.

OCT4 expression and purification

Sf9 insect cells were cultured with EX-Cell 420 media (Sigma-Aldrich) supplemented with 10% fetal calf serum and penicillin/streptomycin. *OCT4* cDNA was cloned into pAcG2T transfer vector which contains GST tag and transferred by homologous recombination to baculoviral bright linear DNA (BD Biosciences, Heidelberg, Germany) containing a *GFP* gene. To obtain recombinant OCT4, Sf9 cells in 1 L suspension cultures were infected with baculovirus at a multiplicity of infection (MOI) of 10. Five days post-infection cells were harvested by centrifugation at 4°C for 10 min at 2000 g and washed twice with 50 mL PBS. As recombinant OCT4 localizes in the nucleus of Sf9 cells, nuclear extraction was conducted as described [50]. Briefly, cell pellets were suspended in hypotonic buffer (10 mM Na-HEPES, pH 7.9, 10 mM KCl, 0.1 mM EDTA, 0.1 mM EGTA, 1 mM DTT and 0.5 mM PMSF) and incubated for 15 min on ice. Cells were then lysed with 25 strokes of a Dounce homogenizer. The cell lysate including nuclei was centrifuged at 4600 rpm at 4°C for 10 min, resuspended in nuclear lysis buffer (20 mM Na-HEPES, pH 7.9, 400 mM KCl, 1 mM EDTA, 1 mM EGTA, 10% glycerol, 1 mM DTT) and incubated at 4°C for 30 min with shaking. Nuclear lysates were filtrated through 5-µm and 0.45-µm filters followed by affinity chromatography on glutathione sepharose to isolate GST-tagged OCT4. All steps were carried out at 4°C. After measurement of protein content, the column eluates were pooled to obtain a final concentration of 1 mg/mL and frozen in 25% glycerol. The purity of the OCT4 preparations was analyzed by silver staining and Western blotting using an OCT4 antibody (Cell Signaling Technology, Frankfurt, Germany).

Determination of the effect of NPs on OCT4 DNA-binding activity

Electrophoretic mobility shift assays (EMSAs) were performed using Odyssey® Infrared EMSA kit (LI-COR Bioscience, Cambridge, UK). Briefly, recombinant OCT4 was incubated with 1 µl of IRDye® 700 infrared dye-labeled double-stranded oligonucleotide (5′-GCCGAATTTGCATATTTGCATGGCTG-3′), 2 µl of 10 × binding buffer, 2.5 mM DTT, 0.25% Tween-20 and 1 µg of poly(dI-dC) in a total volume of 20 µl for 20 min at RT. Samples were separated on 4% native polyacrylamide gels in 0.5 × Tris-borate-EDTA. The gel was scanned by infrared fluorescence detection on the Odyssey® imaging system. DNA-binding activity of encapsulated OCT4 was determined directly after NP formulation, after storage at 4°C, RT and in cell culture media at 37°C.

Determination of the effect of NLS density on NP cell surface binding and uptake

Rhodamine isothiocynate (RITC)-coupled BSA was used to explore the effect of an NLS on the cell surface binding and cell uptake of S-NPs. NP encapsulation of BSA-RITC was performed as described [28]. NPs were purified and protein content was determined by fluorometry (FLUOstar Optima, BMG Labtech, Ortenberg, Germany; λex 540 nm; λem 625 nm). As a classical NLS the octapeptide CPKKKRKV (Bio Basic Canada Inc., Ontario, Canada) was used. NLS tagging to NPs was performed via N-succinimidyl 3-[2-pyridyldithio]-propionate (Pierce Biotechnology, Rockford, IL), a SH-NH_2 cross-linker utilizing the N-terminal SH group in the NLS and cationic amines in chitosan. S-NPs with low (L-NLS; 0.25 NLS/nm^2), intermediate (I-NLS; 0.5 NLS/nm^2) and high (H-NLS; 2 NLS/ nm^2) NLS density were synthesized. NLS tagging and characterization of the modified NPs was performed as detailed previously [28].

For NP treatment, human primary fibroblasts were plated in 96-well plates (2 × 10^4 cells/well) and cultured in RPMI-1640 medium supplemented with 10% fetal calf serum, 2 mM glutamine and 2 mM sodium pyruvate. After 48 h cells were washed with PBS and

incubated with purified NP-encapsulated BSA-RITC in serum-containing phenol-red free RPMI-1640. The non-modified and NLS-modified S-NPs were added to the cells at a concentration of 100, 250 and 500 µg/mL. After 24 h, culture supernatants were removed and cells were washed twice with PBS. The amount of cell-associated NPs was calculated by fluorometry from standard curves as described [28, 44].

Based on the preferential affinity of wheat germ agglutinin (WGA) to chitosan, FITC-coupled WGA was exploited to distinguish between cell surface-absorbed and internalized NPs. In non-permeabilized cells at 4°C WGA-FITC is not internalized and only labels extracellular chitosan NPs, whereas in permeabilized cells at RT WGA-FITC can enter the cell and label both surface-bound and internalized chitosan NPs. Therefore, fibroblasts were grown in two 96-well plates and loaded with the non-modified or NLS-modified S-NPs as described above. After 24 h, cells were washed twice with PBS. In the first plate, cells were fixed with 4% paraformaldehyde (PFA) for 15 min, washed with PBS, and permeabilized with 0.1% Triton X-100 for 15 min. Cells were then incubated with 100 µL of 10 µg/mL WGA-FITC (Sigma-Aldrich) for 15 min at RT followed by washings in PBS. In the second plate, cells were incubated on ice for 15 min and then directly treated with WGA-FITC for 15 min on ice. After three washings in PBS, the amount of bound WGA-FITC was determined by fluorometry (λex: 494 nm; λem 518 nm) in both plates as described [44]. Results are expressed as mean ± SD from three experiments performed in triplicate.

Measurement of NP nuclear localization by FRET spectroscopy

The effect of NLS density on nuclear delivery of S-NPs was assessed in intact human fibroblasts by Förster resonance energy transfer (FRET) fluorometry. To this end, the nuclear DNA dye Hoechst 33258 and FITC from FITC-coupled BSA were used as FRET donor and acceptor, respectively. Formulation and encapsulation of BSA-FITC in unmodified and the different versions of NLS-modified S-NPs was performed as described above and detailed previously [28]. Fibroblasts were seeded at a density of 2×10^4 cells/well in 96-well plates, treated with 250 µg/mL of the NP versions after 48 h and incubated for another 24 h. After aspiration of the culture supernatants cells, cells were stained with Hoechst dye (1.5 µg/mL). Cells were washed 3 times with PBS then analyzed by FRET spectroscopy. Three readings were obtained in the FRET channel (λex 366 nm; -λem 518 nm) either for Hoechst-stained and NP-treated cells, for NP-treated cells or for Hoechst-stained cells. FRET was determined from the increase in FITC emission due to a nuclear colocalization of both dyes. FRET efficiency was calculated as described [28].

Detection of OCT4 nuclear delivery by confocal laser scanning microscopy

Human fibroblasts were seeded on coverslips in 24-well plates at a density of 5×10^5 cell/well. After 24 h cells were treated with either 50 µg/mL of OCT4 encapsulated in S-NPs or soluble OCT4 and incubated for another 24 h. Following washes in PBS, cells were stained with Hoechst 33258 (1.5 µg/mL) for 5 min, fixed with 4% PFA and permeabilized with 0.1% Triton X-100 in PBS. WGA-Alexafluor 488 (Life Technologies, Darmstadt, Germany) was added to the cells for 15 min at RT. Cells were then washed twice with PBS and incubated in blocking buffer (1% BSA in PBS) for 30 min. OCT4 antibody (1:100) was incubated overnight at 4°C. After three washes in blocking buffer, FITC-conjugated goat anti-rabbit IgG (1:500; Promega, Mannheim, Germany) was applied for 1 h at RT. Coverslips were washed in PBS, mounted in fluorescence-mounting medium (DAKO, Hamburg, Germany) and examined by confocal microscopy (Eclipse Ti, Nikon, Tokyo, Japan).

ACKNOWLEDGMENTS AND FUNDING

This study was supported by the French Government excellence initiative managed by the French National Research Agency under the program "Investissements d'Avenir" (ANR-11-LABX-0021) to A.L. and the Deutsche Forschungsgemeinschaft (GRK 1302) to K.S.O.

CONFLICTS OF INTEREST

The authors declare no conflicts of interest.

REFERENCES

1. Okita K, Yamanaka S. Induced pluripotent stem cells: opportunities and challenges. Philos Trans R Soc Lond B Biol Sci. 2011; 366:2198–2207.
2. Robinton DA, Daley GQ. The promise of induced pluripotent stem cells in research and therapy. Nature. 2012; 481:295–305.
3. Takahashi K, Tanabe K, Ohnuki M, Narita M, Ichisaka T, Tomoda K, Yamanaka S. Induction of pluripotent stem cells from adult human fibroblasts by defined factors. Cell. 2007; 131:861–872.
4. Li Y, Shen Z, Shelat H, Geng YJ. Reprogramming somatic cells to pluripotency: a fresh look at Yamanaka's model. Cell Cycle. 2013; 12:3594–3598.
5. Sun N, Longaker MT, Wu JC. Human iPS cell-based therapy: considerations before clinical applications. Cell Cycle. 2010; 9:880–885.
6. Ruiz S, Fernandez-Capetillo O. Reducing genomic instability in iPSCs. Oncotarget. 2015; 6:34045–34046.

7. Stadtfeld M, Nagaya M, Utikal J, Weir G, Hochedlinger K. Induced pluripotent stem cells generated without viral integration. Science. 2008; 322:945–949.
8. Okita K, Hong H, Takahashi K, Yamanaka S. Generation of mouse-induced pluripotent stem cells with plasmid vectors. Nat Protoc. 2010; 5:418–428.
9. Warren L, Manos PD, Ahfeldt T, Loh YH, Li H, Lau F, Ebina W, Mandal PK, Smith ZD, Meissner A, Daley GQ, Brack AS, Collins JJ, et al. Highly efficient reprogramming to pluripotency and directed differentiation of human cells with synthetic modified mRNA. Cell Stem Cell. 2010; 7:618–630.
10. Yu J, Hu K, Smuga-Otto K, Tian S, Stewart R, Slukvin II, Thomson JA. Human induced pluripotent stem cells free of vector and transgene sequences. Science. 2009; 324:797–801.
11. Kaji K, Norrby K, Paca A, Mileikovsky M, Mohseni P, Woltjen K. Virus-free induction of pluripotency and subsequent excision of reprogramming factors. Nature. 2009; 458:771–775.
12. VandenDriessche T, Ivics Z, Izsvák Z, Chuah MK. Emerging potential of transposons for gene therapy and generation of induced pluripotent stem cells. Blood. 2009;114:1461–1468.
13. Sommer CA, Sommer AG, Longmire TA, Christodoulou C, Thomas DD, Gostissa M, Alt FW, Murphy GJ, Kotton DN, Mostoslavsky G. Excision of reprogramming transgenes improves the differentiation potential of iPS cells generated with a single excisable vector. Stem Cells. 2010; 28:64–74.
14. Ben-Porath I, Thomson MW, Carey VJ, Ge R, Bell GW, Regev A, Weinberg RA. An embryonic stem cell-like gene expression signature in poorly differentiated aggressive human tumors. Nat Genet. 2008; 40:499–507.
15. Marzi I, Cipolleschi MG, D'Amico M, Stivarou T, Rovida E, Vinci MC, Pandolfi S, Dello Sbarba P, Stecca B, Olivotto M. The involvement of a Nanog, KLF4 and c-MYC transcriptional circuitry in the intertwining between neoplastic progression and reprogramming. Cell Cycle. 2013; 12:353–364.
16. Corominas-Faja B, Cufí S, Oliveras-Ferraros C, Cuyàs E, López-Bonet E, Lupu R, Alarcón T, Vellon L, Iglesias JM, Leis O, et al. Nuclear reprogramming of luminal-like breast cancer cells generates SOX2-overexpressing cancer stem-like cellular states harboring transcriptional activation of the mTOR pathway. Cell Cycle. 2013; 12:3109–3124.
17. Bareiss PM, Paczulla A, Wang H, Schairer R, Wiehr S, Kohlhofer U, Rothfuss OC, Fischer A, Perner S, Staebler A, Wallwiener D, Fend F, Fehm T, et al. SOX2 expression associates with stem cell state in human ovarian carcinoma. Cancer Res. 2013; 73:5544–5555.
18. Schaefer T, Wang H, Mir P, Konantz M, Pereboom TC, Paczulla AM, Merz B, Fehm T, Perner S, Rothfuss OC, Kanz L, Schulze-Osthoff K, Lengerke C. Molecular and functional interactions between AKT and SOX2 in breast carcinoma. Oncotarget. 2015; 6:43540–43556.
19. Zhou H, Wu S, Joo JY, Zhu S, Han DW, Lin T, Trauger S, Bien G, Yao S, Zhu Y, Siuzdak G, Schöler HR, Duan L, et al. Generation of induced pluripotent stem cells using recombinant proteins. Cell Stem Cell. 2009; 4:381–384.
20. Kim D, Kim CH, Moon JI, Chung YG, Chang MY, Han BS, Ko S, Yang E, Cha KY, Lanza R, Kim KS. Generation of human induced pluripotent stem cells by direct delivery of reprogramming proteins. Cell Stem Cell. 2009; 4:472–476.
21. Nemes C, Varga E, Polgar Z, Klincumhom N, Pirity MK, Dinnyes A. Generation of mouse induced pluripotent stem cells by protein transduction. Tissue Eng Part C Methods. 2014; 20:383–392.
22. Agnihotri SA, Mallikarjuna NN, Aminabhavi TM. Recent advances on chitosan-based micro- and nanoparticles in drug delivery. J Control Release. 2004; 100:5–28.
23. Pan Y, Li YJ, Zhao HY, Zheng JM, Xu H, Wei G, Hao JS, Cui FD. Bioadhesive polysaccharide in protein delivery system: chitosan nanoparticles improve the intestinal absorption of insulin *in vivo*. Int J Pharm. 2002; 249:139–147.
24. Vila A, Sánchez A, Janes K, Behrens I, Kissel T, Vila Jato JL, Alonso MJ. Low molecular weight chitosan nanoparticles as new carriers for nasal vaccine delivery in mice. Eur J Pharm Biopharm. 2004; 57:123–131.
25. Enríquez de Salamanca A, Diebold Y, Calonge M, García-Vazquez C, Callejo S, Vila A, Alonso MJ. Chitosan nanoparticles as a potential drug delivery system for the ocular surface: toxicity, uptake mechanism and *in vivo* tolerance. Invest Ophthalmol Vis Sci. 2006; 47:1416–14125.
26. Gaur S, Wen Y, Song JH, Parikh NU, Mangala LS, Blessing AM, Ivan C, Wu SY, Varkaris A, Shi Y, Lopez-Berestein G, Frigo DE, Sood AK, et al. Chitosan nanoparticle-mediated delivery of miRNA-34a decreases prostate tumor growth in the bone and its expression induces non-canonical autophagy. Oncotarget. 2015; 6:29161–29177.
27. Harush-Frenkel O, Debotton N, Benita S, Altschuler Y. Targeting of nanoparticles to the clathrin-mediated endocytic pathway. Biochem Biophys Res Commun. 2007; 353:26–32.
28. Tammam SN, Azzazy HM, Breitinger HG, Lamprecht A. Chitosan Nanoparticles for Nuclear Targeting: The Effect of Nanoparticle Size and Nuclear Localization Sequence Density. Mol Pharm. 2015; 12:4277–4289.
29. Radzisheuskaya A, Silva JC. Do all roads lead to Oct4? the emerging concepts of induced pluripotency. Trends Cell Biol. 2014; 24:275–284.
30. Radzisheuskaya A, Chia Gle B, dos Santos RL, Theunissen TW, Castro LF, Nichols J, Silva JC. A defined OCT4 level governs cell state transitions of pluripotency entry and differentiation into all embryonic lineages. Nat Cell Biol. 2013; 15:579–590.
31. Jerabek S, Merino F, Schöler HR, Cojocaru V. OCT4: dynamic DNA binding pioneers stem cell pluripotency. Biochim Biophys Acta. 2014; 1839:138–154.

32. Stefanovic S, Pucéat M. Oct-3/4: not just a gatekeeper of pluripotency for embryonic stem cell, a cell fate instructor through a gene dosage effect. Cell Cycle. 2007; 6:8–10.

33. Kim JB, Sebastiano V, Wu G, Araúzo-Bravo MJ, Sasse P, Gentile L, Ko K, Ruau D, Ehrich M, van den Boom D, Meyer J, Hübner K, Bernemann C, et al. Oct4-induced pluripotency in adult neural stem cells. Cell. 2009; 136:411–419.

34. Bosnali M, Edenhofer F. Generation of transducible versions of transcription factors Oct4 and Sox2. Biol Chem. 2008; 389:851–861.

35. Thier M, Münst B, Edenhofer F. Exploring refined conditions for reprogramming cells by recombinant Oct4 protein. Int J Dev Biol. 2010; 54:1713–1721.

36. Zhang H, Ma Y, Gu J, Liao B, Li J, Wong J, Jin Y. Reprogramming of somatic cells via TAT-mediated protein transduction of recombinant factors. Biomaterials. 2012; 33:5047–5055.

37. Singh SM, Panda AK. Solubilization and refolding of bacterial inclusion body proteins. J Biosci Bioeng. 2005; 99:303–10.

38. Jarvis DL. Baculovirus-insect cell expression systems. Methods Enzymol. 2009; 463:191–222.

39. Thier M, Münst B, Mielke S, Edenhofer F. Cellular Reprogramming Employing Recombinant Sox2 Protein. Stem Cells Int. 2012; 2012:549846.

40. Huang M, Ma Z, Khor E, Lim LY. Uptake of FITC-chitosan nanoparticles by A549 cells. Pharm Res. 2002; 19:1488–1494.

41. Braun GB, Friman T, Pang HB, Pallaoro A, Hurtado de Mendoza T, Willmore AM, Kotamraju VR, Mann AP, She ZG, Sugahara KN, Reich NO, Teesalu T, Ruoslahti E. Etchable plasmonic nanoparticle probes to image and quantify cellular internalization. Nat Mater. 2014; 13: 904–911.

42. Cho EC, Xie J, Wurm PA, Xia Y. Understanding the role of surface charges in cellular adsorption versus internalization by selectively removing gold nanoparticles on the cell surface with a I2/KI etchant. Nano Lett. 2009; 9: 1080–1084.

43. Gottstein C, Wu G, Wong BJ, Zasadzinski JA. Precise quantification of nanoparticle internalization. ACS Nano. 2013; 7:4933–4945.

44. Tammam SN, Azzazy HM, Lamprecht A. A high throughput method for quantification of cell surface bound and internalized chitosan nanoparticles. Int J Biol Macromol. 2015; 81:858–866.

45. Cho SJ, Choi HW, Cho J, Jung S, Seo HG, Do JT. Activation of pluripotency genes by a nanotube-mediated protein delivery system. Mol Reprod Dev. 2013; 80: 1000–1008.

46. Khan M, Narayanan K, Lu H, Choo Y, Du C, Wiradharma N, Yang YY, Wan AC. Delivery of reprogramming factors into fibroblasts for generation of non-genetic induced pluripotent stem cells using a cationic bolaamphiphile as a non-viral vector. Biomaterials. 2013; 34:5336–5343.

47. Lee J, Sayed N, Hunter A, Au KF, Wong WH, Mocarski ES, Pera RR, Yakubov E, Cooke JP. Activation of innate immunity is required for efficient nuclear reprogramming. Cell. 2012; 151:547–558.

48. Cho HJ, Lee CS, Kwon YW, Paek JS, Lee SH, Hur J, Lee EJ, Roh TY, Chu IS, Leem SH, Kim Y, Kang HJ, Park YB, et al. Induction of pluripotent stem cells from adult somatic cells by protein-based reprogramming without genetic manipulation. Blood. 2010; 116:386–395.

49. Trinder P. Determination of blood glucose using an oxidase-peroxidase system with a non-carcinogenic chromogen. J Clin Pathol. 1969; 22:158–161.

50. Malak PN, Dannenmann B, Hirth A, Rothfuss OC, Schulze-Osthoff K. Novel AKT phosphorylation sites identified in the pluripotency factors OCT4, SOX2 and KLF4. Cell Cycle. 2015; 14:3748–3754.